Applications of Porous Inorganic-Organic Hybrid Solid in Membrane Reactors and Catalysis for Hydrogen Production

---

A thesis submitted in fulfilment of the requirements for the

Degree of Doctor of Philosophy in Chemical Engineering

Department of Chemical and Process Engineering,

University of Canterbury,

New Zealand

Ben, Hang Yin

2016

Contents

ACKNOWLEDGEMENT

First of all, I would like to express my sincere gratitude to my supervisor, Dr Alex Yip for his supervision throughout my PhD study at the University of Canterbury. I really appreciate his thoughtful and thorough guidance, his consistent patience and his invaluable support and trust on me during the past years. I have been very happy to study and work with him, a very young and generous scientist, who has also become a true friend in my life. I would also like to extend my gratitude to my Co-supervisor, Dr. Jungkyu Choi for his suggestions and help throughout my study and work.

Secondly, I would like to thank my group mates, Matthew MacDonald, Iman Hashemi and Vincent. Aside from the immeasurable amount of support and help you have provided, you have made the lab and office more than just a work area, but an interesting place full of joy. Also, special thanks to the helpful and humorous technicians in CAPE, Stephen Hood, Leigh, Stephen Beuzenberg, Michael, Frank, Glenn and Tim, for all your help and support to my research work during both good and bad times.

Next, I have my warm gratitude to my friends in Christchurch, David Zhang, Jack Wu, Xing, Simon, Cheng Li and Yanjie. The life in New Zealand becomes very happy and colourful with you all around.

My deepest gratitude is extended to my family. It is more than just words to show how much I feel indebted to my parents, for giving me the opportunity to pursue my dream and happiness. Furthermore, I am especially grateful to have my wife Yvonne and my daughter Mona. This little family has become the source of my happiness, the strength behind all my work and the meaning of my whole life.

Last but not least, I am grateful to Royal Society of New Zealand for the financial support and to University of Canterbury for giving me the opportunity of PhD study in New Zealand.

ABSTRACT

Hydrogen based energy system is considered to be a promising solution to address the energy shortage and environment pollution issues. Due to the increasing demand of hydrogen, different processes have been developed to produce this useful molecule in an efficient and economical way, such as the water gas shift reaction (WGSR) which is one of the important approaches in industry at present. In the meantime, the by-product CO_2 generated in WGSR must be separated to produce the high purity product H_2 and to reduce the greenhouse gas emission. Membrane gas separation technology provides an environmental friendly and low cost solution to separate the mixture products in WGSR. Derived from the membrane technology, membrane reactor (MR) is an integrated unit by combining the heterogeneous catalysis and membrane separation process, which owns the instinct advantages of simplified facilities and improved productivity in many applications.

In this work, the objective is to develop a porous hybrid solid membrane reactor system for hydrogen production and separation in WGSR. Herein, zeolitic imidazolate framework-8 (ZIF-8) was firstly screened out from various proposed porous materials as the candidate membrane material of the MR for WGSR, since this new emerging material was a novel catalysts host and in the meantime the ZIF-8 membrane showed promising H_2/CO_2 and H_2/CO separation performance. Later on, the applicability of ZIF-8 material was firstly examined from the practical perspectives of catalyst and membrane under different environments. The results showed the stability of ZIF-8 strongly depends on the gas phase environment, whereas the ZIF-8 structure remained unchanged under inert atmosphere at 300 ℃ for 24 h. Subsequently, the ZIF-8 membrane was successfully fabricated with a simple polishing procedure which was developed to repair the defect membrane. The gas separation performance of the well-prepared ZIF-8 membrane was evaluated with respect to a simulated syngas stream in the presence and absence of steam. In addition, a synthesis method was developed for

a core-shell metal/ZIF-8 composite catalyst which consists of a ZIF-8 core incorporated with the metal nanoparticles and a ZIF-8 protect membranous layer formed from secondary crystallization. The catalyst exhibited high selectivity and anti-poisoning property in the alkenes hydrogenation reactions. Finally, WGSR were carried out in the conventional packed bed reactor and the ZIF-8 membrane based MR. MR advantages were demonstrated and the required improvement in MR development was discussed. This study concluded that the ZIF-8 membrane based MR could provide benefit on higher CO conversion and purified hydrogen in WGSR compared to the traditional packed bed reactor. However, the porous material ZIF-8 may have bright application future in the applications of catalysis and separation membrane under the mild conditions, although progress modification of the ZIF-8 structure is inevitable in the applications under harsh conditions, like MR for WGSR.

ABBREVIATIONS

Å	Angstroms
$\alpha_{i/j}$	Separation factor
CMR	Catalytic membrane reactor
FID	flame ionization detector
GC	gas chromatography
$GtCO_2$	Gigatonnes carbon dioxide
ΔH_{298}^{0}	Reaction enthalpy
H/C	Conversion ratio of 1-hexene to cis-cyclooctene
HTS	High temperature shift
Hmim	2-methylimidazole
Kp/ Keq	Equilibrium constant
LTS	Low temperature shift
MMbbl/d	Million barrels per day
Metal/MOF	In the structure and on the surface of MOF
Metal@MOF	Distributed throughout the structure of MOF
MOFs	Metal organic frameworks
MMM	Mixed-matrix membrane
PBR	Packed Bed Reactor
Stage cut	Permeate flow rate / Feed flow rate
SDA	Structure directing agents
SEM	Scanning electron microscopy
TGA	Thermo-gravimetric analysis

T	Absolute temperature
TEM	Transmission electron microscopy
TCD	Thermal conductivity detector
WGSR	Water gas shift reaction
wt%	Weight per cent
XRD	X-ray diffraction
x_i	Mole fraction of species i in the feed side
y_i	Mole fraction of species i in the permeate side
ZIFs	Zeolitic imidazolate frameworks
θ	X-ray diffraction angle of the peak

LIST OF TABLES

LIST OF FIGURES

Chapter 1
Introduction

Nowadays, an incredible huge amount of energy is consuming around the world because of the rapid population growth and industry development. The current extensive exhaustion of fossil fuel including oil and coal, will potentially lead the human beings to a serious energy and economic crisis in the future. Based on the projections of the International Energy Outlook 2014 prepared by U.S Energy Information Administration, the world liquid fuels consumption will increase by one third from 87 MMbbl/d in 2010 to 119 MMbbl/d in 2040, as shown in Figure 1.1, while the crude oil price will continuously increase by 100% till then [1]. In the meantime, the pollution emissions, especially the greenhouse gas CO_2, from the fossil fuel combustion is fearfully damaging the global environments and threatening the fragile ecological balance of the planet. According to the information provided by International Energy Agent, annul CO_2 emissions from fuel combustion have been up to 32 $GtCO_2$ in 2013 [2]. Hence, exploring the new energy source and improving the energy utilization efficiency is an extremely urgent mission we are facing at this moment.

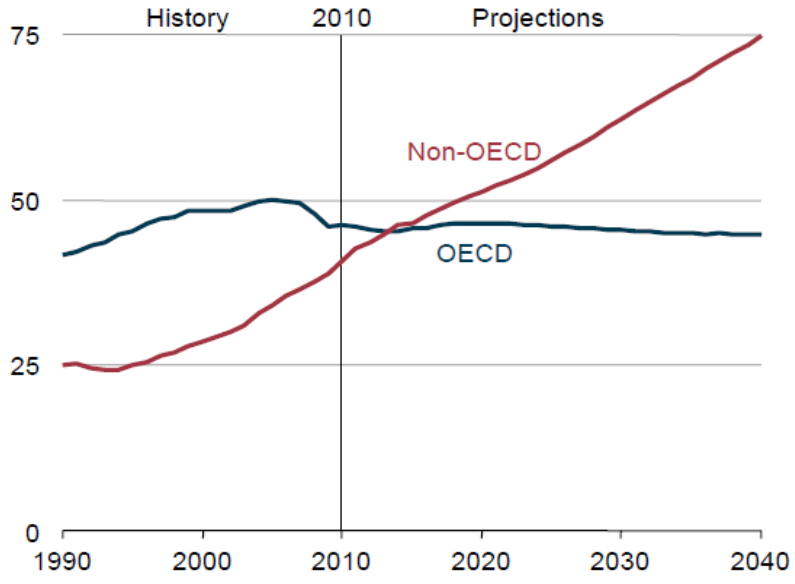

Figure 1.1 OECD and Non-OECD petroleum and other liquid fuels consumption, reference case, 1990-2040 (million barrels per day) [1].

Plenty forms of substitutable energies, including the solar energy, tide energy, wind energy, nuclear energy etc. have been extensively developed and applied to alternate the traditional fossil fuel energy system [3]. However, the utilizations of these alternative energies are strongly limited by timeliness and producing areas. Therefore, the development of the proper energy carrier is essential before these substitutable energies could be widely generalized. Among various possible energy carriers, hydrogen is the most promising fuel with the advantages of high energy density, environment friendly combustion emission, abundant resource as well as ease of distribution [4 - 9]. The physicochemical properties of hydrogen are listed in Table 1.1 and the Volumetric and gravimetric energy densities of common fuels are listed in Table 1.2.

Table 1.1 The physicochemical properties of hydrogen.

Atomic number	1	
Chemical formula of hydrogen molecular	H_2	
Molecular weight	2.02	g / mol
Density, at 101.33 kPa and 273.15 K	0.0899	g / L
Liquid Density, at 101.33 kPa and 273.15 K	70.97	g / L
Melting point, at 101.33 kPa	14.01	K
Boiling point, at 101.33 kPa	20.28	K
Kinetic diameter of hydrogen molecular	0.289	nm
Specific heat capacity, at 101.33 kPa and 298 K	14300	J / (kg K)

Table 1.2 Volumetric and gravimetric energy densities of common fuels. [10]

Materials	Energy per kilogram (MJ/kg)	Energy per liter (MJ/L)
Hydrogen (liquid)	143	10.1
Nature gas (liquid)	53.6	22.2
LPG propane	49.6	25.3
Gasoline (petrol)	46.4	34.2
Diesel	45.4	34.6

To date, hydrogen is largely utilized in the hydro cracking process in the petroleum industry, and consumed in the fertilizer synthesis, food industry and other areas [9, 11]. Most of the commercial hydrogen product is produced from the steam reforming reaction (SRR) of nature gas shown in Eq. 1-1 and coal gasification (CG) shown in Eq. 1-2 followed by water gas shift reaction (WGSR) shown in Eq. 1-3 [9, 12]. Herein, SRR is a strongly endothermic reaction and WGSR is an exothermic reversible catalytic reaction as the chemical equations listed below [13 - 15].

$$\mathrm{CH_4} + H_2O \leftrightarrow CO + 3H_2 \qquad \Delta H_{298}^0 = 206\ kJ/mol \qquad (1\text{-}1)$$

$$C + H_2O \leftrightarrow CO + H_2 \qquad \Delta H_{298}^0 = 131.3\ kJ/mol \qquad (1\text{-}2)$$

$$\mathrm{CO} + H_2O \leftrightarrow CO_2 + H_2 \qquad \Delta H_{298}^0 = -41.09\ kJ/mol \qquad (1\text{-}3)$$

In WGSR, the downstream mixture contains H_2, CO_2, the unreacted CO, water vapour and trace amount of sulphur-containing substances etc. The capture and separation of the main by-product CO_2 and unreacted CO are the critical step to produce the purified hydrogen and to eliminate the greenhouse gas emission in this process [9, 16, 17].

Compared to the traditional separation methods, membrane gas separation technology provides the benefits of low energy consumption, small footprint and environmental friendly properties [18 - 22]. Hence, membrane technology has attracted extensive researchers and engineers' interests on H_2 purification and CO_2 capture [9, 23 - 28]. The inorganic membranes, which have outstanding permeability and promising thermal/chemical stabilities are considered as the best candidates to utilize under the harsh application conditions, like in WGSR. Especially the microporous crystalline membranes, such as zeolite and metal organic frameworks (MOFs), are the most promising option for high temperature gas separation because of the excellent gas

separation performance with molecular sieve mechanism and the relative low price to other inorganic membranes [29 - 34] On the other hand, these microporous materials have been successfully functionalized with the incorporated nanoparticles in their pores, cavities or channels and these grafted nanoparticle/porous support composites have been proved of excellent catalysts in some reactions [35 - 38].

Hence, the concept of a porous hybrid solid catalytic membrane reactor system formed by combining the two distinct functions, gas separation and catalysis reaction, is a promising and meaningful solution for hydrogen production. In this study, the objectives are (1) to investigate and synthesis the appropriate microporous materials of the hybrid catalytic membrane for hydrogen production and separations, (2) to conduct research on the synthesis and characterizations of the porous gas separation membrane and the nanoparticles incorporated porous catalysts and (3) to carry out the WGSR with the integrated porous hybrid membrane reactor system. In conclusion, the aim of the study is to develop a solid membrane reactor system for WGSR with the new material for hydrogen production and separation.

This dissertation is filed and constructed with eight chapters. The brief descriptions of the chapters are listed below.

Chapter 1: A brief introduction of this study, including the motivations, the general backgrounds, aim of the thesis and the overview of the whole dissertation were explained in this chapter.

Chapter 2: The background knowledge of this study was reviewed. This chapter emphatically introduces the general information of water gas shift reaction, the development progress of the microporous materials, the utilization of the membrane technology and the fabrication and applications of membrane reactors.

Chapter 3: The fabrication methods and characterization results of various microporous materials were described in this chapter. After considering the gas separation and catalysis performance of the synthesized materials, zeolitic imidazolate framework-8 (ZIF-8) was selected as the raw material for the hybrid membrane reactor.

Chapter 4: Thermal stability of ZIF-8 under inert and oxidative environments from the practical perspective was evaluated. The synthesized ZIF-8 samples were firstly treated under various environments at different temperatures and then characterized with x-ray diffraction (XRD) and scanning electron microscopy (SEM). Later on, the ZIF-8 thermal behaviour analysis was conducted with thermo-gravimetric analysis (TGA). Finally, hydrogen reduction and CO oxidation of Au/ZIF-8 was performed to verify the structure stability.

Chapter 5: The synthesis method of the well-integrated ZIF-8 membrane and the repair procedure to avoid undesired membrane defects were presented in this chapter. The gas separation performance of the well-prepared ZIF-8 membrane with respect to a simulated syngas (50% H_2, 25% CO_2 and 25% CO) in the presence and absence of steam were investigated. The thermal stability on the use of ZIF-8 membrane for H_2 separation under wet conditions was also examined.

Chapter 6: The performance of the ZIF-8 based membrane reactor for water gas shift reaction was demonstrated. The improvements of WGSR conducted with the membrane reactor compared to traditional packed bed were presented. The limitation of employing ZIF-8 membrane reactor in WGSR was highlighted.

Chapter 7: A synthesis method for core-shell metal/ZIF-8 composite was reported in this chapter. Subsequently, the selective catalytic performance of the prepared

composites in the hydrogenation reaction was characterized. Furthermore, the anti-poisoning property of the synthesized catalysts was demonstrated.

Chapter 8: The key findings of this study were concluded and the future study was proposed.

Reference

[1] J. Conti, P. Holtberg, S. Napolitano, A.M. Schaal, International Energy Outlook 2014: World Petroleum and Other Liquid Fuels, U.S. Energy Information Administration, Washington, 2014.

[2] F. Birol, CO2 emissions from fuel combustion highlights (2015 edition), International Energy Agency, France, 2015.

[3] M. Jefferson, Sustainable energy development: performance and prospects, renew energy 31(2006) 571-582

[4] C.J. Winter, J. Nitsch, Hydrogen as an energy carrier, Springer-Verlag New York Inc., New York, NY, 1988

[5] F. Barbir, Transition to renewable energy systems with hydrogen as an energy carrier, Energy, 34(3) (2009) 308-312

[6] G. Cipriani, V.D. Dio, F. Genduso, D.L. Cascia, R. Liga, R. Miceli, Perspective on hydrogen energy carrier and its automotive applications, Int. J. Hydrogen. Energ., 39(16) (2014) 8482-8494

[7] T.N. Vezirolu, F. Barbir, Hydrogen: the wonder fuel, Int. J. Hydrogen. Energ., 17(6) (1992) 391-404

[8] B. Sorensen, Hydrogen and Fuel Cells Emerging Technologies and Applications, Elsevier, Oxford, UK, 2005

[9] T. Yang, T.S. Chung, High performance ZIF-8/PBI nanocomposite membranesfor high temperature hydrogen separation consisting of carbon monoxide and water vapor, Int. J. Hydrogen. Energy. 38(2013) 229-239

[10] K. Mazloomi, C. Gomes, Hydrogen as an energy carrier: Prospects and challenges, Renew. Sust. Energy. Rew. 16(2012) 3024-3033

[11] M.Momirlan, T.N.Veziroglu, The properties of hydrogen as fuel tomorrow in sustainable energy system for a cleaner planet. Int J Hydrogen Energy, 30(2005) 795-802

[12] M.Momirlan, T.N.Veziroglu, Current status of hydrogen energy, Renew Sust. Energ. Rev, 6(2002) 141-179

[13] B.R.J. Smith, M. Loganathan. M.S. Shantha, A Review of the Water Gas Shift Reaction Kinetics, Int. J. Chem. React. Eng. 8(2010) R4

[14] C. Ratnasamy, J.P. Wagner, Water Gas Shift Catalysis, Catal. Rew. 51(2009) 325-440

[15] C. Wheeler, A. Jhalani, E.J. Klein, S. Tummala, L.D. Schmidt, The water-gas-shift reaction at short contact times, J. Catal. 223(2004) 191-199.

[16] T.C. Merkel, M. Zhou, R.W. Baker, Carbon dioxide capture with membranes at an IGCC power plant. J. Membr. Sci 389(2012) 441-450.

[17] S.S. Hla, Y. Sun, G.J. Duffy, L.D. Morpeth, A. Ilyushechkin, A. Cousins, D.G. Roberts, J.H. Edwards, Kinetics of the water-gas shift reaction over a La0.7Ce0.2FeO3 perovskite-like catalyst using simulated coal-derived syngas at high temperature, Int. J Hydrogen. Energy., 30(2005) 795-802

[18] P. Bernardo, E.Drioli, G.Golemme. Membrane gas separation:a review/state of the art. Ind. Eng. Chem. Res 48(2009) 4638-4663

[19] H. Strathmann, Membrane separation process: Current relevance and future opportunities, AIChE Journal. 47(2001) 1077-1087

[20] Y. Yampolskii, B.D. Freeman, Membrane Gas Separation, WILEY, 2010

[21] J. Shi, Q. Yuan, C.K. Gao, Membrane technology handbook, Chemical Industry Press, Beijing, 2000.

[22] R.W. Baker, Membrane separation system: recent development and future direction, Noyes Data Corporation Park Ridge, New Jersey USA. 1991

[23] S. Adhikari, S. Fernando, Hydrogen membrane separation technology, Ind. Eng. Chem. Res., 45(3)(2006) 875-881

[24] S.J. Lee, S.M. Yang, S.B. Park, Synthesis of Palladium Impregnated Alumina Membrane for Hydrogen Separation, J. Membr. Sci., 96(3)(1994) 223-232

[25] J. Fan, H. Ohya, T. Suga, H. Ohashi, K. Yamashita, S. Tsuchiya, M. Aihara, T. Takeuchi, Y. Negishi, High flux zirconia composite membrane for

hydrogen separation at elevated temperature, J. Membr. Sci., 170(1)(2000) 113-125

[26] S. Lu, B.T. Low, .T.S. Chung, A.R. Greenberg, Polymeric membranes for the hydrogen economy: Contemporary approaches and prospects for the future, J. Membr. Sci., 327(1-2)(2009) 18-31

[27] F.Y. Li, Y.C. Xiao, O.Y. Kang, T.S. Chung, UV-Rearranged PIM-1 Polymeric Membrane for Advanced Hydrogen Purification and Production, Adv. Energy. Mater. 2(12)(2012) 1456-1466.

[28] S. Yun, S.T. Oyama, Correlations in palladium membranes for hydrogen separation: A review, J. Membr. Sci., 375(1-2)(2011) 28-45

[29] H. Wang, Y.S. Lin, Synthesis and modification of ZSM-5/silicalite bilayer membrane with improved hydrogen separation performance, J. Membr. Sci., 396(2012) 128-137

[30] M. Hong, J.L. Falconer, R.D. Noble, Modification of Zeolite Membranes for H_2 Separation by Catalytic Cracking of Methyldiethoxysilane, Ind. Eng. Chem. Res., 44(11)(2005) 4035-4041

[31] S. Battersby, M.C. Duke, S. Liu, V. Rudolph, J.C.D.D. Costa, Metal doped silica membrane reacto: operational effects of reaction and permeation for water gas shift reaction, J. Membr. Sci., 316(1-2)(2008) 46-52

[32] Y. Li, F. Liang, H. Bux, W. Yang, J. Caro, Zeolitic imidazolate framework ZIF-7 based molecular sieve membrane for hydrogen separation, J. Membr. Sci., 354(2010) 48-54

[33] Y. Pan, B. Wang, Z. Lai, Synthesis of ceramic hollow fiber supported zeolitic imidazolate framework-8 (ZIF-8) membranes with high hydrogen permeability, J. Membr. Sci., 421-422(2012) 292-298

[34] Z. Xie, J. Yang, J. Wang, J. Bai, H. Yin, B. Yuan, J. Lu, Y. Zhang, L. Zhou, C. Duan, Deposition of chemically modified α-Al2O3 particles for high performance ZIF-8 membrane on a macroporous tube, Chem. Commun., 48(2012) 5911-5989

[35] A. Corma, H. Garcia and F.X.L.i. Xamena, Engineering Metal Organic Frameworks for Heterogeneous Catalysis, Chem. Rev., 110(2010) 4606-4655.

[36] M. Meilikhov, K. Yusenko, D. Esken, S. Turner, G.V. Tendoloo and R.A. Fischer, Metals@MOFs– loading MOFs with Metal Nanoparticles for Hybrid Functions, Eur. J. Inorg. Chem., 24(2010) 3701-3714

[37] L.Y. Chen, H.R. Chen, R. Luque and Y.W. Li, Metal-organic framework encapsulated Pd nanoparticles: towards advanced heterogeneous catalysts, Chem. Sci., 5(2014) 3708-3714.

[38] P.Z. Li, K. Aranishi and Q. Xu, ZIF-8 immobilized nickel nanoparticles: highly effective catalysts for hydrogen generation from hydrolysis of ammonia borane, Chem. Commun., 48(2012). 3173-3175

Chapter 2
Literature Review

2.1 Water Gas Shift Reaction (WGSR)

2.1.1 General Information

Water gas shift reaction (WGSR) is a traditional chemical process which has been employed to produce hydrogen from the hydrocarbons since hundred years ago [1 - 4]. While, the produced hydrogen is conventionally used in the fertilizer industry, petroleum industry, food industry, the power generation and transportation technology which is rapidly developed in recent years. At present, WGSR is still employed widely for the decarburization of fuel gas and adjusting the CO/H_2 ratio to conduct the syngas which is generated from gasification [5]. Nowadays, WGSR is also found emerging significant application in fuel cell processing and has attracted extensive research attention again [4, 6 - 8]

WGSR is taken place from CO and steam to produce CO_2 and H_2 under the catalyst environment, as Eq. 1-3 expressed. The equation shows WGSR is an exothermic reversible reaction, which means the equilibrium constant of the reaction would decrease with increasing the reaction temperature, as shown in Figure 2.1. In the meantime, the high reaction temperature is still kinetically favourable for the fast reaction rate in WGSR. Therefore, the reaction temperature is a trade-off factor between kinetics and thermodynamics in WGSR [9 - 11] Meanwhile, the pressure would not seriously influence the reaction equilibrium theoretically because there is no volume difference before and after the reaction [1, 3].

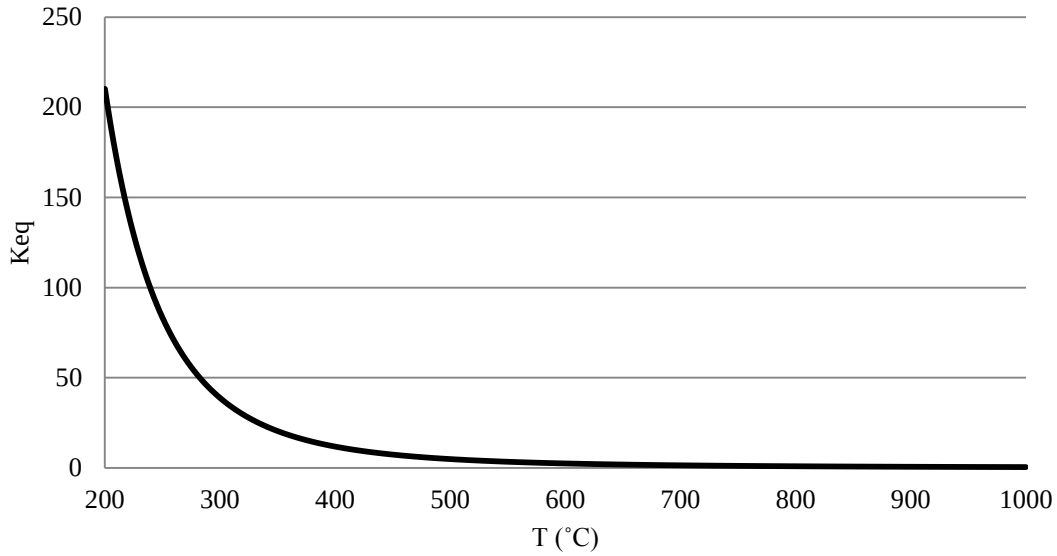

Figure 2.1 Equilibrium constant of WGSR as the function of temperature. It is derived from the experienced equation Kp=exp[((4577.8)/T)-4.33] [3].

In order to obtain the high CO conversion while maintaining the reaction rates, the industrial WGSR is always conducted with a series of adiabatic steps, normally combined with high temperature shift (HTS) and low temperature shift (LTS). Practically, the effluent gas including around 3-5% of CO from the high reaction rate step, which is the HTS (350˚C-550˚C), is then introduced to the LTS (190˚C-250˚C), under which step is the thermodynamic favor conditions, the purer hydrogen and higher CO conversion (up to 99.7%) could be achieved then [1 - 4].

2.1.2 Water Gas Shift Catalysts

As aforementioned, the industrial WGSR is normally carried out in two steps: high temperature shift and low temperature shift. Correspondingly, the catalysts utilized in the two steps, HTS and LTS are different: where Fe-based catalysts for the HTS and Cu-based catalysts for the LTS [2, 3].

High temperature shift and Fe-based catalysts

Fe_2O_3-Cr_2O_3 is the conventional catalyst for HTS and has been commercialized for over 60 years. The HTS catalyst was named Fe-based or iron-chromium catalyst because their main compositions are iron and chromium. Normally, these iron-chromium oxide catalysts contain 80-90 wt% Fe_2O_3, 10 wt% Cr_2O_3 with little amount of MgO, CuO and other remaining volatiles, whereas the chromium in the catalyst plays the role of the stabilizer for iron oxide crystallites and the structure promoter to enhance the catalytic activity [12 - 16]. In some cases, the HTS catalysts could be deactivated by thermal sintering and chemical deposition on the catalysts surface. Hence, in order to protect the catalyst, the inlet temperature in HTS is always maintained around 350˚C, while the temperature would increase along the reactor and can reach 550˚C maximally at the end of the reactor. On the other hand, it is important to control the space velocity at around 3-9 seconds and to operate at a reasonable steam to CO ratio in HTS [2, 17]. A higher steam/CO ratio in HTS leads to a higher CO conversion of around 97%, but higher cost in the same time, whereas the lower steam/CO ratio would cause coke formation, methanation and Fischer-Tropsch reactions, these possible side reactions are listed in Table 2.1 [10, 18, 19].

Table 2.1 Possible undesired side reactions of HTS under low steam/CO ratio [19].

$2CO \leftrightarrow C + CO_2$
$CO + H_2 \leftrightarrow C + H_2O$
$CO + 3H_2 \leftrightarrow CH_4 + H_2O$
$4CO + 2H_2O \leftrightarrow CH_4 + 3CO_2$
$CO_2 + 2H_2 \leftrightarrow C + 2H_2O$
$CO_2 + 4H_2 \leftrightarrow CH_4 + 2H_2O$
$C + 2H_2 \leftrightarrow CH_4$

Low temperature shift and Cu-based catalysts

$ZnO\text{-}CuO\text{-}Al_2O_3$ is customarily employed as the LTS catalyst with certain compositional concentrations. The typical industrial LTS catalysts are composted of 32-33 wt% ZnO, 34-53 wt% CuO and 15-33 wt% Al_2O_3. The copper acts as the active species in the catalyst, while ZnO provides the catalyst support and Al_2O_3 is almost inactive [2, 3, 20 - 23]. Since WGSR is thermodynamically favored at lower temperature, the CO concentration could be reduced to lower than 0.1% after LTS carried out at the temperature lower than 300˚C. However, the serious concern of LTS is the catalyst deactivation during the practical operation, which is caused by the thermal sintering [24] and the sulphur poisoning [2, 25]. Herein, the anti-poisoning catalyst is highly desired in WGSR and ZnO applied in the LTS catalyst could act to protect the Cu catalyst [24].

Noble metal catalysts

Due to the inherent limitation of the existing commercial WGSR catalysts, the noble metal catalysts, including Pt group-based catalysts and Au-based catalysts have been developed in order to meet the specific requirements in fuel cell applications [1, 26 - 29]. Wheeler et al compared the catalytic performance of these noble metals in WGSR and found the catalytic activities are in the order of Ni>Ru>Rh>Pt>Pd. These Pt group-based catalysts are quite active at the temperature of 250-400 ˚C and have a better tolerance to the poisoning substance which is highly desired for fuel cell [1, 28]. In the past 10 years, the gold catalyst has attracted many research interests since the extraordinary activity of the support Au was found for CO oxidation [30]. In the meantime, the Au-based catalysts were also found with excellent catalytic activities in WGSR, especially in the LTS temperature range of 180-250 ˚C, as shown in Figure 2.2 [31]. Again, the Au particle size and dispersion were also reported seriously affecting the catalytic activity in WGSR. Hence, the particle size control plays a

crucial role during the Au-based catalysts preparation [27]. However, the high price of the noble metals limits the applications of these catalysts and most of the employed noble metal catalysts were in the forms of deposited on partially reducible oxides, like TiO_2, iron oxides and mixed oxides [27 - 30].

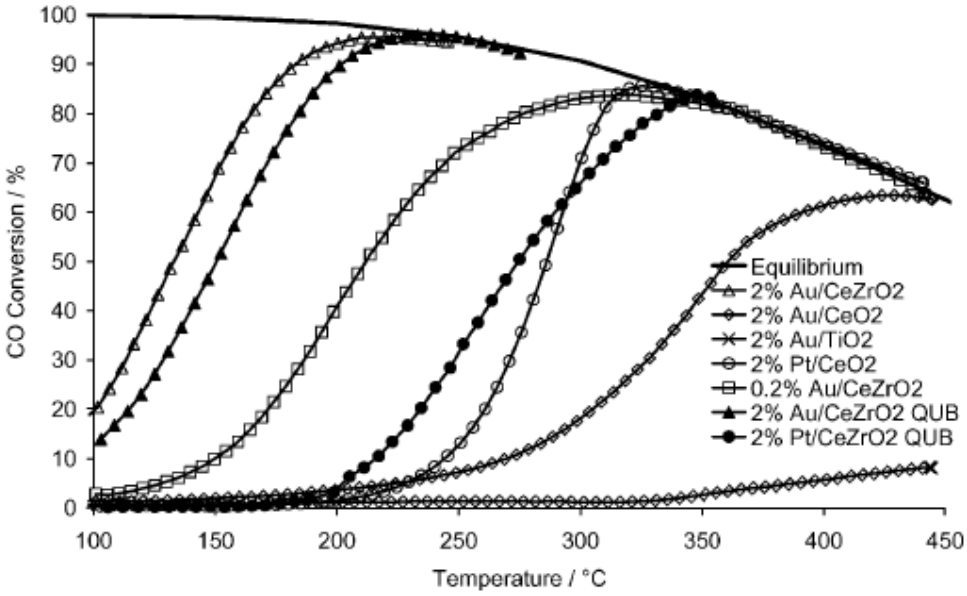

Figure 2.2 CO conversion in WGSR over Pt-group and Au based catalysts [31].

2.2 Microporous Materials – Zeolites and Metal organic frameworks (MOFs)

2.2.1 Zeolites

In 1756, the first zeolites were found by the Swedish mineralogist Cronstedt. He called these mineral materials with the Greek word "zeolites" which literally means "boiling stone" [32]. However, the first artificial synthesized zeolites were not developed until 1800s' and the systematic study of zeolite was actually started from 20^{th} century when many various zeolite structures were found and applied in industries since then [33].

The definition of zeolite is the crystalline, microporous aluminosilicates with 3D structure complex. The general formula of zeolite is $(SiO_2)_x(AlO_2)_yzMO_xaH_2O$, which implies the zeolite compositions primarily includes silicate, alumina and other elements such as sodium, manganese, titanium etc. [33]. Till now, there are 229 unique zeolite frameworks have been identified, and over 40 naturally occurring zeolite frameworks are known [34]. The most common zeolite structures are framework type A (LTA), framework type Y (FAU), framework type P (NaP-GIS) and framework type MFI (ZSM-5, silicate-1, TS-1) as shown in Figure 2.3 [34].

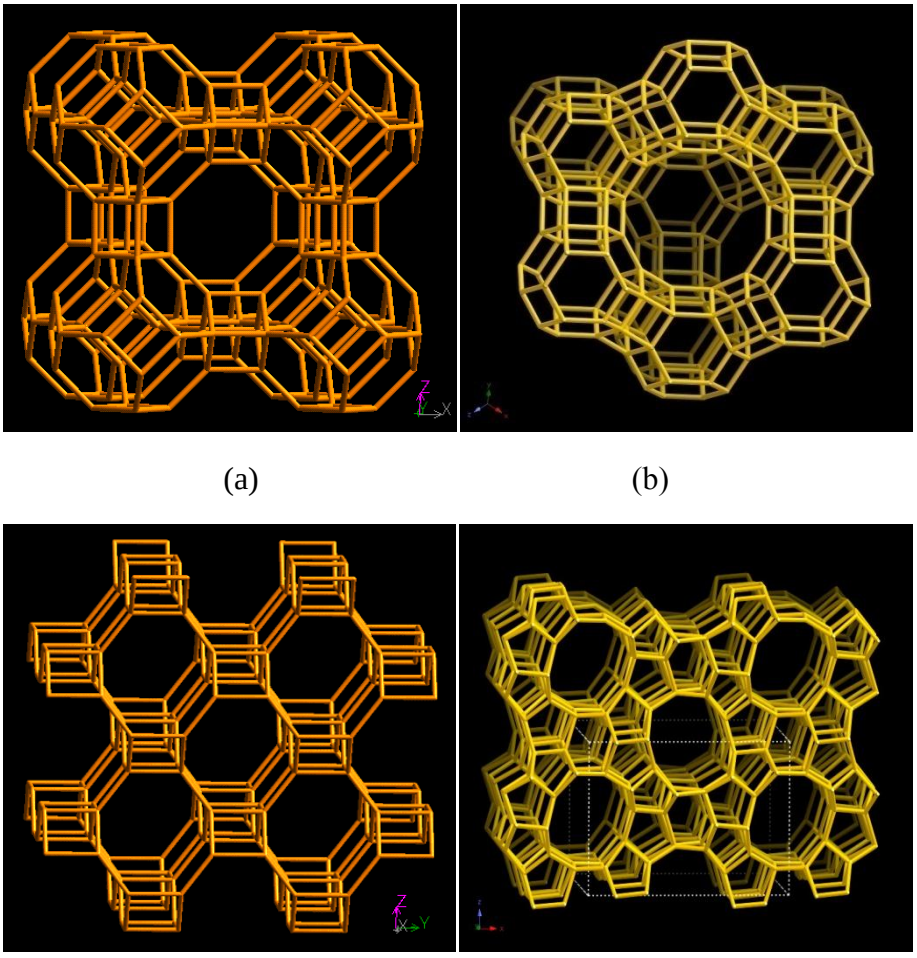

(a) (b)

(c) (d)

Figure 2.3 The frame structures of the most common zeolites; (a) LTA, (b) FAU, (c) GIS and (d) MFI[34].

Generally, the laboratory synthesis of zeolites is carried out by hydrothermal methods. In which approach, the desired amount of silica source, aluminum source, alkali and other demanded components are mixed in the autoclave and heated in the auto-generated pressure. The organic structure directing agents (SDA) plays an important role of controlling the formations of the zeolite frameworks since the first crystallization always happens around these organic templates. Herein, the synthesis temperature is always limited to the decomposition point of the organic template and the stirring is also an important factor in some zeolite synthesis procedures [33, 35, 36].

Zeolites are widely used in chemical industry due to their promising pore structures and the thermal and chemical stabilities. Firstly, zeolite is the valuable commercial catalysts/catalyst hosts for many important reactions in oil and gas industries [37, 38]. In addition, zeolite membranes are considered a promising solution for the energy efficient separation of gas and solutions [39 - 41]. Especially for the LTA, MFI and FAU membranes, with the suitable pore sizes to separate many important molecular pairs, have been extensively studied in the past decades. Furthermore, zeolites are also found important applications in the industries of adsorption, sensor and hydrogen storage etc. [42 - 44].

NaP zeolite – GIS

NaP zeolite has a gismondine (GIS) – like frameworks with the intersecting channels of 0.31×0.45 nm and 0.28×0.48 nm in the directions of [100] and [010], respectively, as shown in Figure 2.4 [34]. The eight-ring structured channels with the micro-size pores enable NaP – GIS zeolite to separate the small gas molecular pairs, like hydrogen and helium [45]. In addition, it is also used as the extraction detergent to remove and immobilize the toxic elements, heavy metals and ammoniums from the waste spices [46].

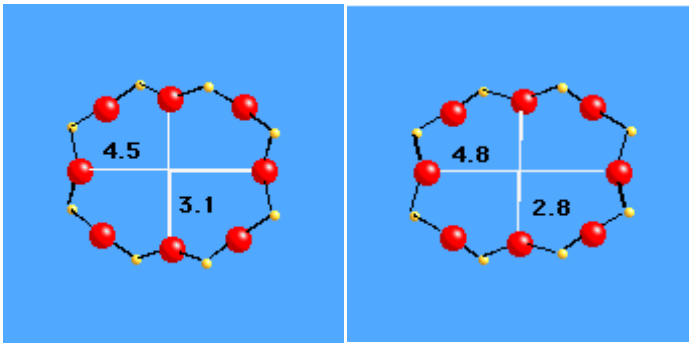

Figure 2.4 The pore profile of NaP-GIS zeolite in Angstroms [34].

Several publications could be found about the studies of the NaP - GIS zeolite synthesis and applications. Mouhtaris et al. reported their synthesized NaP - GIS from sulphocalcic lignite fly ash, however impurities were found in their products [47]. Albert et al. successfully synthesized highly crystallized NaP - GIS zeolite with the low silica compositions [48]. Sharma et al. synthesized a knobby surfaced NaP – GIS zeolite and evaluated hydrogen adsorption ability of the synthesized samples [49]. Dong et al. fabricated the NaP – GIS gas separation membrane through the in-situ hydrothermal method on a porous α-alumina support and examined hydrogen separation performance of the membrane [45]. Huo et al. evaluated the thermal stability of the NaP – GIS zeolite and found the zeolite structure would convert to phillipsite phase after high temperature treatment [50].

MFI zeolite

In MFI structure, there are two intersecting ten-ring pores, with the dimensions of 0.51×0.55 nm and 0.53×0.56 nm in the directions of [100] and [010] respectively, as shown in Figure 2.5 [34]. The two most important MFI zeolites are ZSM-5 and Silicate-1. ZSM-5, abbreviation of Zeolite Socony Mobil-5 was first developed by Mobil Oil Company as a heterogeneous catalyst in petroleum industry in 1975 [51], while Silicate-1 is an alumina free MFI molecular sieve structure [52]. The MFI zeolites are outstanding catalysts in many reactions by utilizing their catalytic

activities and molecular sieve screening abilities, especially in the hydrocarbon isomerization reactions [53, 54]. In addition, the MFI zeolite membrane becomes very popular for gas separation because of the thermal stability and suitable pore size of the framework [10, 39, 41, 55 - 57].

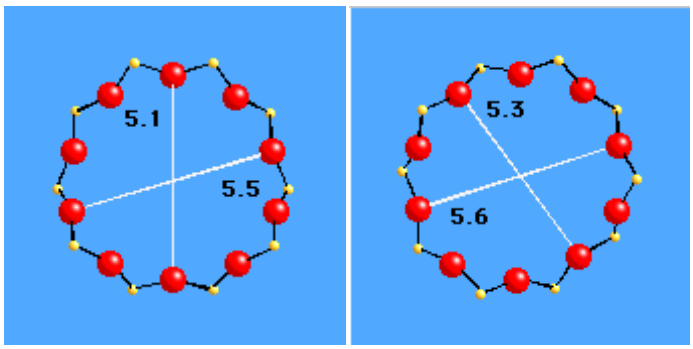

Figure 2.5 The pore profile of MFI zeolite in Angstroms [34].

Many works have been conducted towards the MFI zeolite synthesis and applications. Young et al. used ZSM-5 catalysts for selective xylene isomerization reaction in early 1980s' [54]. Besides, many ZSM-5 supported metal catalysts were prepared for various selective catalytic processes, including the propane dehydrogenation [58], benzene methylation [59] and steam reforming [60] etc. Aside from catalysts, Vos et al. reported their works on fabricating silica membrane for gas separation, and later on they further reported their methods to improve the performance of this hydrophobic MFI zeolite membrane [61, 62]. Gas separation ZSM-5 membrane was fabricated and modified with chemical crack deposition method to promote the performance for hydrogen purifications [63]. The ZSM-5 based membrane reactor for WGSR showed considerable and stable performance under the harsh reaction conditions [64].

2.2.2 Metal Organic Frameworks - MOFs

Metal organic framework (MOF), is defined as the crystals composite with the ionic nods netted by the organic ligands. The solids which are classified as MOFs usually

possess the inherent properties like incredible high surface areas (>3000 m^2/g), nano-porosity with tunable structures, varieties of pore sizes and topologies as well as robustness with strong bonding etc. [65 - 70]. A specific MOF geometrical structure could be designed by decorating with different ligands, ionic nods and sorts of connecting methods, as shown in Figure **2.6** [71]. Diverse MOF materials have been identified since the first prototype MOF-5 was developed a decade ago, while numbers of MOFs have already been commercialized in the market, such as Zeolitic imidazolate framework-8 (ZIF-8) [66]. Although MOFs have not been extensively used in industry yet because of the high production cost [68], the bright future of the materials has been widely accepted considering their outstanding properties and application potentials.

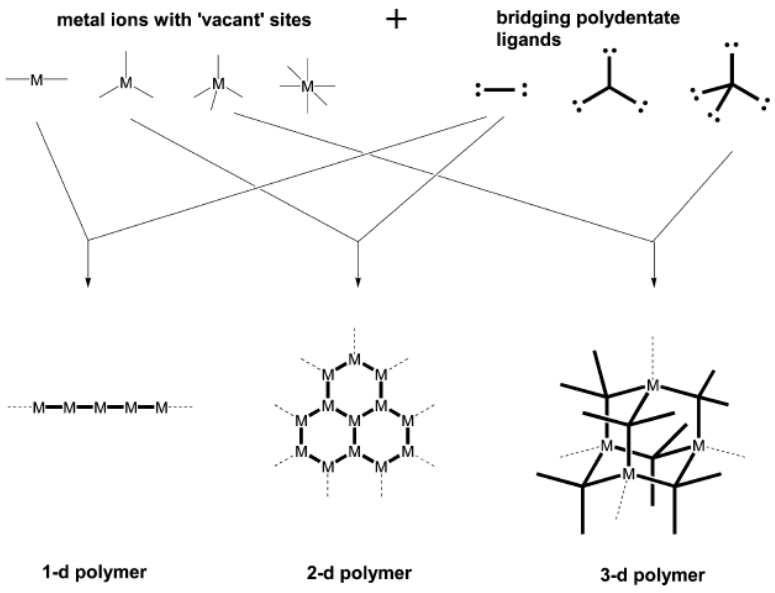

Figure 2.6 The schematic diagram of MOF formation [71].

Many research efforts have been made on MOF development in past years, and in the meantime many new MOF are continuously emerging for various interesting industrial applications. Currently, many methods, including conventional hydrothermal synthesis, microwave-assisted synthesis, electrochemical synthesis,

mechano-chemical synthesis and sono-chemical synthesis etc. have been employed for MOF synthesis [67]. Except for the common synthesis aspects like temperature, pH and pressure, the factors such as adding mineralizers, precursors, solvent and insolvent directing agents etc. are also considered in the synthesis process in order to obtain the specific structures [72]. For example, different conditions have been used, through conventional synthesis or microwave synthesis, with or without additives of sodium formate and from different ionic resources ($ZnCl_2$ or $Zn(NO_3)_2$), to synthesis ZIF-8 particles and films, . The result shows that these changes would dramatically affect the ZIF-8 crystallinity, morphology and thermal stability [73, 74]. Hence, an appropriate synthesis method is essential to produce the reliable MOF product for a specific application. Stock and Biswas reviewed the developed synthesis methods and the influencing factors in MOF synthesis process [72].

Nowadays, MOF materials are extensively studied in the application areas of separation and adsorption, catalysis, hydrogen storage, drug delivery, optical application and sensors etc. Benefits from the adjustable pore sizes, some MOF materials were utilized to fabricate the molecular sieve membrane for gas and liquid separations [75, 76]. In addition, MOF nanoparticles could be incorporated to polymeric membrane to form the mixed-matrix membrane (MMM) with the enhanced adsorption and molecular filtration [77]. Likewise, MOF solids are also considered as the remarkable catalyst materials. On one hand, the metal nods and the organic ligands in MOF structures could act as the catalysts in some reactions. On the other hand, MOF could also be employed as the catalyst support deposited with other catalytic elements in its cavities so as to improve the catalytic performance [78, 79]. As shown in Figure 2.7, there are roughly three states that the catalyst particles deposited on/in the MOF microstructures. In the states of Metal/MOF as shown in Figure 2.7a, the deposited particles are larger than the cavity of the structure and attached on the surface of the MOF pores. Figure 2.7b and Figure 2.7c are defined as Metal@MOF, in which particles are distributed throughout the structure, while larger

particles with a broad dimension distribution in structure (b) and the particles well isolated in the pore frames with the narrow dimension distributions in structure (c). The formation of these states could be seriously affected by the loading methods, including chemical vapor deposition, solution impregnation, solid grinding and encapsulation etc. [80, 81].

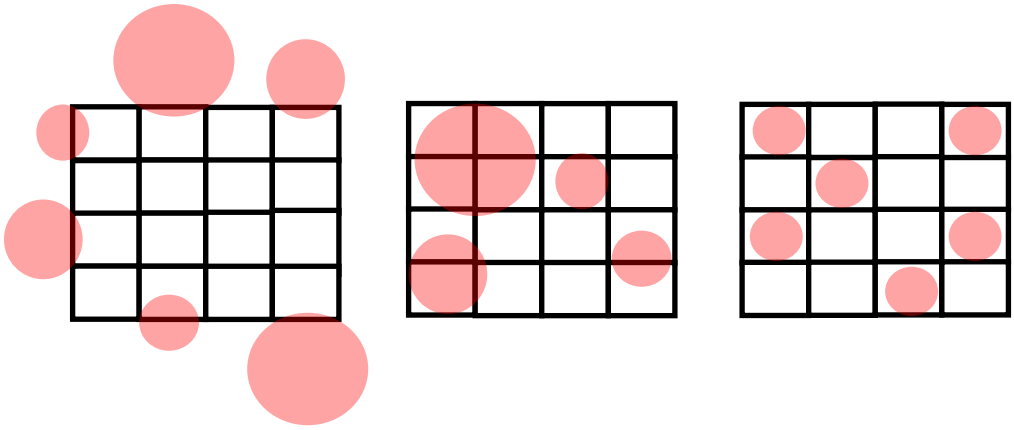

Figure 2.7 States of the ionic catalyst particles in MOF structure, (a) Metal/MOF and (b) & (c) Metal@MOF [80].

Zeolitic Imidazolate Frameworks – ZIFs

Despite many MOF materials are reported very stable and robust under many conditions, their structure stabilities are still very sensitive to high polar solvent, acid and hydrothermal treatment, and this instability limits the viability of MOF materials in many chemical industrial applications. Zeolites, by contact, are more stable than MOF materials under harsh conditions benefit from their tetrahedral $Si(Al)O_4$ covalent bonds in the frames. Herein, the MOF material which owns better stability with the zeolite-like Si (Al)-O-Si (Al) structure is highly desired. Zeolitic imidazolate frameworks (ZIFs) materials, a subclass of MOFs, are composed with the transition metals linked by the imidazolate (IM) bridging ligands. Coincidently, the M-IM-M

bond angel in ZIF structure is 145 º, the same with the angle of Si (Al)-O-Si (Al) in zeolite frames. By owning this zeolite structure similarity, ZIF materials were found to be exceptional chemical and solvent stability [82]. Aside from the robustness, ZIF also have the general property advantages of most MOF materials, like high surface area and the tunable structures. Up to now, over 150 ZIF structures have been developed with variety numbers of zeolite-like topologies. Some of the representative ZIF structures are shown in Figure 2.8 [83].

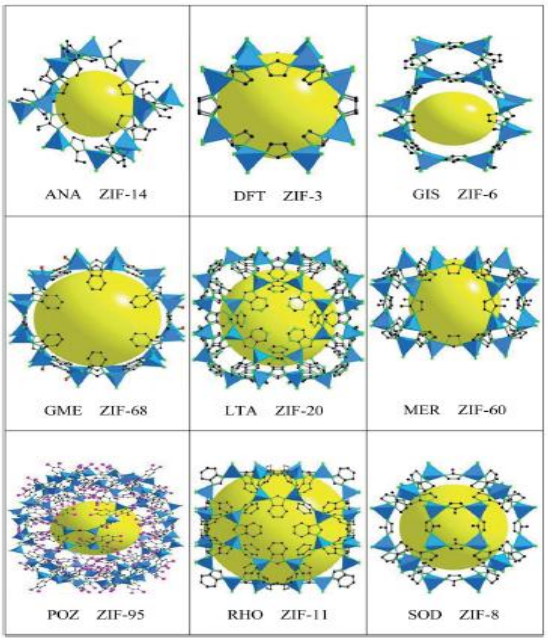

Figure 2.8 Representative ZIF crystal structures [83].

The inherent properties enable ZIF materials a promising candidate for many applications, like separation and adsorption, catalysis and drug delivery etc. Among these applications, separation membrane and catalysis are considered the most promising utilizations of ZIF materials. Many ZIF membranes have been developed through different synthesis methods and been employed for gas and liquid separation [84, 85]. Herein, ZIF-7 and ZIF-8 are the most studied for gas separation membrane, especially for H_2 purification and propylene/propane separation [86, 87]. ZIF material based catalysts were synthesized and used in many important reactions. For examples,

Wang et al. reported an encapsulation strategy for incorporating platinum (Pt) nanoparticles within the matrix of ZIF-8 and the catalytic performance of this Pt/ZIF-8 was examined in alkene hydrogenation reaction [88]. Jiang et al. reported a simple grinding method for depositing gold (Au) nanoparticles onto ZIF-8, and this Au/ZIF-8 composite exhibited an outstanding catalytic performance in the CO oxidation reaction [89]. Li et al. prepared the nickel/ZIF-8 composite by chemical vapor deposition method and the catalyst was employed in hydrolysis reaction of ammonia borane [90]. The TEM images of their metal/ZIF samples are shown in Figure 2.9.

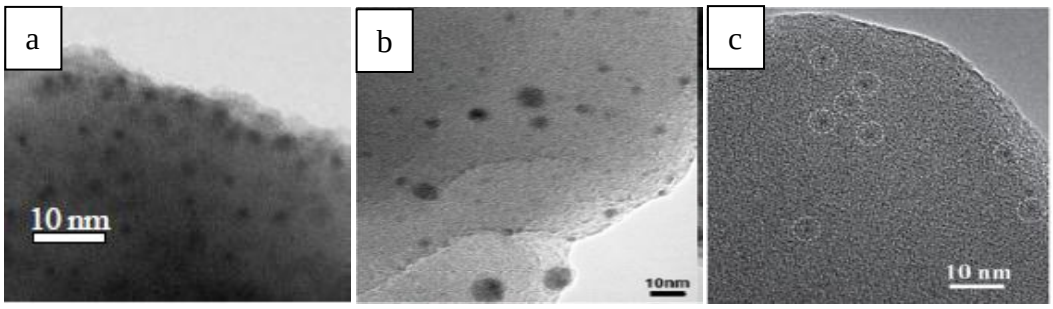

Figure 2.9 TEM images of some metal/ZIF catalyst samples; (a) Pt/ZIF-8 [88], (b) gold/ZIF-8 [89] and (c) Ni/ZIF-8 [90].

2.3 Gas Separation Membrane

2.3.1 General Information

A membrane is a layer of material which serves as a selective barrier between two phases and remains impermeable to specific particles, molecules, or substances when they exposed to the action of a driving force. Some components are allowed passing through the membrane into a permeate stream, whereas others are retained by it and accumulate in the retentate side [91, 92]. Nowadays, membrane technology is wildly employed in diverse application fields, including water treatment, bio-filtration, oil and gas industry and agriculture etc. [93]. Gas separation membrane technology is gradually developing and spreading in gas industry because of the operation

simplicity and less energy demand etc. comparing to the conventional gas separation methods, like pressure swing adsorption and cryogenic distillation. The estimate market for gas separation membrane is growing very quickly of around 15% annually and roughly utilized in the application fields of nitrogen generator, carbon dioxide capture, hydrogen recovery and vapor removal [94].

The gas permeation process in different membrane is controlled by different mechanism, including Knudsen diffusion, molecular Sieving, solution-diffusion, surface diffusion and capillary condensation etc., where the molecular sieving and solution diffusion mechanism are the most common mechanism in applications. As shown in Figure 2.10a, gas molecular is separated by their molecular size over the nano-scale membrane pores through molecular sieving mechanism, which is the dominant mechanism for inorganic membrane. However, gas separation process in most dense polymeric membranes is dominated by solution-diffusion mechanism which is based on the different solubility and diffusivity of the gas molecules in polymer chain as shown in Figure 2.10b [93].

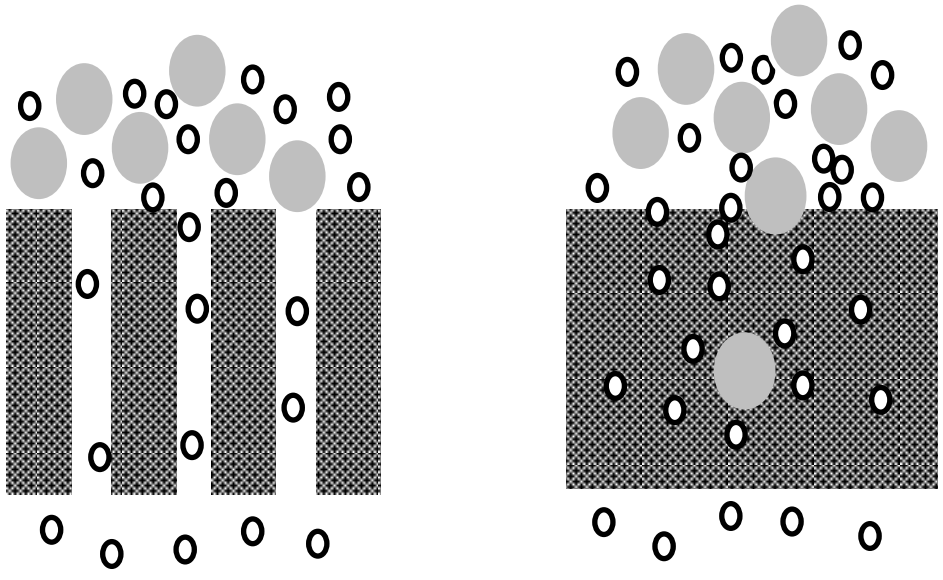

(a) Molecular sieving (b) Solution diffusion

Figure 2.10 Schematic diagram of (a) molecular sieving and (b) solution-diffusion mechanism.

In general, membrane could be divided into two categories by configuration, symmetric membrane and asymmetric membrane. The symmetric membrane is formed uniformly in the cross-section whereas the asymmetric membrane is usually combined with a thin, dense layer acts as the selective layer on top and a thick, porous layer as the bottom support. In addition, membrane could be categorized to nature membrane and synthetic membrane by materials, where the synthetic membrane is further divided into inorganic membrane and polymeric membrane. Generally, the polymer materials are more flexible and easier to form membrane into different patterns comparing to the inorganic materials. However, most of the polymeric membrane's application is seriously limited by the thermal instability and low permeability. Mixed-matrix membranes (MMM) have been developed by mixing the inorganic materials into the polymeric matrix to improve the separation factor and permeability. MMM is a practical product because it composites the advantages of the two materials. Nevertheless, it seems that more aspects need to be considered during their fabrication process. It is also important to note that the selection of the membrane material and formation strongly depends on the application and practical environments in the specific industry [95].

Since the first membrane was found by Nollet in 1748, this technology has been studied for more than 200 years, from tiny lab scale test to very large industrial scale applications. Today, many of these industrial applications process hundreds of square meters membrane area to meet the permeation and separation requirements. Hence, it is necessary to incorporate this large amount of membrane to an easy-handled packed membrane module. Correspondingly, several of membrane module appearances have been launched to meet the market demands, including the plate and frame module, tubular module, capillary module, spiral wound module and hollow fiber module. Each of the appearance has their unique features and shortages when applied in practical sites, as summarized in Table 2.2, whereas the hollow fiber module and the

spiral wound are the two common types that are usually selected for the large amount capacity in industry [96].

Table 2.2 The features of different membrane modules.

	Price	*Packing Density*	*Clean*	*Pressure Drop*	*Mechanical Resistance*
Hollow fiber module	Low	High	Difficult	High	Good
Spiral wound module	Medium	Medium	Medium	Medium	Good
Capillary module	Medium	Medium	Easy	Medium	Week
Plate and frame module	High	Low	Easy	Medium	Week
Tubular module	High	Low	Easy	Low	Week

2.3.2 Inorganic Membranes

The inorganic membrane exhibits excellent gas separation performance, especially under the harsh conditions due to their structure robustness. Various inorganic membranes have been developed and utilized in different application fields, including the zeolite membrane, metallic membrane, ceramic membrane, MOF membrane etc.

Dense metallic membranes, like Pd membrane, with excellent hydrogen selectivity were developed for high temperature hydrogen separation and purification [97]. The protons and electrons in the metallic membrane could capture and carry the dissociated hydrogen molecular from the feed side, and subsequently release the association H_2 at the permeate side. Although, metallic membrane possesses promising H_2 selectivity, their high cost and brittleness are the inevitable drawbacks

of commercialization. In contrast, zeolite membranes could provide outstanding gas separation performance with a relative low price. These membranes generally possess very uniform micro pore size [40, 41]. For example, the developed LTA membrane with the pore size of 0.41 nm is a feasible option for vapor removal from alcohol through prevaporation [98]. Recently, MOF membrane has extensively studied and examined for gas separation [75, 76]. The tailored pore structure enables MOF materials to be the candidates for different gas pairs separations, for instant, ZIF-7 with the pore size of 0.27 nm is a good choice for H_2 separation while ZIF-8 with the pore size of 0.34 nm is a good choice for propylene/propane separation [86, 87]. Besides, the organic ligands of the structure make MOF materials more compatible with the organic polymers and thus are easier to incorporate into the polymer matrix for MMM [77].

Despite many studies conducting on inorganic gas separation membrane, there are not many commercialized inorganic gas separation membrane being used in industry at this moment. This is because the current fabrication method makes the inorganic membrane very difficult for large scale production and handling. Besides, some emerging crystalline membranes (silicate-1 and MOFs) are still not hydrothermal stable enough to be utilized under the demanded conditions. Hence, further membrane material modification and novel technical fabrication methods are highly demanded before inorganic gas separation membrane is feasible for large scale industry application.

2.3.3 Membranes Reactors

According to the definition of IUPAC, a membrane reactor (MR) system is a unit combines the functions of catalytic reactions and membrane separation process. Although the membrane reactor concept has already been proposed in 1950s', the considerable development of this technology has only been achieved in the last 30

years that benefit from the emerging inorganic materials and high temperature membrane system [9].

The MRs could be classified into two types according to placements of membranes and catalysts, as shown in Figure 2.11. The packed bed membrane reactor (Figure 2.11(a)) is constructed with the packed catalyst layer and the inert membrane layer, while the catalytic membrane reactor has the catalytic active membrane layer, whether the catalyst is incorporated in the porous membrane structure (Figure 2.11(b)) or the membrane has the inherent catalytic activity (Figure 2.11(c)) [99]. There are mainly three MR configurations according to the functions, which are the extractor, distributor and active contactor, as shown Figure 2.12. For example, in the MR for water gas shift reactions, the membrane separation process is usually utilised to improve the catalytic reaction conversions, either to shift the thermodynamic equilibrium or to enhance the reaction rate by selective removal of product H_2 [9 - 11]. The distributor type membrane reactor is usually used to enhance the reaction selectivity. For example, the membrane could control the oxygen concentration and distribution in the reaction chamber of MR resulted with the high product selectivity and reactant conversions in the partial oxidation reactions [99].

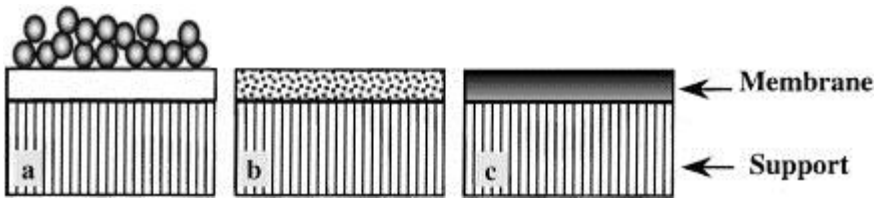

Figure 2.11 The two membrane reactor types: (a) packed bed membrane reactor; (b) and (c) catalytic membrane reactors. [99]

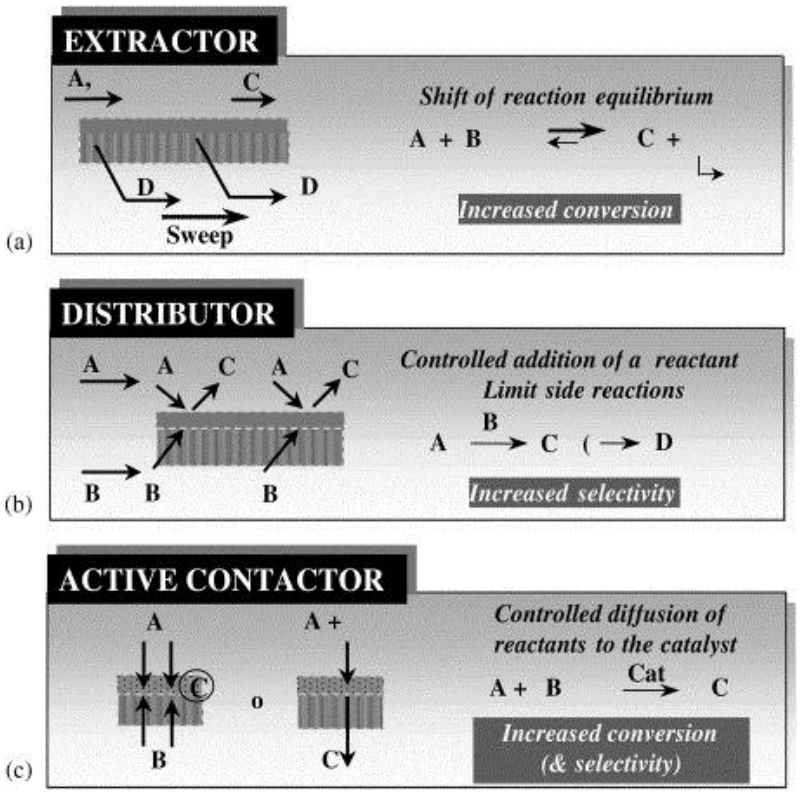

Figure 2.12 The three main membrane functions in a membrane reactor [99].

Up to now, various chemical reactions have been conducted in membrane reactor process, including the dehydrogenation reactions, hydrogenation reactions, partial oxidative reactions and catalytic decomposition reactions etc. [9]. Herein, water gas shift reaction, a well-known exothermic reaction to produce the hydrogen was also extensively carried out in different membrane reactors. There are many advantages by using a MR for water gas shift reaction, including 1) a higher CO conversion with respect to the equilibrium, 2) higher recovery of the concentrated hydrogen product and 3) the capture of the greenhouse gas CO_2 etc. [9-11]. Kikuchi et al. fabricated a palladium membrane reactor with Fe-Cr catalyst for high temperature water gas shift reaction and obtained 100% CO conversion at 400 ℃ under 5 atm [100]. According to Brunetti et al., the employment of MR could reduce the amount of catalyst requested in the conventional packed bed reactor due to the improvement on the reaction kinetic [101].

Pd dense membrane based membrane was firstly used for water gas shift reaction to produce high purity hydrogen due to the extremely high selectivity [100]. However, the Pd metal is very expensive and the membrane is very sensitive to the sulfur poisoning [10]. Zeolite membrane based water gas shift reaction membrane reactors were studied with silicate-1 membrane and modified ZSM-5 membrane because these membranes own higher permeance, but they also have the relative low H_2/CO_2 selectivity comparing to the dense metal membranes [10, 63, 64]. Recently, MOF materials were found as a promising option for hydrogen separation membrane with the tailorable pore size and mild synthesis conditions comparing to Zeolite membranes [86, 87]. However, the thermal instabilities of MOF membranes make them inapplicable under the high temperature water gas shift reaction conditions [10].

In addition, the performance of MR system also highly depends on the operation conditions coupling with the engineering properties of membrane and catalysts. Basile et al. and Giessler et al. investigated the effects of the water to CO molar ratio on the equilibrium conversions and they reported that the higher water/CO ratio would enhance the CO conversion, but excess water would seriously decline the membrane performance [9, 102]. Brunetti et al. found that higher operation pressure would enhance the CO conversion and improve the catalyst efficiency in WGSR MR because of the enhanced separation performance of the membrane process [101]. Giessler et al. reported their findings on the effect of space velocity (SV) and they claimed that MR conversion increased at higher SV comparing to the traditional packed bed reactor [102]. Battersby et al. also found the same trend that the higher SV resulted better improvement of MR performance in WGSR, however, these improvements of CO conversion by using MR was indistinctive with only about 10% higher than packed bed reactor [9]. This is because these studies were all conducted with the high SV in order to maximize the H_2 separation performance of the membrane. However, in the meantime, the high SV had weakened the MR function of adjusting the gas compositions in the reaction chamber.

Reference

[1] C. Wheeler, A. Jhalani, E.J. Klein, S. Tummala, L.D. Schmidt, The water-gas-shift reaction at short contact times, J. Catal., 223(2004) 191-199.

[2] B.R.J. Smith, M. Loganathan. M.S. Shantha, A Review of the Water Gas Shift Reaction Kinetics, Int. J. Chem. React. Eng., 8(2010) R4

[3] C. Ratnasamy, J.P. Wagner, Water Gas Shift Catalysis, Catal. Rew., 51(2009) 325-440

[4] Y. Choi, H.G. Stenger, Water gas shift reaction kinetics and reactor modelling for fuel cell grade hydrogen, J. Power. Sources., 124(2003) 432–439

[5] S.S. Hla, D. Park, G.J. Duffy, J.H. Edwards, D.G. Roberts, A. Ilyushechkin, L.D. Morpeth, T. Nguyen, Kinetics of high-temperature water-gas shift reaction over two iron-based commercial catalysis using simulated coal-derived syngases, Chem. Eng. J., 146(2009) 148-154

[6] K.G. Azzam, I.V. Babich, K. Seshan, L. Lefferts, Bifunctional catalysts for single-stage water-gas shift reaction in fuel cell applications. J. Catal. 251(1)(2007) 153-171

[7] V. Galvita, T. Schroder, B. Munder, K. Sundmacher, Production of hydrogen with CO_x-content for PEM fuel cells by cyclic water gas shift reactor, Int. J Hydrogen. Energy., 33(4)(2008) 1354-1360

[8] M.G. Beaver, H.S. Caram, S. Sircar, Selection of CO_2 chemisorbent for fuel-cell grade H_2 production by sorption-enhanced water gas shift reaction, Int. J Hydrogen. Energy., 34(7)(2009) 2972-2978

[9] A. Basile, A. Criscuoli, F. Santella and E. Drioli, Membrane reactor for water gas shift reaction, Gas. Sep. Purif. 10(1996) 243-254

[10] S. Battersby, M.C.Duke, S. Liu, V. Rudolph, J.D.D. Costa, Metal doped silica membrane reactor: Operational effects of reaction and permeation for the water gas shift reaction, J. Membra. Sci., 316(1-2)(2008) 46-52

[11] K. Gosiewski, K. Warmuzinski, M. Tanczyk, Mathematical simulation of WGS membrane reactor for gas from coal gasification, Catal. Today. 156(3-4)(2010) 229-236

[12] J.C. Gonzales, M.C. Gonzales, M.A. Laborde, N. Moreno, Effect of temperature and reduction on the activity of high temperature water gas shift catalysts. Appl. Catal., 20(1986) 3–13.

[13] G.C. Chinchan, R.H. Logan, M.S. Spencer, Water-gas shift reaction over an iron oxide/chromium oxide catalyst. II: Stability of activity. Appl. Catal., 12(1)(1984) 69–88.

[14] A. Boudjemaa, C. Daniel, C. Mirodatos, M. Trari, A. Auroux, R. Bouarab, In situ DRIFTS studies of high-temperature water –gas shift reaction on chromium-free iron oxide catalysts, Cr. Chim. 14(6)(2011) 534-538

[15] Y. Lei, N.W. Cant, D.L. Trimm, Kinetics of water-gas shift reaction over a rhodium-promoted iron-chromium oxide catalyst, Chem. Eng. J. 114(1-3)(2005) 81-85

[16] T. Salmi, S. Bostrom, L.E. Lindfors, A dynamic study of the water-gas shift reaction over an industrial ferrochrome catalyst, J. Catal. 112(2)(1988) 345-356

[17] C.N. Satterfield, Heterogeneous Catalysis in Industrial Practice, 2nd ed. McGraw-Hill: New York, (1991)

[18] E. Xue, M. O'Keeffe, J.R.H. Ross, Water-gas shift conversion using a feed with low steam to carbon monoxide ratio and containing sulphur, Catal. Today. 30(1-3)(1996) 107-118

[19] J. Xu, G.F. Froment, Methane Steam Reforming, Methanation and Water-Gas Shift: I. Instrinsic Kinetics, AIChE Journal. 35(1) (1989) 88-96.

[20] K.M.V. Bussche, G.F. Froment, A steady-state kinetic model for methanol synthesis and the water gas shift reaction on a commercial $Cu/ZnO/Al_2O_3$ catalyst, J. Catal., 161(1)(1996) 1-10

[21] T. Shishido, M. Yamamoto, D. Li, Y. Tian, H. Morioka, M. Honda, T. Sano, K. Takehira, Water-gas shift reaction over Cu/ZnO and Cu/ZnO/Al_2O_3 catalysts prepared by homogeneous precipitation, Appl. Catal. A-Gen., 303(1)(2006) 62-71

[22] I. Atake, K. Nishida, D. Li, T. Shishido, Y. Oumi, T. Sano, K. Takehira Catalytic behaviour of ternary Cu/ZnO/Al_2O_3 systems prepared by homogeneous precipitation in water-gas shift reaction, J. Mol. Catal. A-Chem., 275(1-2)(2007) 130-138

[23] A.A.G. Lima, M. Nele, E.L. Moreno, H.M.C. Andrade, Composition effects on the activity of Cu-ZnO-Al_2O_3 based catalysts for the water gas shift reaction: A statistical approach, Appl. Catal. A-Gen., 171(1)(1998) 31-43

[24] M.V. Twigg, M.S. Spencer, Deactivation of supported copper metal catalysts for hydrogenation reactions, Appl. Catal. A-Gen, 212(1)(2001) 161-174

[25] H.F. Rase, Chemical Reactor Design for Process Plants: Volume two – Case Studies and Design Data, John Wiley and Sons, 1977

[26] A. Venugopal, J.Aluha, .M.S. Scurrell, The water-gas shift reaction over Au-based, bimetallic catalysts. The Au-M (M=Ag, Bi, Co, Cu, Mn, Ni, Pb, Ru, Sn, Tl) on Iron(III) oxide system, Catal. Lett., 90(1-2)(2003) 1-6

[27] S. Gil, A. Romero, A.D. Lucas, P. Sanchez, F. Dorado, A.R.D.L. Osa, J.M. Garcia-Vargas, J.L. Valverde, Nano-Scale Au supported on carbon materials for the low temperature water gas shift (WGS) reaction, Catal., 1(2011) 155-174

[28] A.A. Phatak, N. Koryabkina, S. Rai, J.L. Ratts, W. Ruettinger, R.J. Farrauto, G.E.Blau, W.N. Delgass, F.H. Ribeiro, Kinetics of the water–gas shift reaction on Pt catalysts supported on alumina and ceria, Cataly. Today., 123(2007) 224–234

[29] H. Sakurai, A. Ueda, T. Kobayashi, M. Haruta, Low-temperature water-gas shift reaction over gold, depositedon TiO_2, Chem. Commun., 3(1997) 271-272

[30] M. Haruta, S. Tsubota, T. Kobayashi, H. Kageyama, M.J. Genet, B. Delmon, Low-temperature oxidation of CO over gold supported on TiO_2, α-Fe_2O_3, and Co_3O_4, J. Catal. 144(1)(1993) 175-192

[31] R. Burch, Gold catalysts for pure hydrogen production in the water-gas shift reaction: activity, structure and reaction mechanism, Phys. Chem. Chem. Phys. 8(2006) 5483-5500

[32] A. F. Cronstedt, Ron och beskriting om en obekant barg ant, som kallas zeolites. Akad Handl Stackholm 17(1756)120–130

[33] S.M. Auerbach, K.A. Carrado, P.K. Dutta, Handbook of zeolite science and technology, Marcel Dekker Inc., New York, (2003)

[34] http://www.iza-online.org/

[35] C.S. Cundy, P.A. Cox, The hydrothermal synthesis of zeolites: Precursors, intermediates and reaction mechanism. Microporous Mesoporous Mater. 82(2005) 1–78

[36] V. Valtchev, L. Tosheva, Porous Nanosized Particles: Preparation, Properties, and Applications. Chem. Rev. 113(2013) 6734–6760.

[37] S. Kulprathipanja, Zeolites in industrial separation and catalysis, Focus on catalysts, Viley-VCH,Weinheim, Germany (2010)

[38] O.C. –L, J. Hazen, D.G. Casey, Zeolite catalyst systems, Zeolites, 16(1)(1994) 80

[39] E.E. Mcleary, J.C. Jansen, F. Kapteijn, Zeolite based films, membranes and membrane reactors: Process and prospects, Micro. Meso. Mater. 90(1-3)(2006) 198-220

[40] J. Caro, M. Noack, Zeolite membranes – Recent developments and progress, Micro. Meso. Mater. 115(3)(2008) 215-233

[41] N. Kosinov, J. Gascon, F. Kapteijn, E.J.M. Hensen, Recent developments in zeolite membranes for gas separation, J. Membr. Sci. 499(2016) 65-79

[42] S. Kulprathipanja, R.B. James, Overview in Zeolites adsorptive separation; Zeolites in industrial separation and catalysis, Viley-VCH,Weinheim, Germany (2010)

[43] P. Yang, X. Ye, C. Lau, Z. Li, X. Liu, J. Lu, Design of efficient zeolite sensor material for n-hexane, Anal. Chem. 79(4)(2007) 1425-1432

[44] L. Regli, A. Zecchina, J.G. Vitillo, D. Cocina, G. Spoto, C. Lamberti, K.P. Lillerud, U. Olsbye, S. Bordiga, Hydrogen storage in Chabazite zeolite frameworks, Phys. Chem. Chem. Phys. 7(2005) 3197-3203

[45] J. Dong, Y.S. Lin, In situ synthesis of P-type zeolite membrane on porous α-alumina supports, Ind. Eng. Chem. Res. 37(1998) 2404-2409

[46] DW. Breck, Zeolite molecular sieves: structure, chemistry and use. Wiley, New York (1974).

[47] T.H. Mouhtaris, D. Charistos, N. Kantiranis, A. Filippidis, A. Kassoli-Fournaraki, A. Tsirambidis, GIS-type zeolite synthesis from Greek lignite sulphocalcic fly ash promoted by NaOH solutions. Micro. Meso. Mater. 61(2003) 57-67

[48] B.R. Albert, A.K. Cheetham, J.A.Stuart, C.J. Adams, Investigating on P zeolites: synthesis, characterization, and structure of highly crystalline low-silica NaP, Micro. Meso. Mater. 21(1-3)(1998) 133-142

[49] P. Sharma, J. Yeo, M.H. Han, C.H. Cho, Knobby surfaced, mesoporous, single-phase GIS-NaP1 zeolite microsphere synthesis and characterization for H_2 has adsorption, J. Mater. Chem. A. 1(2013) 2602-2612

[50] Z. Huo, X. Xu, Z. Lv, J. Song, M. He, Z. Li, Q. Wang, L. Yan, Y. Li, Thermal study of NaP zeolite with different morphologies, J. Therm. Anal. Calorim. 111(2013) 365-369

[51] R. J. Argauer, M. Kensington, G.R. Landolt, US Patent 3702886 (1972)

[52] C-Y. Hsu, A.S.T. Chiang, R. Selvin, R.W. Thompson, Rapid synthesis of MFI zeolite nanocrstals, J. Phy. Chem. B. 109(40)(2005) 18804-18814

[53] O. Cappellazzo, G. Cao, G. Messina, M. Morbidelli, Kinetics of shape selective xylene isomerisation over a ZSM-5 catalyst, Ind. Eng. Chem. Res. 30(10)(1991) 2280-2287

[54] L.B. Young, S.A. Butter, W.W. Keading, Shape selective reactions with zeolite catalysts:III. Selectivity in xylene isomerisation, toluene-methanol alkylation, and toluene disproportionation over ZSM-5 zeolite catalysts, J. Catal. 76(2)(1982) 418-432

[55] L. Sandstrom, E. Sjoberg, J. Hedlund, Very high flux MFI membrane for CO_2 separation, J. Membr. Sci. 390(1-2)(2011) 232-240

[56] T. Matsufuji, K. Watanabe, N. Nishiyama, Y. Egashira, M. Matsukata, K. Ueyama, Permeation of hexane isomers through an MFI membrane, Ind. Eng. Chem. Res. 39(7)(2000) 2434-2438

[57] Q. Zhao, J. Wang, N. Chu, X. Yin, J. Yang, C. Kong, A. Wang, J. Lu, Preparation of high permeance MFI membrane with the modified secondary growth method on the macroporous α-alimina tubular support, J. Membr. Sci. 320(1-2)(2008) 303-309

[58] Y. Zhang, Y. Zhou, Y. Li, Y. Wang, Y. Xu, P. Wu, effect of calcinations temperature on catalytic properties of PtSnNa/ZSM-5 catalyst for propane dehydrogenation, Catal. Commun. 8(7)(2007) 1009-1016

[59] J.V.D. Mynsbrugge, M. Visur, U. Olsbye, P. Beato, M. Bjorgen, V.V. Speybroeck, S. Svelle, Methylation of benzene by methanol: Single-site kinetics over H-ZSM-5 and H-beta zeolite catalysts, J. Catal. 292(2012) 201-212

[60] T. Kawabata, H. Matsuoka, T. Shishido, D. Li, Y. Tian, T. Sano, K. Takehira, Steam reforming of dimethyl ether over ZSM-5 coupled with $Cu/ZnO/Al_2O_3$ catalyst prepared by homogeneous precipitation, Appl. Catal. A-Gen. 308(2006) 82-90

[61] R.M.D. Vos, H. Verweij, Improved performance of silica membranes for gas separation, J. Membr. Sci. 143(1-2)(1998) 37-51

[62] R.M.D. Vos, W.F. Maier, H. Verweij, Hydrophobic silica membranes for gas separation, J. Membr. Sci. 158(1-2)(1999) 277-288

[63] H. Wang, Y.S. Lin, Synthesis and modification of ZSM-5/silicalite bilayer membrane with improved hydrogen separation performance, J. Membr. Sci. 396(2012) 128-137

[64] X. Dong, H. Wang, Z. Rui, Y.S. Lin, Tubular dual-layer MFI zeolite membrane reactor for hydrogen production via the WGS reaction: Experimental and modelling studies, Chem. Eng. J. 268(2015) 219-229

[65] O.M. Yaghi, H. Li, Hydrothermal synthesis of a Meral-organic framework containing large rectangular channels, J. Am. Chem. Soc. 117(41)(1995) 10401-10402

[66] H. Li, M. Eddaoudi, M. O'Keeffe, O.M. Yaghi, Design and synthesis of an exceptional stable and highly porous metal organic framework, Nature. 402(1999) 276-279

[67] S.T. Meek, J.A. Greathouse, M.D. Allendorf, Metal-organic frameworks: A rapidly growing class of versatile nanoporous materials, Adv. Mater. 23(2011) 249-267

[68] H.C. Zhou, J.R. Long, O.M. Yaghi, Introduction to Metal –organic frameworks, Chem. Rev. 112(2012) 673-674

[69] J.L.C. Rowsell, O.M. Yaghi, Metal-organic frameworks: a new class of porous materials, Micro. Meso. Mater. 73(2004) 3-14

[70] S.G. Telfer, What are these things called MOFs, Chem. N. Z. Adv. Mater. Nanotech. 74(2010) 9-14

[71] S.L. James, Meral-organic frameworks, Chem. Soc. Rev. 32(2006) 276-288

[72] N. Stock, S. Biswas, Synthesis of metal-organic frameworks (MOFs): Routes to various MOF topologies, morphologies, and composites, Chem. Rev. 112(2012) 933-969

[73] J. Cravillon, R. Nayuk, S. Springer, A. Feldhoff, K. Huber, M. Wiebcke, Controoling zeolitic imidazolate framework nano- and microcrystal formation:

Insight into crystal growth by time-resolved in situ static light scattering, Chem. Mater. 23(2011) 2130-2141

[74] M.C. McCarthy, V. Varela-Guerrero, G.V. Barnett, H-K, Jeong, Synthesis of zeolitic imidazolate framework films and membranes with controlled microstructures, Langmuir. 26(18)(2010) 14646-14641

[75] A. Betard, R.A. Fischer, Metal-organic framework thin film: from fundamentals to applications, Chem. Rev. 112(2012) 1055-1083

[76] W. Li, Y. Zhang, Q. Li, G. Zhang, Metal-organic framework composite membranes: synthesis and separation applications, Chem. Eng. Sci. 135(2015) 232-257

[77] H.B.T. Jeazet, C. Staudt, C. Janiak, Metal-organic frameworks in mixed-matrix membranes for gas separation, Dalton. Tran. 41(2012) 14003-14027

[78] A. Corma, H. Garcia, F.X.L.I. Xamena, Engineering metal organic frameworks for heterogeneous catalysis, Chem. Rev. 110(2010) 4606-655

[79] J.Y. Lee, O.K. Farha, J. Roberts, K.A. Scheidt, S.B.T. Nguyen, J.T. Hupp, Metal organic framework materials as catalysts, Chem. Soc. Rew. 38(2009) 1450-1459

[80] D. Esken, S. Turner, O.I. Lebedev, G.V. Tendeloo, R.A. Fisher, Au@ZIFs: stabilization and encapsulation of cavity size matching gold clusters inside functionalized zeolite imidazolate frameworks, ZIFs, Chem. Mater. 22(2010) 6393-6401

[81] T. Tsuruoka, H. Kawasaki, H. Nawafune, K. Akamatsu, Controlled sele-assembly of metal-organic frameworks on metal nanoparticles for efficient synthesis of hybrid nanostructures, ACS. Appl. Mater. Interfaces. 3(2011) 3788-3791

[82] K.S. Park, Z. Ni, A.P. Cote, J.Y. Choi, R. Huang, F.J. Uribe-Romo, H.K. Chae, M. O'keeffe, O.M. Yaghi, Exceptional chemical and thermal stability of zeolitic imidazolate frameworks, PNAS. 103(27)(2006) 10186-10191

[83] B. Chen, Z. Yang, Y. Zhu, Y. Xia, Zeolitic imidazolate framework materials: Recent progress in synthesis and applications, J. Mater. Chem. A. 2(2014) 16811-16831

[84] V.M.A. Melgar, J. Kim, M.R. Othman, Zeolitic imidazolate framework membranes for gas separation: A review of synthesis methods and gas separation performance, J. Ind. Eng. Chem. 28(2015) 1-15

[85] B.R. Pimentel, A. Parulkar, E-K. Zhou, N.A. Brunelli, R.P. Lively, Zeolitic imidazolate frameworks: Next generation materials for energy-efficient gas separations, Chem. Sus. Chem. 7(2014) 3202-3240

[86] Y. Li, F. Liang, H. Bux, W. Yang, J. Caro, Zeolitic imidazolate framework ZIF-7 based molecular sieve membrane for hydrogen separation, J. Membr. Sci. 354(2010) 48-54

[87] Y. Pan, T. Li, G. Lestari, Z. Lai, Effective separation of propylene/Propane binary mixtures by ZIF-8 membranes, J. Membr. Sci. 390-392(2012) 93-98

[88] P. Wang, J. Zhao, X. Li, Y. Yang, Q. Yang, C. Li, Assembly of ZIF nanostructures around free Pt nanoparticles: efficient size-selective catalysts for hydrogenation of alkenes under mild conditions, Chem. Comm. 49(2013) 3330-3332

[89] H-L. Jiang, B. Liu, T. Akita, M. Haruta, H. Sakurai, Q. Xu, Au@ZIF-8: CO oxidation over gold nanoparticles deposited to metal-organic framework, J. Am. Chem. Soc. 131(2009) 11302-11303.

[90] P-Z. Li, K. Aranishi, Q. Xu, ZIF-8 immobilized nickel nanoparticles: highly effective catalysts for hydrogen generation from hydrolysis of ammonia borane, Chem. Comm. 48(2012) 3173-3175

[91] P. Bernardo, E. Drioli, G. Golemme, Membrane gas separation: a review/state of the art. Ind. Eng. Chem. Res. 48(2009) 4638-4663

[92] H. Strathmann, Membrane separation process: Current relevance and future opportunities, AIChE Journal. 47(2001) 1077-1087

[93] E. Drioli, L. Giorno, Comprehensive Membrane Science and Engineering, Elsevier, Amsterdam, (2010)

[94] R. Baker, Future directions of membrane gas-separation technology, Ind. Eng. Chem. Res. 41(2002) 1393-1411.

[95] J. Shi, Q. Yuan, C.K. Gao, Membrane technology handbook, Chemical Industry Press, Beijing, 2000

[96] S. P. Nunes, K.-V. Peinemann, Membrane Technology: in the Chemical Industry, Second, Revised and Extended Edition, WILEY-VCH Verlag GmbH & Co. KGaA, Weinheim, 2006.

[97] P. P. Mardilovich, Y. She, Y. H. Ma, M. H. Rei, Defect-Free Palladium Membranes on Porous Stainless-Steel Support, AIChE Journal, 44 (1998) 310-322.

[98] D. Liu, Y. Zhang, J. Jiang, X. Wang, C. Zhang, X. Gu, High-performance NaA zeolite membranes supported on foure-channel ceramic hollow fivers for ethanol dehydration, RSC. Adv. 5(2015) 95866-95871

[99] A. Julbe, D. Farrusseng, C. Guizard, Porous ceramic membranes for catalytic reactors – overview and new ideas, J. Membr. Sci. 181(2001) 3-20

[100] S. Uemiya, N. Sato, H. Ando, E. Kikuchi, The water gas shift reaction assisted by a palladium membrane reactor, Ind. Eng. Chem. Res., 30(1991) 585-589

[101] A. Brunetti, G. Barbieri, E. Drioli, K.-H. Lee, B. Sea, D.-W. Lee, WGS Reaction in a Membrane Reactor Using a Porous Stainless Steel Supported Silica Membrane. Chem. Eng. Proc: Proc. Intens. 46(2007) 119–126

[102] S. Giessler, L. Jordan, J.C. Diniz da Costa, G.Q.M. Lu, Performance of hydrophobic and hydropholic silica membrane reactors for the water gas shift reaction, Separ. Purif. Technol. 32(2003) 255-264.

Chapter 3

Synthesis of Micro-porous Materials

3.1 Introduction

Porous solids have attracted many research interests because of their outstanding performance in the applications of catalysis, adsorption, separation and ion exchange etc. Many of their distinguishable properties benefit from their highly ordered pore structures, whereas these porous materials could be classified to micro-porous (less than 2 nm), mesoporous (2 nm – 50 nm) and macroporous (larger than 50 nm) according to the range of the pore size [1].

Zeolite, first found by Swedish mineralogist Cronstedt, is the most used porous materials in industry at this moment [2]. The definition of zeolite is the crystalline, micro-porous aluminosilicates with 3D strecture complex, which has the compositions primarily includes silicate, alumina and other elements such as sodium, manganese, titanium etc. [3]. Till now, there are 229 unique zeolite have been found and identified from both naturally and artificial synthesized [4]. In the recent years, a new emerging group of materials, called metal organic frameworks (MOFs) has become very attractive in the porous material research society. The solids defined as MOFs are mainly composed with the ionic end nods and the organic ligands, while these materials usually possess the inherent properties like incredible high surface area, nano-porosity with tenable structures, varieties of pore sizes and topologies as well as the robustness with strong bonding etc. Interestingly, the specific MOF geometrical structure could be designed and synthesized by decorating with different ionic and organic ligands pairs [5 - 10].

Nowadays, both Zeolite and MOFs have been the important porous materials in the research and industries for their promising application potentials in many areas, like catalysis and gas separations. Herein, the zeolite material of GIS-NaP and the MOF material ZIF-8 were extensively studied in the applications of the catalysis and gas separation membranes. They both have the intersecting channels with the micro-size pores enable them the promising structures for catalyst host and the molecular sieve gas separation membranes. Besides, they were reported as the robustness and thermal stable structures which could be employed in many harsh conditions [11 - 15]. MIL-47, a member of MOFs family, which compose vanadium nods connected by terephthalate

linkers, is also a noticeable porous material with excellent gas adsorption properties and promising structure stability [16 - 17].

Hence, these porous solids (GIS – NaP, ZIF-8 and MIL-47) were firstly selected as the candidate materials of the membrane reactor and catalyst host in this study. In this chapter, the micro-porous materials of ZIF-8, GIS - NaP and MIL-47 were prepared through the hydrothermal synthesis method and the crystallization mechanisms of these materials were examined. Then, the composite catalysts with these porous material supports were prepared and characterized with various methods. Finally, ZIF-8 was selected as the raw material of the membrane system after considering its fabrication feasibility and the application potentials in catalysis and gas separation membrane processes

3.2 Methodology

3.2.1 Materials

Zinc nitrate hydrate (>99.99%), 2-methylimidazole (Hmim), methanol (>99.8%), sodium formate, sodium metasilicate, sodium hydroxide (>98%), sodium aluminate, vanadium (III) chloride (97%), terephthalic acid (98%), gold (III) chloride trihydrate (>99.99%), sodium borohydride (>98%) were purchased from Sigma–Aldrich. Deionized (DI) water was used to prepare all required samples and solutions. All of the chemicals were used as received without any further treatment.

3.2.2 Characterization Methods

Scanning electron microscopy (SEM) and transmission electron microscopy (TEM) images were recorded using a JEOL 700F and a Philips CM-200, respectively. X-ray diffraction (XRD) patterns of the samples were collected using a Philips PW1700 instrument equipped with a Co Ka radiation source.

3.2.3 Sample Preparation

3.2.3.1 ZIF-8 Synthesis

Typically, ZIF-8 synthesis solution was prepared by dissolving $Zn(NO_3)_2 \cdot 6H_2O$ and 2-Hmim in solvent (methanol or DI water), and then the zinc nitrate solution was mixed with the 2-Hmim solution under stirring. This solution was then hydrothermally treated in an oven at various temperatures for different synthesis durations. The synthesis conditions of these ZIF-8 samples are listed in Table 3.1. Finally, the product solids were washed and collected by centrifuge and then dried overnight in an oven at 80 ℃.

Table 3.1 Synthesis conditions of the ZIF-8 samples.

Sample	*Molar ratio* (Zn^{2+} *: 2-Hmim : HCOONa : MeOH)*	*Temperature (℃)*	*Synthesis Duration (hours)*
ZIF-8 - 1	1 : 4 : 0 : 330	room	4
ZIF-8 - 2	1 : 4 : 0 : 500	room	4
ZIF-8 - 3	1 : 4 : 0 : 1000	room	4
ZIF-8 – 4	1 : 4 : 0 : 1000	room	24
ZIF-8 - 5	1 : 2 : 0 : 330	80	4
ZIF-8 – 6	1 : 4 : 0 : 330	80	4
ZIF-8 – 7	1 : 10 : 0 : 330	80	4
ZIF-8 – 8	1 : 4 : 0 : 330	120	4
ZIF-8 – 9	1 : 2 : 0 : 330	80	1
ZIF-8 – 10	1 : 2 : 0 : 330	80	2
ZIF-8 – 11	1 : 2 : 0 : 330	80	8
ZIF-8 – 12	1 : 2 : 0 : 330	80	24
ZIF-8 – 13	1 : 4 : 0.5 : 330	80	4
ZIF-8 – 14	1 : 4 : 2 : 330	80	4
ZIF-8 – 15	1 : 4 : 4 : 330	80	4
ZIF-8 – 16	1 : 4 : 8 : 330	80	4
ZIF-8-17[18]*	1 : 70 : 0 : 1238	room	0.1

** Solvent is DI water*

3.2.3.2 GIS - NaP Zeolite Synthesis

GIS - NaP zeolite was prepared by dissolving Na_2SiO_3 and NaOH in DI water, and then Na_2AlO_3 was added to the above solution under vigorous stirring. After aged in the air, the solution was hydrothermally treated in an oven at various temperatures for different synthesis durations. The synthesis conditions of the GIS - NaP samples are listed in Table 3.2. Finally, the product solids were washed until pH = 7 ~ 8 and collected by vacuum filtration and then dried in overnight an oven at 50 ℃.

Table 3.2 Synthesis conditions of the GIS - NaP samples.

Sample	*Molar ratio* ($Al_2O_3 : SiO_2 : Na_2O : H_2O$)	*Ageing* *(hours)*	*Temperature* *(℃)*	*Synthesis Duration* *(hours)*
GIS - 1	1 : 10 : 14 : 800	24	100	2
GIS - 2	1 : 10 : 14 : 800	24	100	4
GIS - 3	1 : 10 : 14 : 800	24	100	6
GIS - 4	1 : 10 : 14 : 800	24	100	8
GIS - 5	1 : 10 : 14 : 800	24	100	10
GIS - 6	1 : 10 : 14 : 800	24	100	12
GIS - 7	1 : 10 : 14 : 800	24	100	20
GIS - 8	1 : 10 : 14 : 800	24	100	24
GIS - 9	1 : 15 : 14 : 800	1/12	100	24

3.2.3.3 MIL-47 Synthesis

MIL-47 was synthesized according to the method of Barthelet et al [16]. In general, 1.663 g terephthalic acid and 6.712 g VCl_3 were dissolved in 72.036 g DI water under stirring. The mixture was then carefully poured into a Teflon-lined autoclave and treated at 473 K for 48 hours. The resulting product was washed and collected with vacuum filtration and then dried in a furnace at 573 K for 24 hours.

3.2.4 Preparation of Gold (Au)/support Composites

The Au incorporated porous material composites were prepared by dispersing the micro-porous support suspensions (methanol) in 2 ml of metal precursor solution ($HAuCl_4$ in methanol) and the mixtures were continuously stirred for 2 hours. Subsequently, a 0.15 mmol/ml sodium borohydride/methanol solution was added to the precursor/support mixture under vigorous stirring for 30 min at room temperature. The resulting solids were washed and collected by vacuum filtration and then dried overnight in an oven at 80 ℃.

3.3 Results and Discussions

3.3.1 Characterization of Synthesized ZIF-8 Samples

As shown in Figure 3.1, all the samples have identical XRD patterns, and these XRD patterns are consistent with the simulated ZIF-8 patterns which indicate the standard ZIF-8 structures of all the synthesized samples. However, the appearances of these ZIF-8 samples are quite different and Figure 3.2 shows the SEM images of these synthesized ZIF-8 samples, from where we can find the appearance variations of these ZIF-8 crystals synthesized from different conditions. As shown in Figure 3.2a, Figure 3.2b and Figure 3.2c, the average particle size of ZIF-8 crystals synthesized under room temperature decreased from 180 nm (ZIF-8 - 1) to 70 nm (ZIF-8 - 3), indicating the synthesis solution concentration would dramatically influence the growth of the ZIF-8 crystals. This is because when the synthesis solution concentration is diluted, it is more difficult for the nutrients to meet and to grow surround the ZIF-8 nuclei during the synthesis [19]. ZIF-8 - 3 had a comparable average particle size to that reported by Cravillon et al [20]. While, Figure 3.2d shows the particle size of ZIF-8 - 4 was over 100 nm by prolonging the synthesis duration to 24 hours. In addition, the particle sizes were found around 1 μm, 200 nm and 100 nm in Figure 3.2e, Figure 3.2f and Figure 3.2g of ZIF-8 - 5, 6 and 7 respectively, synthesized at 80 ℃ for 4 hours but adjusting the bridging ligands concentration in the synthesis solutions. This finding implies that

the higher concentration of the bridging ligands in the synthesis solution, the smaller size of the product particles could be obtained. The result is identical to the conclusions reported by others that the excess bridging ligands would depress the ZIF-8 growth because of the ligands competition and deprotonation [20, 21]. Whereas the sample ZIF-8 - 1, 6 and 8 (Figure 3.2h) synthesized under the same conditions but at room temperatures, 80 ℃ and 120 ℃, respectively, the particle size was found increased with the higher reaction rate at higher temperature. Besides, the crystal growth mechanism was also evaluated by comparing the samples of ZIF-8 - 9 to ZIF-8 - 12, which were synthesized for different durations. Figure 3.2i to Figure 3.2l present the changing trend of the particle morphology as the synthesis time prolonged, from where we can find that the particle shape varied as the time-resolved and the rhombic dodecahedral shape ZIF-8 crystals formed after 12 hours. Aside from the particle size growth, the smaller crystals in sample ZIF-8 - 9 also disappeared in sample ZIF-8 - 12 because the Ostwald ripening has taken place during the longer synthesis duration. By comparing the SEM images of sample ZIF-8 - 6 and ZIF-8 - 13 to ZIF-8 - 16 shown in Figure 3.2f and Figure 3.2m to Figure 3.2p, we can find the particle size dramatically increased with higher sodium formate ratio in the synthesis solution. Even more, the ZIF-8 particles were found agglomerated and grew to a large chunk in sample ZIF-8 - 15 and 16 as shown in Figure 3.2o and Figure 3.2p. This size increment is believed caused by the fully deprotonated of 2-Hmim with the appearance of sodium formate in the synthesis solution reported by McCarthy et al [21]. Sample ZIF-8 - 17 was synthesized through the frequently-used aqueous synthesis method and its SEM image is shown in Figure 3.2q. The particle size of ZIF-8 - 17 is around 80 nm, which is very similar to that reported by Lai et al [18].

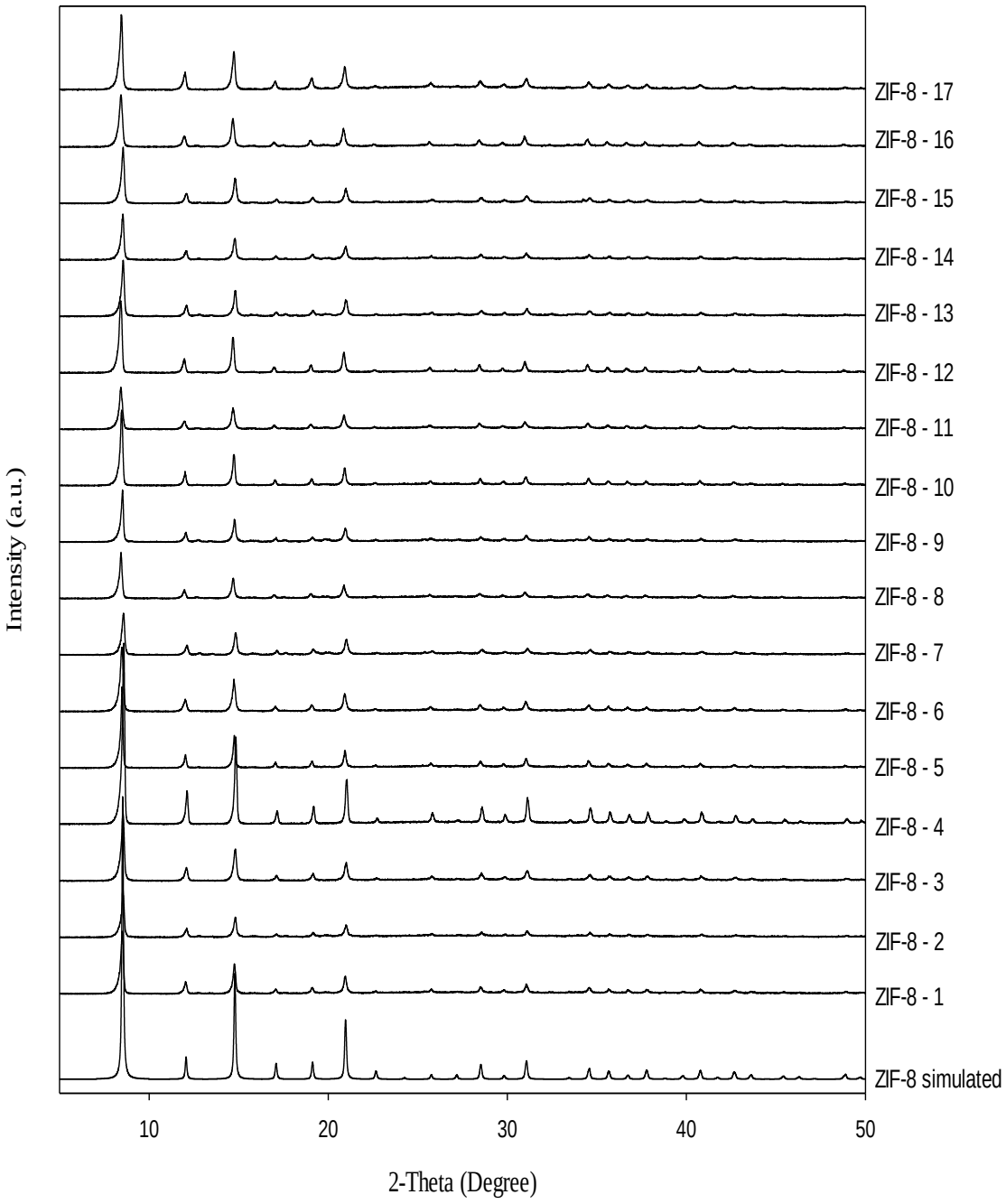

Figure 3.1 XRD patterns of the synthesized ZIF-8 samples.

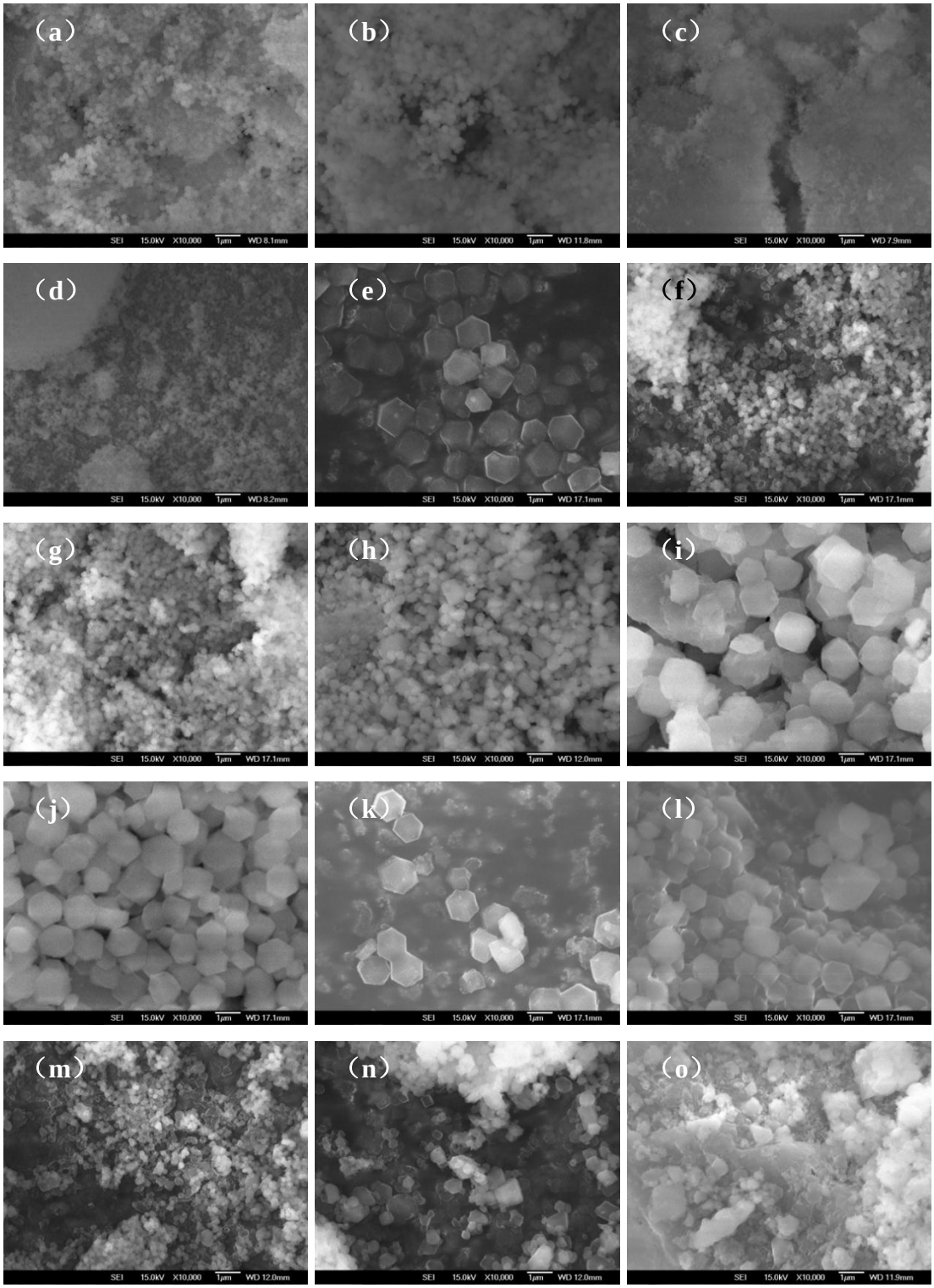
（a）
（b）
（c）
（d）
（e）
（f）
（g）
（h）
（i）
（j）
（k）
（l）
（m）
（n）
（o）

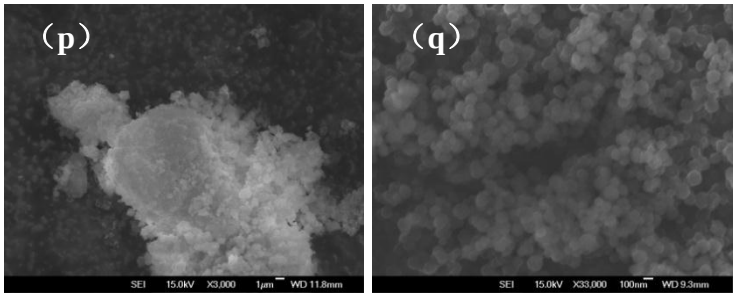

Figure 3.2 SEM images of ZIF-8 samples; images (a) to (q) corresponding to ZIF-8 - 1 to ZIF-8 - 17.

3.3.2 Characterization of Synthesized GIS - NaP Samples

Figure 3.3 illustrates the XRD patterns of the stimulated and synthesized GIS – NaP samples. The identical patterns of the sample GIS - 1, 2 and 3 indicate that the obtained products were well crystallized after 2 hours synthesis at 100 ℃. However, the XRD patterns of these samples were not consistent with that of the stimulated GIS – NaP, but it was NaX zeolite phase. The chartered peaks of GIS – NaP arose in the XRD patterns of sample GIS - 4 and 5 after the synthesis lasted 8 hours at 100 ℃, although the NaX phase still existed in these specimens. Samples of GIS - 6, 7 and 8 obtained after 12 hours crystallization at 100 ℃ have the same XRD patterns with the stimulated GIS – NaP, which confirms the single GIS – NaP zeolite phase without any other impurity phase. In GIS - 9, the SiO_2 ratio was slightly increased and the aging procedure was omitted comparing to other samples. The XRD patterns of GIS - 9 still shows standard GIS – NaP structure which means the aging procedure does not affect the zeolite synthesis in this condition. Hence, we can conclude that the synthesis duration should be longer than 12 hours to obtain the pure single phase of GIS – NaP zeolite.

SEM images of the synthesized GIS – NaP samples are presented in Figure 3.4, which also provide the growth mechanism for the GIS – NaP zeolite crystallization. As shown in Figure 3.4a and Figure 3.4b, the isolated particles were well dispersed in GIS - 1 and 2, while the average sizes of the particles were around 500 nm. In contrast, the particles in Figure 3.4c were still isolated but started to aggregate after 8 hours crystallization of GIS - 4. After 12 hours synthesis, the obtained sample of GIS - 6 presented a sphere shape which was composed of nano-size crystals as shown in Figure 3.4e. On the base

of GIS - 6, the sphere crystals further grew to larger agglomeration with a knobby surface of GIS - 7 after 24 hours, as shown in Figure 3.4f. These study results are similar to the findings reported by Sharma et al. [22] and provide very meaningful information for the control synthesis of GIS – NaP zeolite and its membrane fabrication.

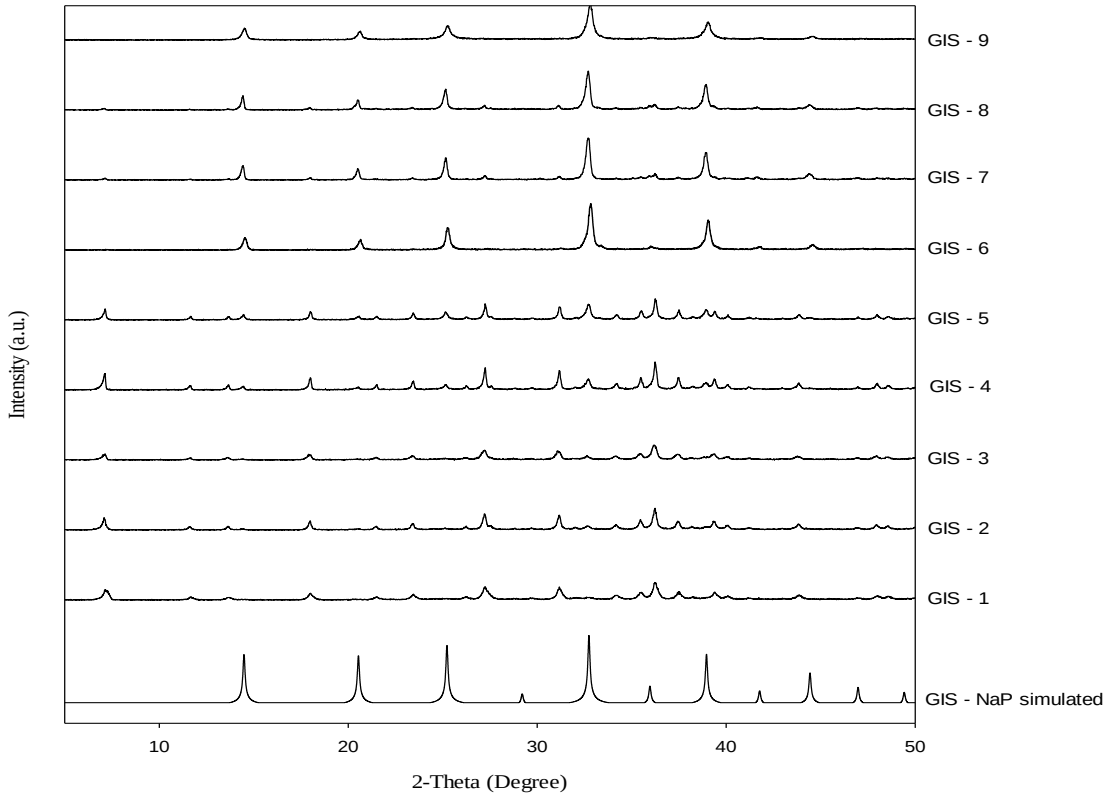

Figure 3.3 XRD patterns of the synthesized GIS - NaP samples.

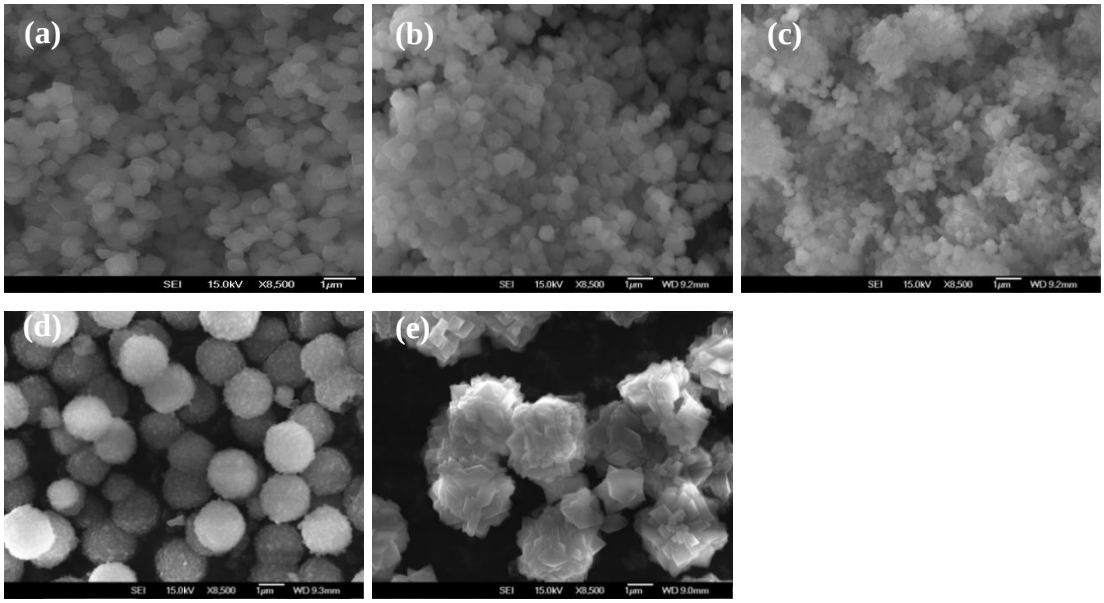

Figure 3.4 SEM images of GIS - NaP samples, (a) GIS - 1, (b) GIS - 3, (c) GIS - 4, (d) GIS - 6 and (e) GIS - 8.

3.3.3 Characterization of Synthesized MIL-47 Samples

The XRD patterns and SEM image of synthesized MIL-47 are shown in Figure 3.5a and Figure 3.5b. Comparison of the synthesized MIL-47 and the stimulated MIL-47 XRD patterns as shown in Figure 3.5a, confirms the pure phase MIL-47 crystals obtained with our synthesis procedure. The SEM image in Figure 3.5b reveals the synthesized MIL-47 particles have a uniform particle size distribution of around 1 μm.

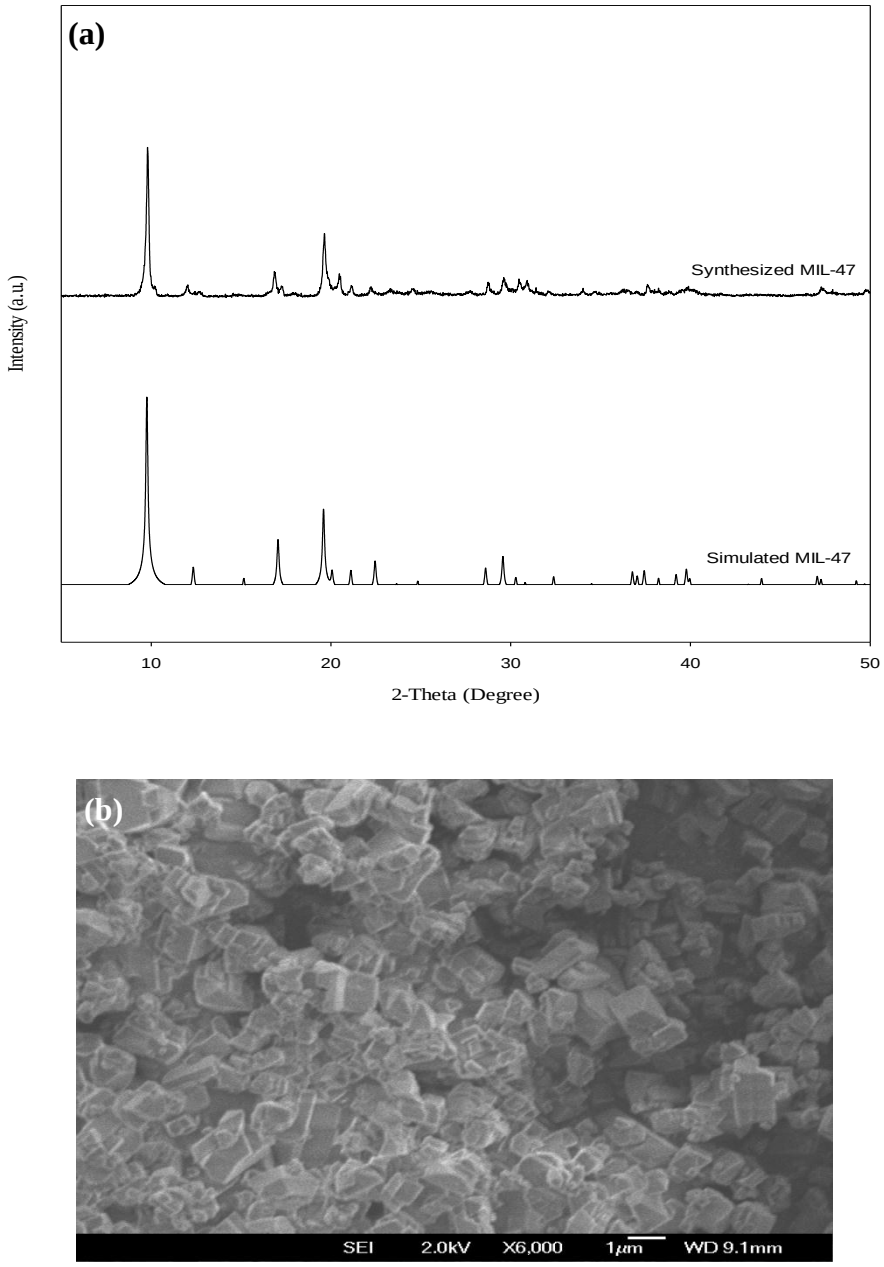

Figure 3.5 XRD patterns (a) and SEM image (b) of synthesized MIL-47.

3.3.4 Characterization of Synthesized Gold/support Samples

The TEM images of the gold (Au)/ZIF-8, Au/MIL-47 and Au/GIS samples are given in Figure 3.6. The gold particles with the average size of 2 – 5 nm were evenly distributed in the Au/ZIF-8 samples with 1, 2.5 and 5 wt% gold loadings as shown in Figure 3.6a,

Figure 3.6b and Figure 3.6c. However, for a higher Au loading (5 wt%), even though most of the gold particles were still very small and isolated, the Au aggregations of different degrees started to be found in Figure 3.6c of sample 3. In general, the isolated gold nano-particles were successfully incorporated and well distributed in the ZIF-8 support of the Au/ZIF-8 samples with the gold loading lower than 5 wt%. In contrast, large gold clusters were observed attaching on the particles surface, rather than in the support MIL-47 structure in Figure 3.6d and Figure 3.6e of sample Au/MIL-47. Although, there were also small amount of fragmentary gold particles in the shell area of the MIL-47 particles, most of the gold were unable to load into the MIL-47 support. Similarly, large gold particles in Au/GIS sample were found aggregated and located on the edges of the GIS - NaP support in Figure 3.6f. The XRD patterns in Figure 3.7 show that the prepared Au/ZIF-8, Au/MIL-47 and Au/GIS all preserved their support structure of ZIF-8, MIL-47 and GIS – NaP, respectively. However, there was no obvious gold diffraction peaks in these samples because of the low gold content and the small size of the loading gold particles [15]. These results indicate that, comparing to MIL-47 and GIS – NaP, ZIF-8 is the most appropriate support for the gold nano-particles in the impregnation preparation method.

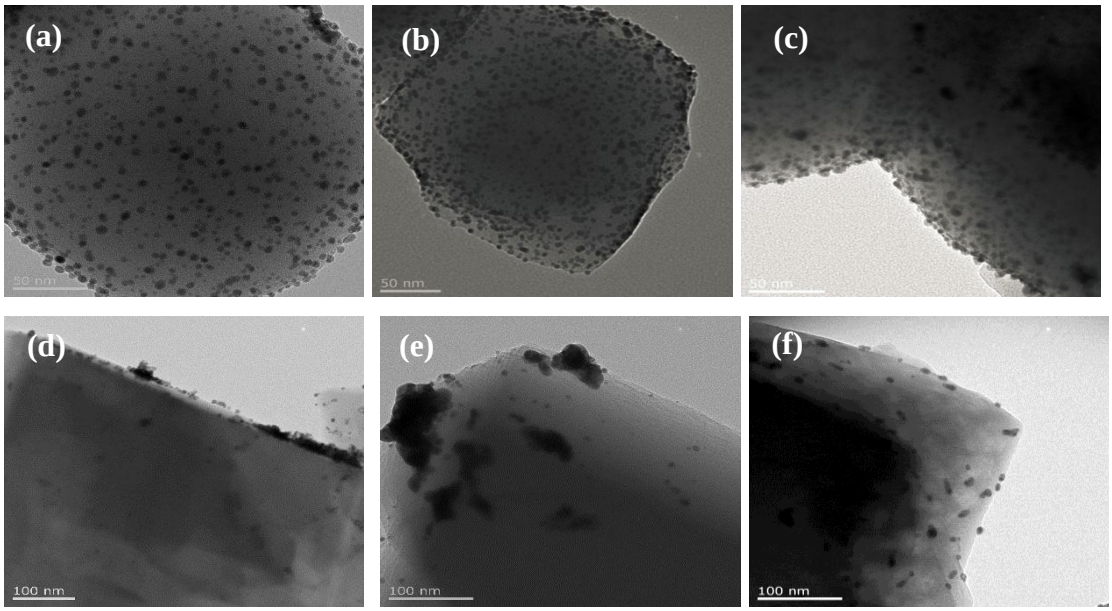

Figure 3.6 TEM images of Au/ZIF-8 with 1 (a), 2.5 (b) and 5 (c) wt% Au loading, Au/MIL-47 (d and e), and Au/GIS (f).

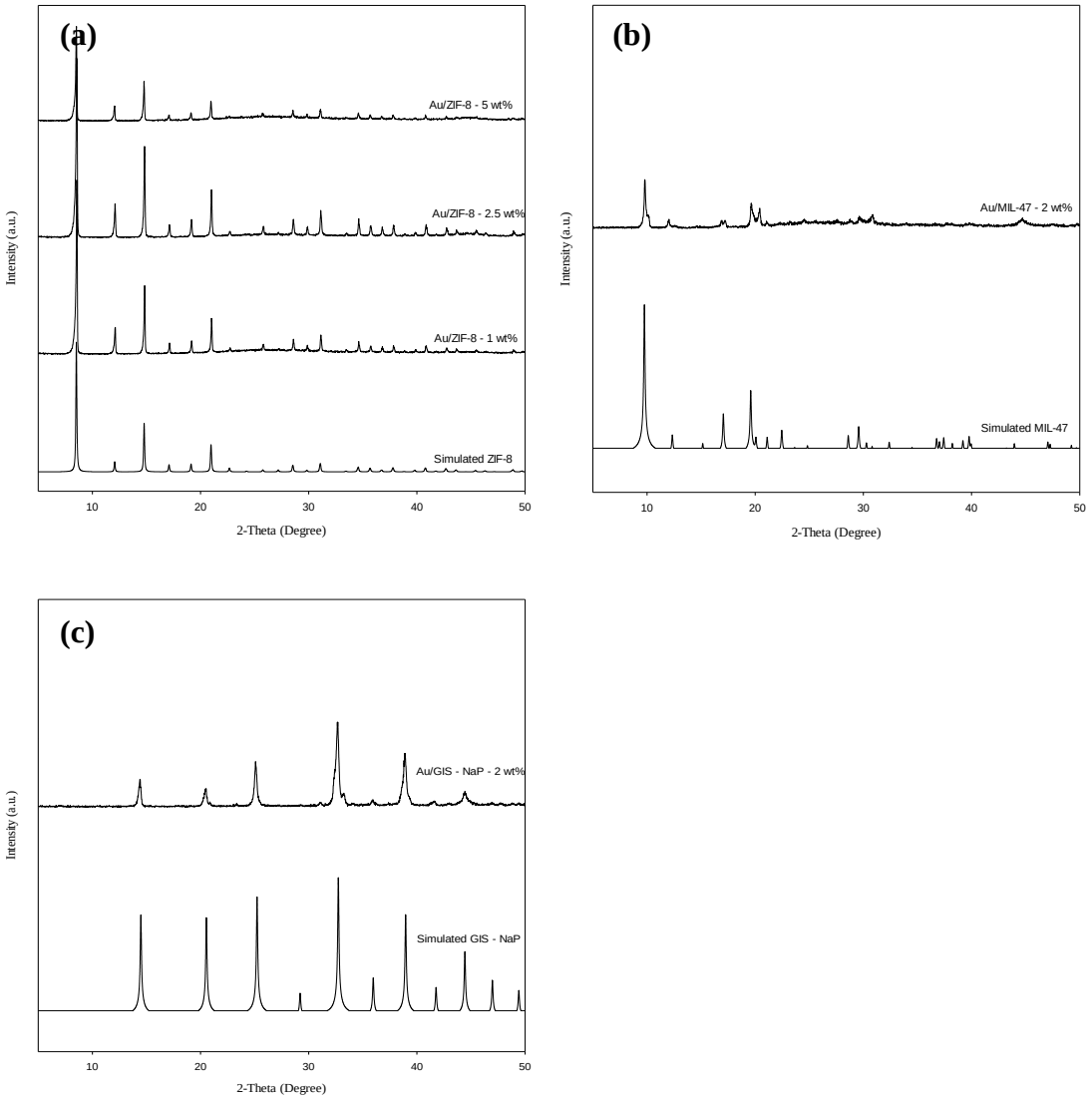

Figure 3.7 XRD patterns of Au/ZIF-8 (a), Au/MIL-47 (b) and Au/GIS - NaP samples (c).

3.4 Conclusion

The micro-porous materials of ZIF-8, GIS - NaP and MIL-47 were successfully prepared through the hydrothermal synthesis method in this study. Besides, the influence of the additive sodium formate in ZIF-8 synthesis was evaluated, and the crystallization mechanism of ZIF-8 and GIS – NaP particles were systematically investigated. In addition, the supported Au nanoparticles composites were prepared with

the three synthesized porous supports and ZIF-8 was found the most appropriate material in this preparation. In conclusion, according to the literature review and the results of this chapter, ZIF-8 was selected as the candidate raw material of the membrane reactor for water gas shift reaction in this dissertation, because 1) ZIF-8 synthesis is controllable and the formations of the produced ZIF-8 could be varied from nano-particles to integrated films, 2) ZIF-8 membrane shows considerable performance for gas separation, especially for hydrogen separation and purification, 3) ZIF-8 was found as a good metal catalysts support with the capacity of controlling the metal particles distribution in its structure.

Reference

[1] M.E. Davis, Ordered porous materials for emerging applications, Nature. 417(2002) 813-821.

[2] A. F. Cronstedt, Ron och beskriting om en obekant barg ant, som kallas zeolites. Akad Handl Stackholm 17(1756)120–130

[3] S.M. Auerbach, K.A. Carrado, P.K. Dutta, Handbook of zeolite science and technology, Marcel Dekker Inc., New York, (2003)

[4] http://www.iza-online.org/

[5] O.M. Yaghi, H. Li, Hydrothermal synthesis of a Meral-organic framework containing large rectangular channels, J. Am. Chem. Soc. 117(41)(1995) 10401-10402

[6] H. Li, M. Eddaoudi, M. O'Keeffe, O.M. Yaghi, Design and synthesis of an exceptional stable and highly porous metal organic framework, Nature. 402(1999) 276-279

[7] S.T. Meek, J.A. Greathouse, M.D. Allendorf, Metal-organic frameworks: A rapidly growing class of versatile nanoporous materials, Adv. Mater. 23(2011) 249-267

[8] H.C. Zhou, J.R. Long, O.M. Yaghi, Introduction to Metal –organic frameworks, Chem. Rev., 112(2012) 673-674

[9] J.L.C. Rowsell, O.M. Yaghi, Metal-organic frameworks: a new class of porous materials, Micro. Meso. Mater. 73(2004) 3-14

[10] S.G. Telfer, What are these things called MOFs, Chem. N. Z. Adv. Mater. Nanotech. 74(2010) 9-14

[11] J. Dong, Y.S. Lin, In situ synthesis of P-type zeolite membrane on porous α-alumina supports, Ind. Eng. Chem. Res. 37(1998) 2404-2409

[12] Z. Huo, X. Xu, Z. Lv, J. Song, M. He, Z. Li, Q. Wang, L. Yan, Y. Li, Thermal study of NaP zeolite with different morphologies, J. Therm. Anal. Calorim. 111(2013) 365-369

[13] Y. Pan, T. Li, G. Lestari, Z. Lai, Effective separation of propylene/Propane binary mixtures by ZIF-8 membranes, J. Membr. Sci. 390-392(2012) 93-98

[14] P. Wang, J. Zhao, X. Li, Y. Yang, Q. Yang, C. Li, Assembly of ZIF nanostructures around free Pt nanoparticles: efficient size-selective catalysts for hydrogenation of alkenes under mild conditions, Chem. Comm. 49(2013) 3330-3332

[15] H-L. Jiang, B. Liu, T. Akita, M. Haruta, H. Sakurai, Q. Xu, Au@ZIF-8: CO oxidation over gold nanoparticles deposited to metal-organic framework, J. Am. Chem. Soc. 131(2009) 11302-11303.

[16] K. Barthelet, J. Marrot, D. Riou, G. Ferey, A breathing hybrid organic – inorganic solid with very large pores and high magnetic characteristics, Angew. Chem. Int. Ed. 41(2)(2002) 281-284

[17] P.L. Llewellyn, S. Bourrelly, C. Vagner, N. Heymans, H. Leclerc, A. Ghoufi, P. Bazin, A. Vimont, M. Daturi, T. Devic, C. Serre, G.D. Weireld, G. Maurin, Evaluation of MIL-47(V) for CO_2-Related application, J. Phys. Chem. C. 117(2013)(2) 962-970.

[18] Y. Pan, Y. Liu, G. Zeng, L. Zhao, Z. Lai, Rapid synthesis of zeolitic imidazolate framework-8 (ZIF-8) nanocrystals in an aqueous system, Chem. Commun. 47 (2011) 2071-2073

[19] J. Yao, L. Li, W.H.B. Wong, C. Tan, D. Dong, H. Wang, Formation of ZIF-8 membranes and crystals in a diluted aqueous solution, Mater. Chem. Phy. 139(2013) 1003-1008

[20] J. Cravillon, R. Nayuk, S. Springer, A. Feldhoff, K. Huber, M. Wiebcke, Controoling zeolitic imidazolate framework nano- and microcrystal formation: Insight into crystal growth by time-resolved in situ static light scattering, Chem. Mater. 23(2011) 2130-2141

[21] M.C. McCarthy, V. Varela-Guerrero, G.V. Barnett, H-K, Jeong, Synthesis of zeolitic imidazolate framework films and membranes with controlled microstructures, Langmuir. 26(18)(2010) 14646-14641

[22] P. Sharma, J. Yeo, M.H. Han, C.H. Cho, Knobby surfaced, mesoporous, single-phase GIS-NaP1 zeolite microsphere synthesis and characterization for H_2 has adsorption, J. Mater. Chem. A. 1(2013) 2602-2612

Chapter 4

Thermal Stability of ZIF-8 under Oxidative and Inert Environments: A Practical Perspective on Using ZIF-8 As A Catalyst Support

This chapter is published as a journal article

Hang Yin, Hyungmin Kim, Jungkyu Choi, Alex C.K. Yip, Chem. Eng. J., 278(2015) 293-300

4.1 Introduction

Metal-organic frameworks (MOFs) are a new class of materials that have received considerable attention in recent years, primarily because of their high specific surface area and pore volume. Also known as porous coordination polymers, these materials consist of infinite crystal lattices that feature metal-ion vertices and organic bridging ligands [1 - 7]. Zeolitic imidazolate frameworks (ZIFs) are a subclass of metal-organic frameworks composed of tetrahedrally coordinated metal ions connected by organic imidazole ligands. They are considered "zeolitic" because of their metal-imidazole-metal angle being similar to the 145 ° Si-O-Si angle observed in zeolites and because of their zeolite-like topologies [8 - 11].

Zeolite imidazole framework-8 (ZIF-8) has attracted extensive research interest because of its simple synthesis and various formulations [10, 12 - 18], its outstanding thermal and chemical stability [8, 19, 20], and its potential applications in catalysis [21 - 24] and gas separation [9, 15, 16, 25, 26]. In many industrial processes, harsh conditions such as high temperatures, high pressures, and the presence of oxidants are required. However, systematic information regarding the structural stability of ZIF-8 under these conditions is still insufficient. Although the authors of numerous previous reports have suggested that ZIF-8 is a structurally sound material on the basis of thermogravimetric analysis (TGA) results for ZIF-8 under air and nitrogen atmospheres [2, 4, 5], we believe the commonly used temperature-increasing method in TGA result in misleading because it overlooks possible structural changes in the materials during long-term isothermal heating. Here, we report a systematic study of the thermal stability of ZIF-8 in the presence of air, argon, and steam, to provide a more realistic assessment of the structural stability of ZIF-8 in industrial gas-phase applications. TGA was performed under isothermal conditions to investigate the trends of ZIF-8 decomposition under air and nitrogen atmospheres at different temperatures. The stability of ZIF-8 as a catalyst support was examined in reaction of the hydrogen reduction of Au in ZIF-8 and the CO oxidation reaction over the reduced Au/ZIF-8.

4.2 Experimental

4.2.1 Materials

Zinc nitrate hydrate (> 99.99%), 2-methyimidazole (Hmim), methanol (> 99.8%) and gold (III) chloride trihydrate (> 99.99%) were purchased from Sigma - Aldrich Chemical Co. Instrument-grade hydrogen, air and argon were purchased from BOC. Deionized (DI) water was prepared in a lab-based water-purification apparatus. All the chemicals were used as received without any further treatment.

4.2.2 Sample Preparation

ZIF-8 was prepared according to the synthesis method reported by Pan et al. [13]. Zn and Hmim solutions were first prepared by dissolving 1.17 g $Zn(NO_3)_2$ $6H_2O$ and 22.7 g Hmim in 8 g and 80 g of DI water, respectively. The Zn solution was then added to the Hmim solution under vigorous stirring for 5 min at ambient temperature. The solid precipitated from the mixture was filtrated through vacuumed filtration and washed with water 3 times. Finally, the solids (ZIF-8) were dried in an oven at 65 ℃ overnight (ZIF-8-D65) or at 100 ℃ for 3 h (ZIF-8-D100) and collected.

The 2 wt % Au loading Au/ZIF-8 was synthesized by impregnating ZIF-8 particles (0.06 g/ml ZIF-8 in 4.4 ml methanol) with 0.8 ml of $HAuCl_4$ in methanol and the mixture was stirred for 3 h, and the Au-containing solid was subsequently collected by filtration. The sample was finally treated in 10% H_2 in Ar at 200 ℃ for 2 h, 400 ℃ for 5 h or 10 h.

4.2.3 Thermal Stability Tests and Characterization

Thermal stability tests were performed using a temperature-controlled tubular furnace (MTI-GSL1500X) with flowing air, Ar, or steam. After the tube furnace was purged with Ar, the ZIF-8-D65 samples (~ 0.1 g) were heated from ambient temperature to the target temperature at 15 K/min. The flow rate of air, Ar, or steam (H_2O/Ar molar ratio

1:1) was 25 ml/min. Scanning electron microscopy (SEM) and transmission electron microscopy (TEM) images were obtained on a JEOL 700F and a Philips CM-200, respectively. To examine the crystal phase transformation of ZIF-8 under different conditions, X-ray diffraction (XRD) analysis was conducted using a Philips PW1700 instrument equipped with a Co-K radiation source. The thermal behavior of ZIF-8 under air and nitrogen flows was assessed using a SDT Q600 thermogravimetric analysis (TGA) system with a temperature ramp rate of 5 K/min and isothermal methods.

4.2.4 CO Oxidation Reaction

The Au/ZIF-8 catalyzed CO oxidation was conducted in a stainless steel fixed bed reactor (i.d. 10 mm). In a standard process, 0.025 g Au/ZIF-8 catalyst was loaded into the reactor at ambient temperature and the reactor was heated to a desired temperature at a rate of 30 K/min. A mixture of gas which contained CO (0.3 sccm), O_2 (3 sccm) and Ar (10 sccm) was introduced to the packed bed reactor. The reactor temperature was controlled using a vertical tubular furnace (MTI-GSL1100) and is monitored by a thermal couple probe extended into the catalyst bed. The reactor effluent was transferred into a gas chromatograph (Buck Scientific 910 GC) to measure reactants and product concentration by thermal conductivity after chromatographic separation in a capillary column (MXT-1, 30 m × 0.53 mm × 1 m).

4.3 Results and Discussion

4.3.1 Structure of ZIF-8

The average size of the ZIF-8 particles formed by the rapid synthesis method [13] was approximately 100 nm (Figure 4.1a). The TEM image (Figure 4.1b) shows that the crystals exhibit a rhombic dodecahedron shape, which is a common ZIF-8 morphology reported in the literature [13]. Figure 4.2a shows that the XRD patterns of the samples ZIF-8-D65 and ZIF-8-D100 are consistent with the simulated ZIF-8 pattern, which suggests that no phase transformation occurred during the drying process. The relative

intensities of the characteristic peaks of ZIF-8-D65, e.g., at 2θ ≈ 5° and 11°, however, differ between the ZIF-8-D100 pattern and the simulated ZIF-8 pattern. This difference is assumed to be caused by insufficient drying, which leaves excess guest molecules remaining in the pores, including residual solvent molecules and organic ligands, which interact with the ZIF-8 structures. We verified this attribution by conducting TGA experiments under increasing temperature. As shown in Figure 4.3, the TGA results reveal that ZIF-8-D65 exhibited a weight loss of approximately 30% under flowing air and nitrogen as the temperature was increased to 200 ℃. The weight-loss percentage was higher than the reported value of 11.8% [13], which indicates the presence of excess residues in the ZIF-8 structure after the sample was dried at 65 ℃ overnight. In addition, Figure 4.3 also demonstrates that the ZIF-8 structure is stable up to 350 ℃ under flowing air and to almost 500 ℃ under flowing nitrogen. Beyond that point, the structure began to collapse quickly, and, finally, 20% of the ZIF-8-D65 sample's initial weight remained after it was heated to 800 ℃ under either atmosphere. On the basis of this result, we confirmed that the ZIF-8 structure is more stable under an inert gas atmosphere than under an air atmosphere. Notably, however, the temperature-increasing method commonly used in TGA does not follow the detection of possible structural changes in the material during long-term isothermal heating.

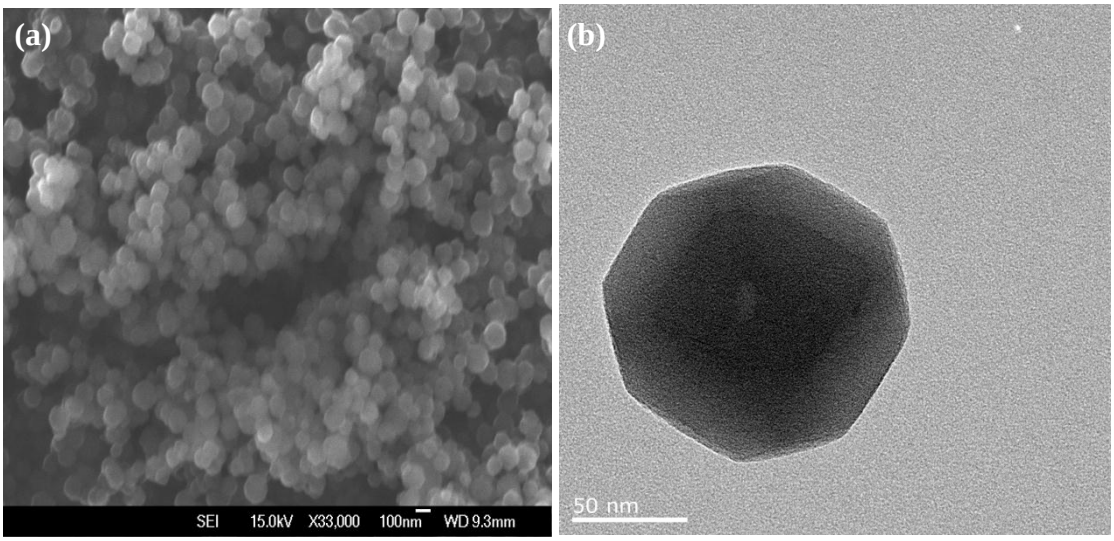

Figure 4.1 (a) SEM and (b) TEM images of the synthesized ZIF-8 samples.

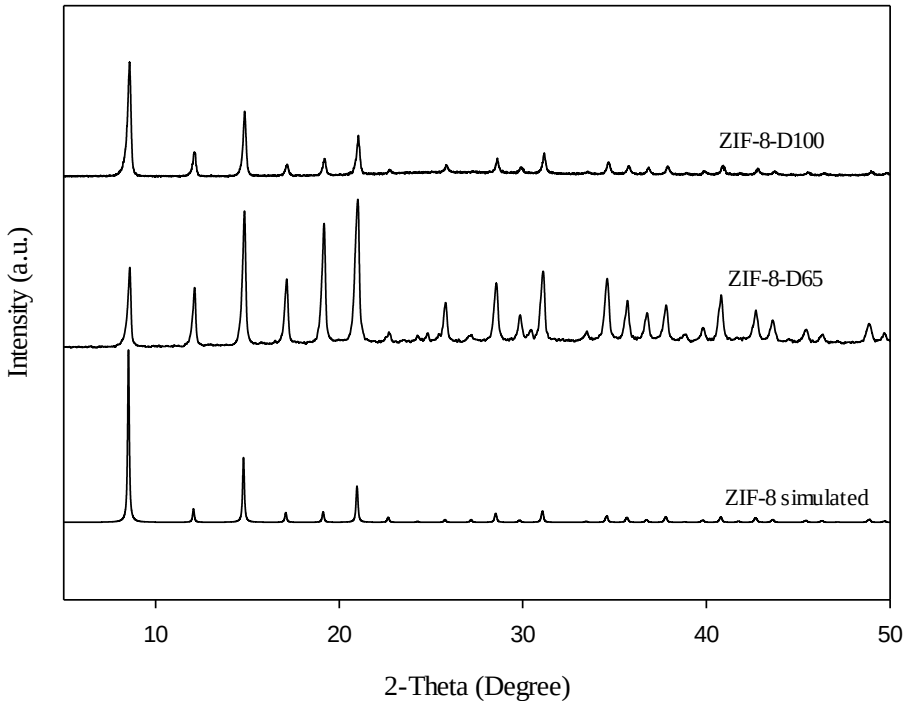

Figure 4.2 XRD patterns of the synthesized ZIF-8 samples and the simulated pattern of ZIF-8.

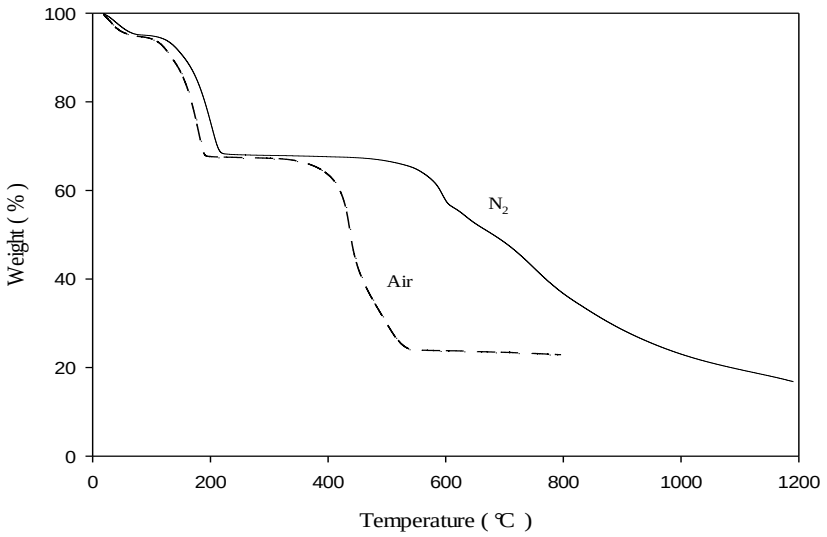

Figure 4.3 TGA results for the ZIF-8-D65 sample.

4.3.2 Thermal Stability Tests

The thermal stability of the ZIF-8 samples was examined at temperatures from 200 ℃ to 500 ℃ under air, argon and steam atmospheres. The powder XRD patterns of the treated ZIF-8 samples are shown in Figure 4.4; these patterns indicate the stability of ZIF-8 under different treatment conditions. The XRD patterns in Figure 4.4a of the ZIF-8 samples treated in air at 200 ℃ for 24 h and at 300 ℃ for 5 h indicate that the samples did not undergo obvious structural alterations compared to the reference ZIF-8 (simulated XRD pattern). However, after the sample were heated in air at 300 ℃ for 24 h and at over 400 ℃ for 5 h, the peaks in the XRD patterns of the ZIF-8 samples disappeared, with the concomitant emergence of characteristic peaks of zinc oxide. These results indicate that ZIF-8 is inappropriate for long-term use in air atmospheres at temperatures greater than 300 ℃, even though the TGA results in Figure 4.3 indicate that the ZIF-8 structure is stable to greater than 350 ℃ under flowing air. In contrast, the structures of the ZIF-8 samples heated at 300 ℃ for 24 h and at 400 ℃ for 5 h under an argon atmosphere were well maintained, as shown in Figure 4.4b, which demonstrates that the ZIF-8 structure is stable under these conditions. Nevertheless, the characteristic XRD peaks of ZIF-8 also disappeared after treatment at 500 ℃ for 5 h under an argon atmosphere. Zinc oxide peaks were not obvious because of the lack of an oxygen source in the inert-gas environment. This result is similarly inconsistent with the TGA results obtained using increasing temperature method, which suggested that ZIF-8 is thermally stable to 500 ℃ under nitrogen, as shown in Figure 4.3. In addition, the ZIF-8 structure of the sample treated under steam at 300 ℃ for 5 h was maintained, although the characteristic peak intensities in the XRD pattern decreased, indicating a dramatic loss of crystallinity, as shown in Figure 4.4c. This loss of crystallinity is most likely caused by hydrolysis between the ZIF-8 ligands and the ambient moisture, which accelerates the decomposition of the ZIF-8 structure [27]. The samples were fully decomposed after exposure to steam at temperatures greater than 400 ℃ for 5 h. Accordingly, we concluded that ZIF-8 was least stable in the steam atmosphere compared to the other two atmospheres.

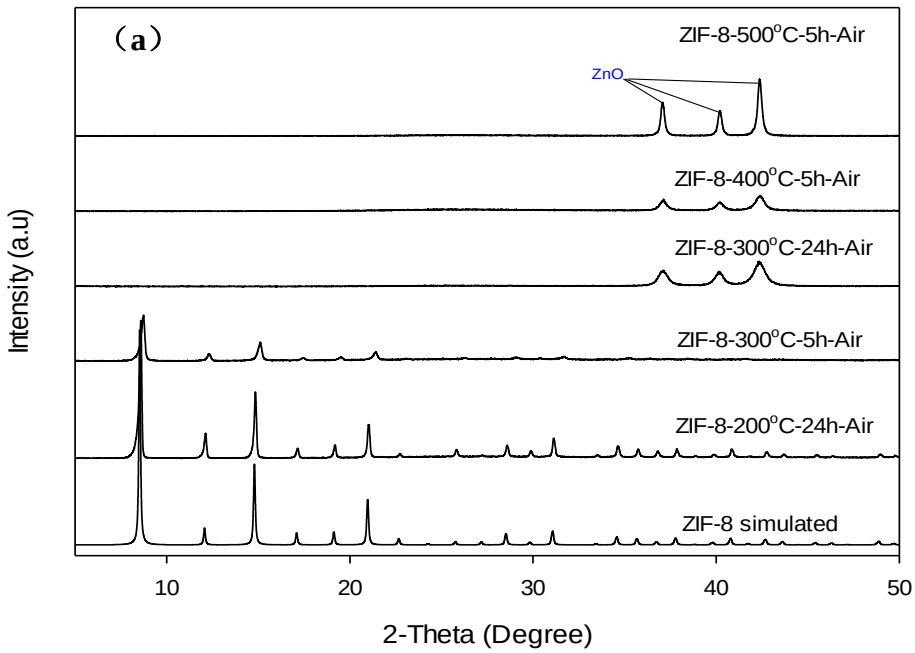
(a)
ZIF-8-500°C-5h-Air
ZnO
ZIF-8-400°C-5h-Air
ZIF-8-300°C-24h-Air
ZIF-8-300°C-5h-Air
ZIF-8-200°C-24h-Air
ZIF-8 simulated
Intensity (a.u)
10
20
30
40
50
2-Theta (Degree)

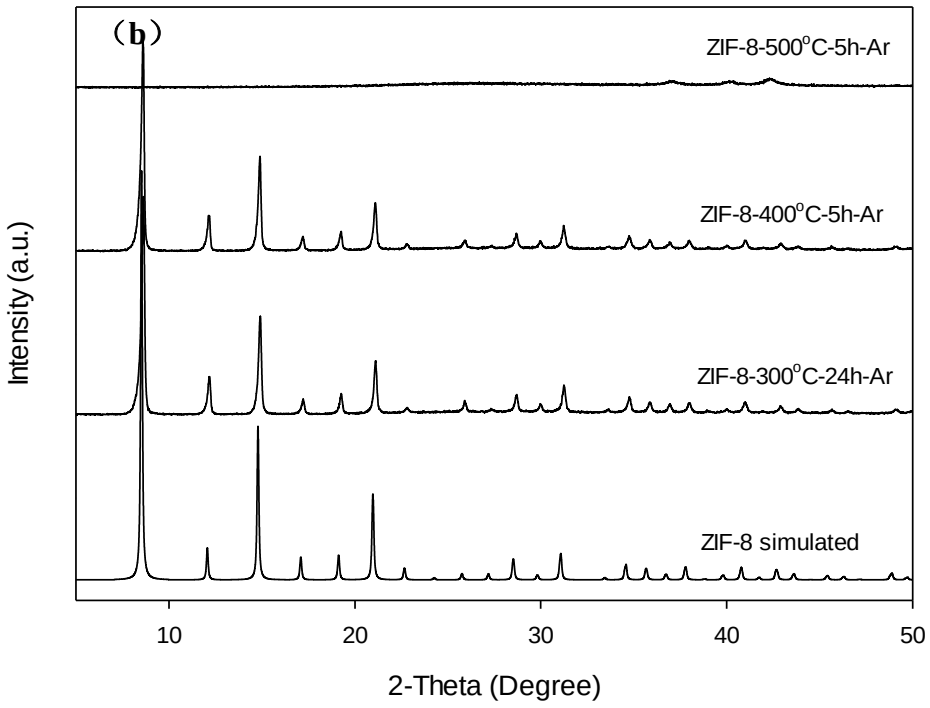
(b)
ZIF-8-500°C-5h-Ar
ZIF-8-400°C-5h-Ar
ZIF-8-300°C-24h-Ar
ZIF-8 simulated
Intensity (a.u.)
10
20
30
40
50
2-Theta (Degree)

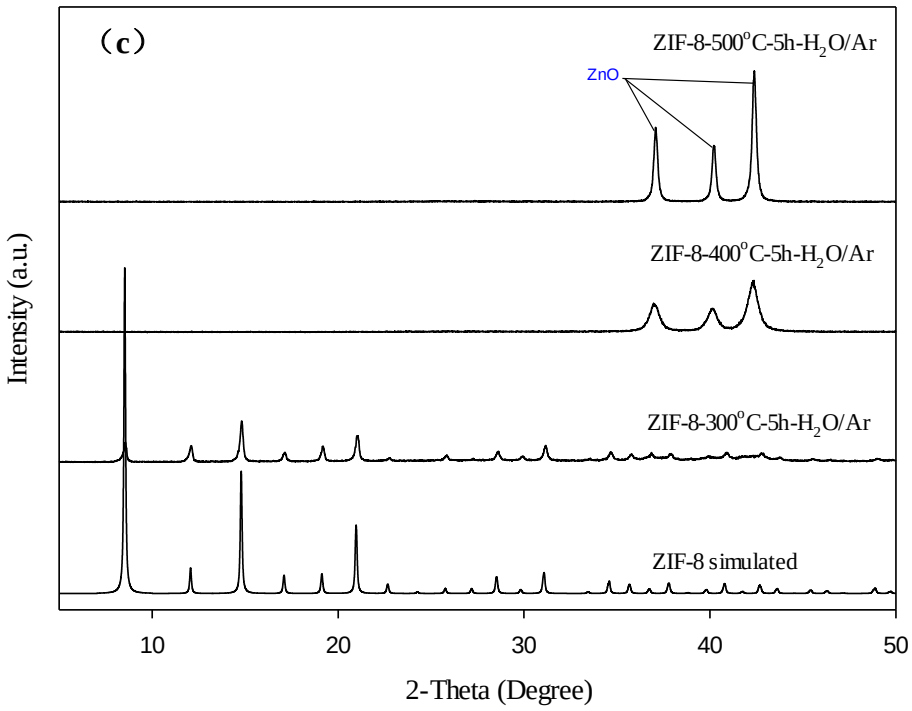

Figure 4.4 XRD patterns of the ZIF-8-D65 sample treated in (a) air, (b) Ar and (c) steam atmosphere at various temperatures and for various durations.

The SEM images corresponding to these treated ZIF-8s are presented in Figure 4.5 and reveal variations in the appearance of the particles after the various treatments. As shown in Figure 4.5a and Figure 4.5d, the samples did not show any obvious variation in appearance compared to the original ZIF-8 samples shown in Figure 4.1a after being treated in air at 300 ℃ for 5 h or in argon at 300 ℃ for 24 h. In contrast, particles with an irregular flocculent shape were observed in the SEM images in Figure 4.5b, Figure 4.5c, and Figure 4.5f, which correspond to the samples treated in air at 300 ℃ for 24 h, in air at 400 ℃ for 5 h, and in steam at 400 ℃ for 5 h, respectively. Notably, the samples treated in argon at 400 ℃ for 5 h (Figure 4.5e) still exhibited the rough appearance of the original ZIF-8; however, the particles size was decreased and became more uniform because of the partial decomposition of the structure. In general, the SEM images agreed well with the XRD results and confirmed the thermal stability trends of ZIF-8 in the described environments.

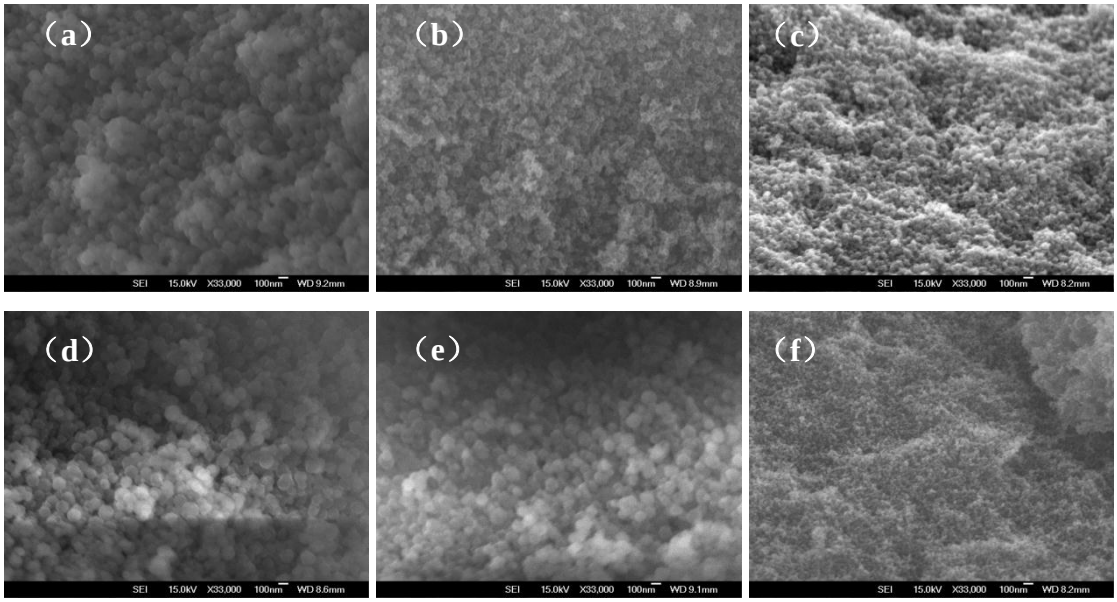

Figure 4.5 SEM images of the ZIF-8-D65 samples treated at (a) 300 ℃ for 5 h, (b) 300 ℃ for 24 h, (c) 400 ℃ for 5 h in air, (d) 300 ℃ for 24 h, (e) 400 ℃ for 5 h in Ar and (f) 400 ℃ for 5 h in steam.

The thermal stability tests indicate that the ZIF-8 is most stable under the argon (inert) atmosphere, where no oxide component exists, followed by the air atmosphere; it exhibited the worst stability under the steam atmosphere. However, the thermal stability of ZIF-8 does not depend only on the treatment temperature and environments; it also depends on the exposure time under respective conditions. Thus, the TGA results acquired using the increasing-temperature method should be recognized as insufficient to evaluate the thermal stability of ZIF-8.

Therefore, to probe the trend of the decomposition of the ZIF-8 structure under the various treatment processes, isothermal TGA tests were conducted under flowing air and nitrogen atmospheres at different temperatures. As presented in Figure 4.6, all the samples exhibited a sharp 30% drop from their original weight during the first minutes as a result of the volatilization of the residual water and organic ligands from the ZIF-8 structure, as previously explained regarding Figure 4.3. After these residual molecules were removed, the weight of the samples remained approximately constant at 300 ℃ under air and at 400 ℃ under nitrogen, with only a slight decrease in weight (an additional 10% of the original weight) after heating for 10 h. These results confirm that

the ZIF-8 structures can be maintained in these environments for at least 10 h. In contrast, the weight of the samples at 400 ℃ under flowing air and at 500 ℃ under flowing nitrogen exhibited substantial weight losses, with only 30% of the original weight remaining after exposure for 4 h; this behavior is identical to the behavior shown in Figure 4.3. These results suggest that the temperature thresholds for ZIF-8 to maintain its structure in oxidative and inert environments are 400 ℃ and 500 ℃, respectively. Although the primary crystal structures of the samples heated at 300 ℃ in air and 400 ℃ in argon for 10 h were maintained, the shape of the resulting ZIF-8 particles as likely to diminish to a certain extent because of the weight loss, as shown in Figure 4.5e, whereas the ZIF-8 structure was fully collapsed when heated for 24 h at 300 ℃ in air, as previously described.

On the basis of these results, we conclude that the ZIF-8 material is suitable for long-term use in applications that involve operation under an inert gas environment at temperatures below 400 ℃ or under air or humid environments at temperatures below 300 ℃.

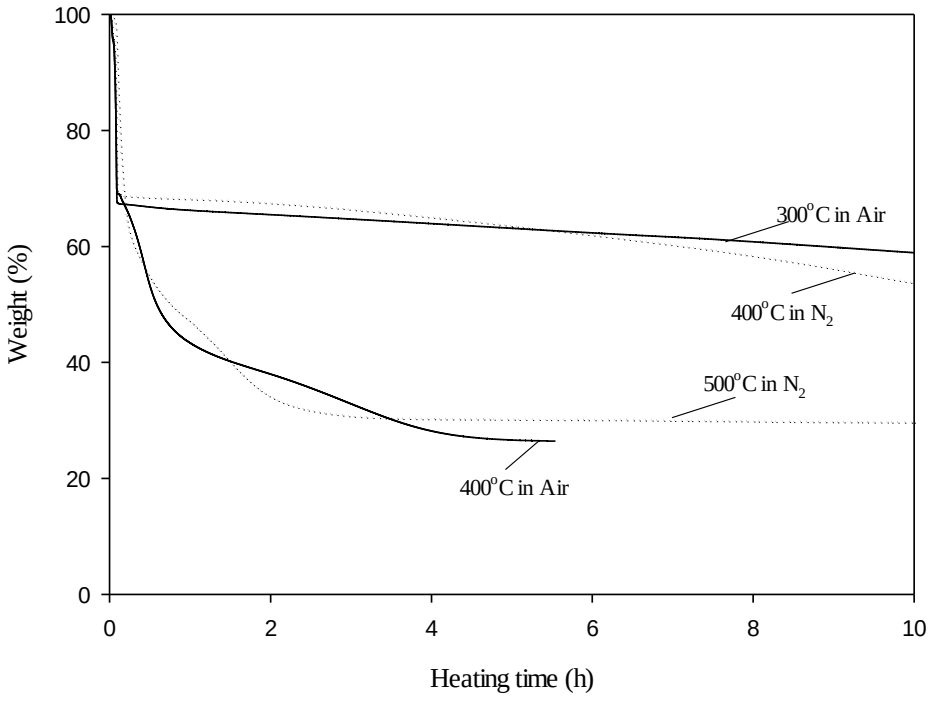

Figure 4.6 Isothermal TGA of the ZIF-8-D65 samples in Air and N_2 at 300 - 500 ℃.

4.3.3 Hydrogen Reduction of Au in ZIF-8 and CO Oxidation over the Reduced Au/ZIF-8 Catalyst

Comprehensive studies of nano-sized Au catalysts have been conducted as Au exhibits excellent catalytic activity toward CO oxidation [28]. Various materials such as metal oxides, zeolites and activated carbons have been used as the supports for Au catalysts [21-23, 28, 29]. In this section, we assess the structural stability of ZIF-8 under the typical preparation conditions of supported Au catalysts (Au/ZIF-8). Au/ZIF-8 was prepared through impregnation of ZIF-8 with gold precursor solution ($HAuCl_4$/ZIF-8), followed by hydrogen reduction at 220 ℃ for 2 h (Au/ZIF-8-220℃-2h), 400 ℃ for 5 h (Au/ZIF-8-400℃-5h) or 400 ℃ for 10 h (Au/ZIF-8-400℃-10h). The selected Au/ZIF-8 was used to catalyze CO oxidation during which the structural stability of the catalyst and its catalytic performance were evaluated.

The TEM images of the $HAuCl_4$/ZIF-8, Au/ZIF-8-220℃-2h, Au/ZIF-8-400℃-5h and Au/ZIF-8-400℃-10h samples are given in Figure 4.7. Figure 4.7a and Figure 4.7b show that the size distribution (average 100 nm) and the crystal shape of $HAuCl_4$/ZIF-8 are very similar to the original ZIF-8 sample (as shown in Figure 4.1a). On the other hand, Figure 4.7c and Figure 4.7d show the general morphology of Au/ZIF-8-220℃-2h and that Au particle with size larger than the pore diameter (1.16 nm) of ZIF-8 were formed. The latter suggests that these Au particles should be located on the external surface of ZIF-8 instead of the channel or within the framework. Some large Au particles with size close to 20 nm resulted from aggregation were also observed (Figure 4.7d). The morphology of the ZIF-8 support changed noticeably after reduction of $HAuCl_4$/ZIF-8 at 400 ℃ for 5 h (Au/ZIF-8-400℃-5h) as shown in Figure 4.7e and Figure 4.7f. The size of Au/ZIF-8-400℃-5h particles decreased slightly as the edges of ZIF-8 support disappeared; while spherical Au particles were also observed. The fragmentary particles (Figure 4.7e) could be due to the partial decomposition of ZIF-8 crystals under heated conditions. Figure 4.7f shows that the average Au particles size in Au/ZIF-8-400℃-5h (approximately 8 nm) was larger than those in Au/ZIF-8-220℃-2h and were distributed evenly on the ZIF-8 structure. Furthermore, Figure 4.7g and Figure 4.7h reveal that the Au/ZIF-8-400℃-10h particles were almost completely decomposed with obvious

aggregation of Au particles. The TEM images indicate that ZIF-8 was not able to maintain the Au particles in its structure at 400 ℃ under H_2/Ar atmosphere. The XRD patterns in Figure 4.8 show that $HAuCl_4$/ZIF-8, Au/ZIF-8-220 ℃-2h and Au/ZIF-8-400 ℃-5h preserved their ZIF-8 structure (compared to the reference patterns), indicating that the supported Au catalyst synthesis procedure via impregnation and the subsequent hydrogen reduction at 220 ℃ for 2 h and at 400 ℃ for 5 h did not alter the crystal phase of the ZIF-8 support. The peak intensities of Au/ZIF-8-400 ℃-5h sample associated with ZIF-8, however, decreased slightly, which indicates a loss of crystallinity to some extent. The results from hydrogen reduction indicate that the Au nano-particles were successfully loaded onto the ZIF-8 support in both Au/ZIF-8-220 ℃-2h and Au/ZIF-8-400 ℃-5h samples. Although the ZIF-8 structure was reasonably stable at 400 ℃ under H_2/Ar atmospheres for as long as 5 h, the Au particles were not completely immobilized under this condition due to weak affinity with the ZIF-8 surface which led to severe aggregation.

CO oxidation was carried out to verify the stability of the Au/ZIF-220 ℃-2h catalyst under an oxidative reaction environment (Figure 4.9). The results show that the catalyst gave a steady CO conversion of 15% in average at 300 ℃ whereas the catalyst activity decreased very rapidly at 400 ℃. This indicates potential structural stability of ZIF-8 at 300 ℃ or below although a minor decrease in conversion was still observed at the initial stage (from ca. 20% to 16% between 2 and 4 h). The large difference between the initial CO conversion at 300 ℃ and 400 ℃ (20% vs 90%) could be attributed to: 1) a much faster reaction kinetic at 400 ℃ and 2) the presence of active Au/ZnO interface resulted from rapid decomposition of ZIF-8 to ZnO at 400 ℃ [29]. The CO conversion at 400 ℃ after 2 h decreased significantly to ca. 20% or below due to the loss of available Au/ZnO interface as Au particles become larger.

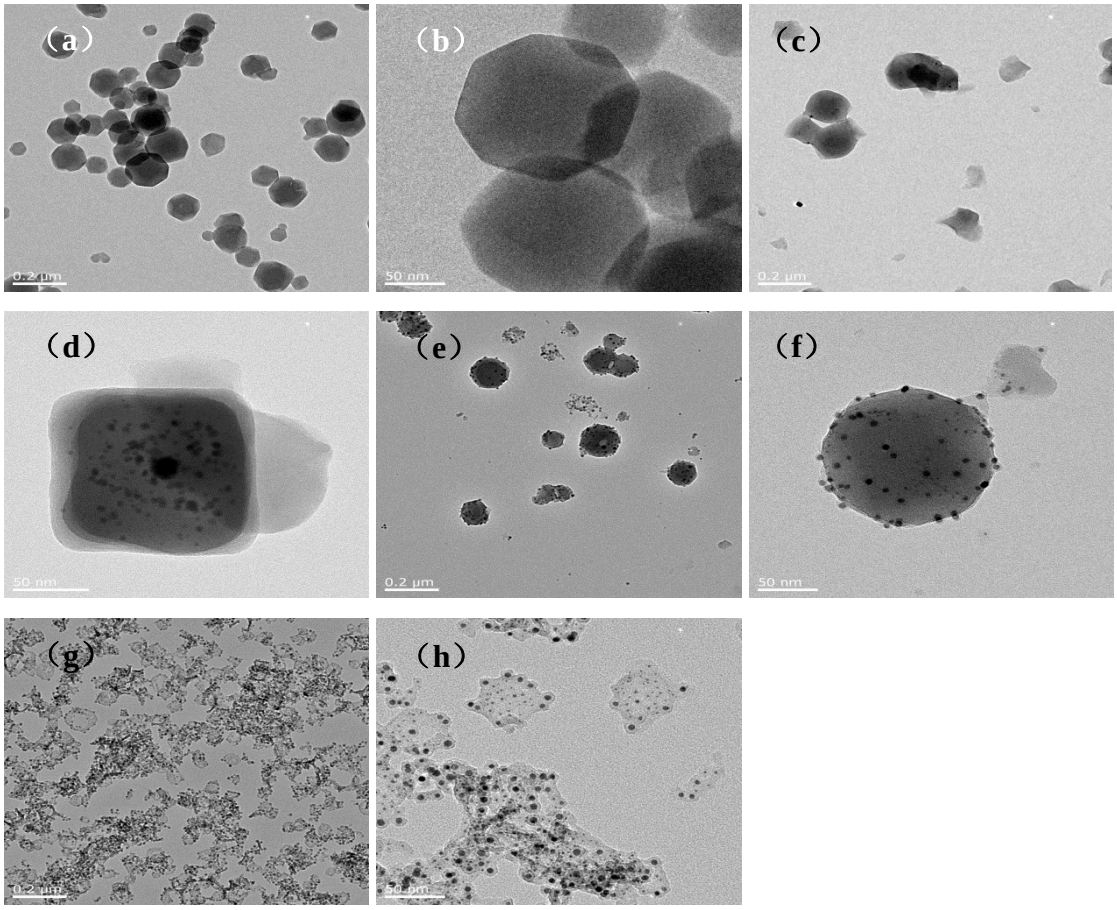

Figure 4.7 TEM images of $HAuCl_4$/ZIF-8 (a and b), Au/ZIF-8-220 ℃ -2h (c and d), Au/ZIF-8-400 ℃ -5h (e and f) and Au/ZIF-8-400 ℃ -10h (g and h).

The XRD patterns of the Au/ZIF-8-220 ℃-2h samples after prolonged period (20 h) of CO oxidation at 300 ℃ and 400 ℃ show that the remaining materials are Au and ZnO resulted from complete decomposition of ZIF-8 (Figure 4.10). The TEM images reveal that most Au particles remained uniform in size (average 15 nm) and were distributed evenly in the decomposed structure after long-term reaction at 300 ℃ (inset of Figure 4.10), while large Au particles (ca. 50 nm) and some fragmentary particles from the support were observed after exposure to oxidative reaction environment at 400 ℃ for 20 h. These results confirmed that progressive modification of the ZIF-8 structure is inevitable during long-term operation at heated conditions, which are consistent with the previous conclusions from the thermal stability tests.

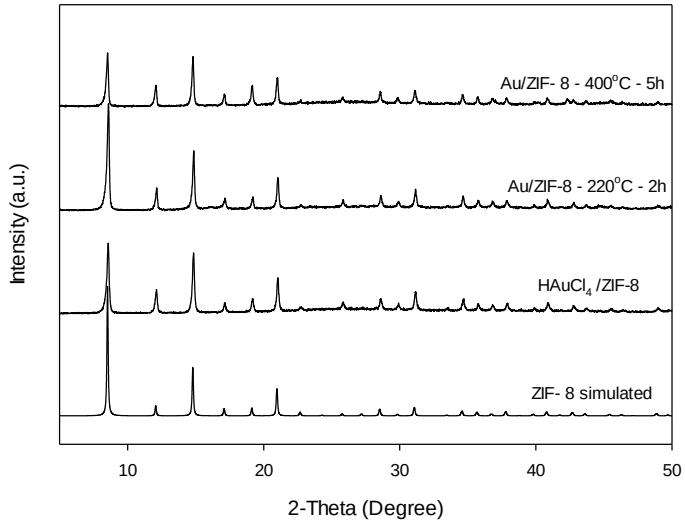

Figure 4.8 XRD patterns of $HAuCl_4$/ZIF-8, Au/ZIF-8-220 ℃-2h and Au/ZIF-8-400 ℃-5h.

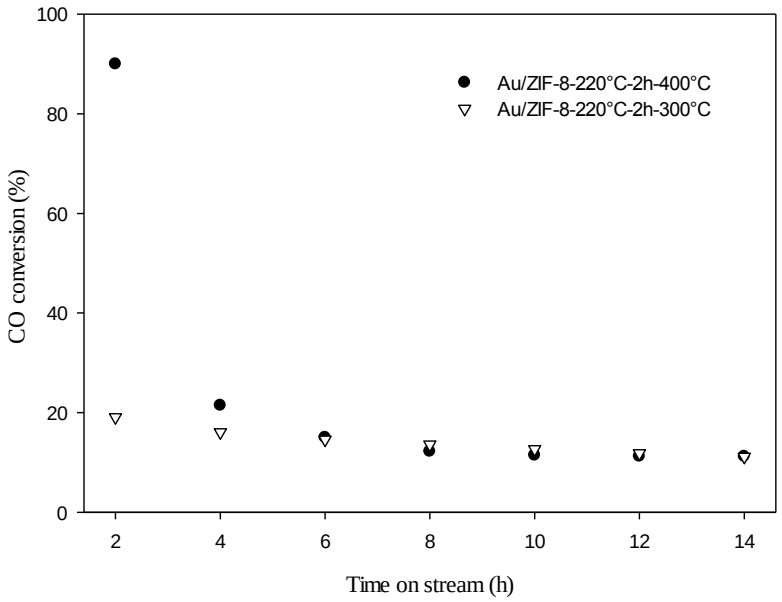

Figure 4.9 CO conversion verse time curves in catalysed CO oxidation over Au/ZIF-8-220 ℃-2h at 300 ℃ and 400 ℃.

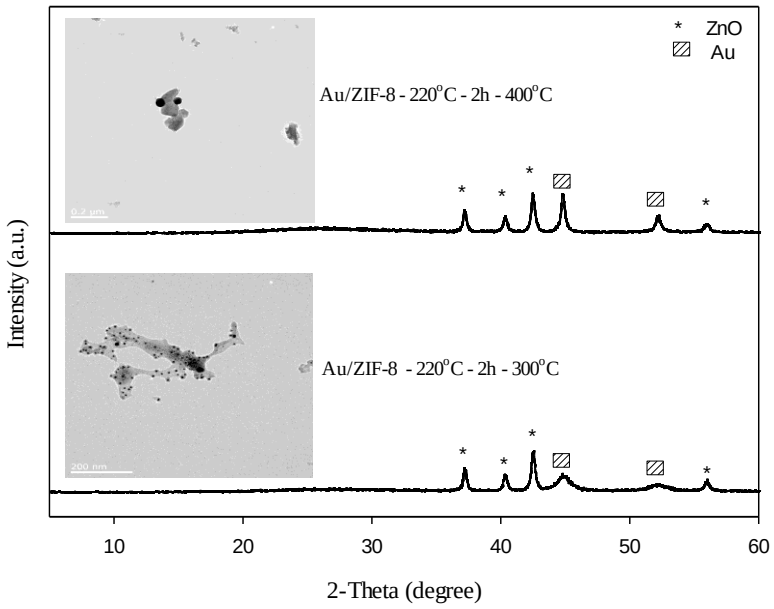

Figure 4.10 XRD patterns and TEM images of Au/ZIF-8-220 ℃-2h after 20 h CO oxidation at 300 ℃ and 400 ℃.

4.4 Conclusions

A comprehensive study was performed to investigate the thermal stability of ZIF-8 under various gaseous environments and to investigate the feasibility of using ZIF-8 in gas-phase applications. In this study, we determined that ZIF-8 exhibits its greatest stability in an inert environment, under which conditions the structure is well maintained when heated at 300 ℃ for 24 h; the next-best stability was observed for ZIF-8 in an air atmosphere, and the worst stability was observed for ZIF-8 under a steam atmosphere. Many TGA results reported in literature regarding the thermal stability of inorganic-organic frameworks could be misleading as the measurement was often carried out for only a short period of time at high temperatures. In this work, isothermal TGA experiments were performed to examine the ZIF-8 decomposition trend in air and nitrogen at different temperatures, these results indicated that the

thermal stability of ZIF-8 depends not only on the treatment conditions but also on the exposure time. We concluded that TGA results could accurately represent the thermal stability of ZIF-8 only if they are recorded isothermally. Furthermore, hydrogen reduction of Au in ZIF-8 and Au/ZIF-8 catalyzed CO oxidation were carried out to verify the structural stability of the framework under general synthesis conditions of supported metal catalysts and oxidative reaction environment, respectively. In summary, ZIF-8 is suitable for use in catalytic reactions and gas-separation processes at temperatures below 300 ℃ in the presence of air or water and under inert gas environments at temperature over 400 ℃. The structural information of ZIF-8 obtained in this work is important and should be considered before one intends to use this framework material in practical situations.

References

[1] S.G. Telfer, What are these things called MOFs?, Chem. in NZ. 74 (2010) 9-14.

[2] H. Li, M. Eddaoudi, M. O'Keeffe, O.M. Yaghi, Design and synthesis of an exceptionally stable and highly porous metal-organic framework, Nature. 402 (1999) 276-279.

[3] S.L. James, Metal-organic frameworks, Chem. Soc. Rev. 32 (2003) 276-288.

[4] J.L.C. Rowsell, O.M. Yaghi, Metal–organic frameworks: a new class of porous materials, Micropor. Mesopor. Mater. 73 (2004) 3-14.

[5] S.T. Meek, J.A. Greathouse, M.D. Allendorf, Metal-organic frameworks: a rapidly growing class of versatile nanoporous materials, Adv. Mater. 23 (2011) 249-267.

[6] H-C. Zhou, J.R. Long, O.M. Yaghi, Introduction to metal-organic frameworks, Chem. Rev. 112 (2012) 673-674.

[7] N. Stock, S. Biswas, Synthesis of metal-organic frameworks (MOFs): routes to various MOF topologies, morphologies, and composites, Chem. Rev. 112 (2012) 933-969.

[8] K. S. Park, Z. Ni, A. P. Côté, J. Y. Choi, R. Huang, F. J. Uribe-Romo, H. K. Chae, M. O'Keeffe, O. M. Yaghi, Exceptional chemical and thermal stability of zeolitic imidazolate frameworks, Proc. Natl. Acad. Sci. USA. 103 (2006) 10186-10191.

[9] M. Shah, H.T. Kwon, V. Tran, S. Sachdeva, H-K. Jeong, One step in situ synthesis of supported zeolitic imidazolate framework ZIF-8 membranes: Role of sodium formate, Micropor. Mesopor. Mater. 165 (2013) 63-69.

[10] J. Cravillon, R. Nayuk, S. Springer, A. Feldhoff, K. Huber, M. Wiebcke, Controlling zeolitic imidazolate framework nano- and microcrystal formation: insight into crystal growth by time-resolved in-situ static light scattering, Chem. Mater. 23 (2011) 2130-2141.

[11] X.C. Huang, Y.Y. Lin, J.P. Zhang, X.M. Chen, Ligand-directed strategy for zeolite-type metal-organic frameworks: zinc(II) imidazolates with unusual zeolitic topologies, Angew. Chem. Int. Ed. 45 (2006) 1557-1559.

[12] J. Cravillon, S. Münzer, S-J. Lohmeier, A. Feldhoff, K. Huber, M. Wiebcke, Rapid room-temperature synthesis and characterization of nanocrystals of a prototypical zeolitic imidazolate framework, Chem. Mater. 21 (2009) 1410-1412.

[13] Y. Pan, Y. Liu, G. Zeng, L. Zhao, Z. Lai, Rapid synthesis of zeolitic imidazolate framework-8 (ZIF-8) nanocrystals in an aqueous system, Chem. Commun. 47 (2011) 2071-2073.

[14] J. Cravillon, C.A. Schröder, H. Bux, A. Rothkirch, J. Caro, M. Wiebcke, Formate modulated solvothermal synthesis of ZIF-8 investigated using time-resolved in situ X-ray diffraction and scanning electron microscopy, CrystEngComm. 14 (2012) 492-498.

[15] H. Bux, F. Liang, Y. Li, J. Cravillon, M. Wiebcke, J. Caro, Zeolitic imidazolate framework membrane with molecular sieving properties by microwave-assisted solvothermal synthesis, J. Am. Chem. Soc. 131 (2009) 16000-16001.

[16] M.C. McCarthy, V. Varela-Guerrero, G.V. Barnett, H-K. Jeong, Synthesis of zeolitic imidazolate framework films and membranes with controlled microstructures, Langmuir 26 (2010) 14636-14641.

[17] X. Liu, H. Jin, Y. Li, H. Bux, Z. Hu, Y. Ban, W. Yang, Metal–organic framework ZIF-8 nanocomposite membrane for efficient recovery of furfural via pervaporation and vapor permeation, J. Mem. Sci. 428 (2013) 498-506.

[18] H. Bux, C. Chmelik, J.M.V. Baten, R. Krishna, J. Caro, Novel MOF-membrane for molecular sieving predicted by IR-diffusion studies and molecular modeling, Adv. Mater. 22 (2010) 4741-4743.

[19] J.J. Low, A.I. Benin, P. Jakubczak, J.F. Abrahamian, S.A. Faheem, R.R. Willis, Virtual high throughput screening confirmed experimentally: porous coordination polymer hydration, J. Am. Chem. Soc. 131 (2009) 15834-15842.

[20] C.O. Ania, E. García-Pérez, M. Haro, J.J. Gutiérrez-Sevillano, T. Valdés-Solís, J.B. Parra, S. Calero, Understanding gas-induced structural deformation of ZIF-8, J. Phys. Chem. Lett. 3 (2012) 1159-1164.

[21] H-L. Jiang, B. Liu, T. Akita, M. Haruta, H. Sakurai, Q. Xu, Au@ZIF-8: CO oxidation over gold nanoparticles deposited to metal−organic framework, J. Am. Chem. Soc. 131 (2009) 11302-11303.

[22] D. Esken, S. Turner, O.I. Lebedev, G.V. Tendeloo, R.A. Fischer, Au@ZIFs: stabilization and encapsulation of cavity-size matching gold clusters inside functionalized zeolite imidazolate frameworks, ZIFs, Chem. Mater. 22 (2010) 6393-6401.

[23] G. Lu, S. Li, Z. Guo, O.K. Farha, B.G. Hauser, X. Qi, Y. Wang, X. Wang, S. Han, X. Liu, J.S. Duchene, H. Zhang, Q. Zhang, X. Chen, J. Ma, S.C.J. Loo, W.D. Wei, Y. Yang, J.T. Hupp, F. Huo, Imparting functionality to a metal–organic framework material by controlled nanoparticle encapsulation, Nat. Chem. 4 (2012) 310-316.

[24] T.T. Isimjan, H. Kazemian, S. Rohani, A.K. Ray, Photocatalytic activities of Pt/ZIF-8 loaded highly ordered TiO_2 nanotubes, J. Mater. Chem. 20 (2010) 10241-10245.

[25] J. Yao, L. Li, W.H.B. Wong, C. Tan, D. Dong, H. Wang, Formation of ZIF-8 membranes and crystals in a diluted aqueous solution, Mater. Chem. Phys. 139 (2013) 1003-1008.

[26] T. Yang, T-S. Chung, High performance ZIF-8/PBI nano-composite membranes for high temperature hydrogen separation consisting of carbon monoxide and water vapour, Int. J. Hydrogen. Energ. 38 (2013) 229-239.

[27] X. Liu, Y. Li, Y. Ban, Y. Pang, H. Jin, H. Bux, L. Xu, J. Caro, W. Yang, Improvement of hydrothermal stability of zeolitic imidazolate frameworks, Chem. Commun. 49 (2013) 9140-9142.

[28] M. Haruta. Nanoparticulate gold catalysts for low-temperature CO oxidation J. New. Mat. Electr. Sys. 7 (2004) 163-172.

[29] Y.S. Bi, G.X. Lv, Advances of catalytic CO oxidation at low-temperature, J. Mol. Catal. (China) 17 (2003) 313-320.

Chapter 5

On the Zeolitic Imidazolate Framework-8 (ZIF-8) Membrane for Hydrogen Separation from Simulated Biomass-derived Syngas

This chapter is published as a journal article

Hang Yin, Hyungmin Kim, Jungkyu Choi, Alex C.K. Yip, Micro. Meso. Mater. (2015) doi:10.1016/j.micromeso.2015.10.033

5.1 Introduction

Biomass is an environmentally friendly renewable energy source that is widely considered as a promising substituent for fossil fuel. Gasification is one of the most attractive biomass conversion technologies for the production of valuable energy products from multiform biomass feedstocks. The primary product of gasification is the producer gas or syngas, which contains hydrogen, carbon monoxide, carbon dioxide, and water vapor. Biomass–derived syngas can be used for power generation, synthesis of Fisher-Tropsch liquid fuel, and other forms of energy after further chemical transformations [1 - 4]. It is noted that the control of the H_2/CO molar ratio and the production of concentrated H_2 are highly desirable for effective utilization of the syngas [5, 6]. New Zealand has abundant biomass resources, including woody waste, agricultural waste, and other commercial crops. Hence, biomass conversion is a promising energy option for New Zealand [7, 8]. In this aspect, a dual fluidized bed (DFB) steam gasifier has been developed as means to produce syngas from biomass resources effectively [1, 3, 4]. In this study, we aim to use the membrane-based separation, which is a promising gas separation technology compared to other traditional methods [9, 10], to produce concentrated H_2 stream in this biomass-derived syngas system.

As a member of metal organic frameworks (MOFs), zeolitic imidazolate frameworks (ZIFs) are novel emerging porous materials composed of divalent metal nodes linked by imidazolate bridging ligands [11 - 16]. ZIF materials are regarded as “zeolitic” because their 145 ° metal-imidazolate-metal angles are very close to the zeolite Si–O–Si angle [14, 17 - 21]. In addition to the general property advantages of most MOF materials, such as the adjustable pore size and the high surface area, ZIFs have high chemical and thermal stability [14, 22, 23]. Over 150 ZIF structures have been developed by incorporating different metals and functional ligand groups, which has resulted in a variety of zeolite-like topologies and special chemical functionalities.

The structure robustness and other advantages make ZIFs promising materials in many application areas, including separation and adsorption [22, 24 - 26], catalysis [27 - 30],

and drug delivery [31]. Among these applications, the most promising utilizations of ZIFs are in separation membranes [32 - 36] and selective sorbents [37]. For example, a supported ZIF-7 membrane was prepared in Caro's group for hydrogen separation and exhibited separation factors for H_2/N_2 of 13.6 and H_2/CO_2 of 18 [32]. A ZIF-8 membrane was fabricated in aqueous solution and was successfully employed to separate a propylene/propane mixture by Lai's group [38]. In addition, a counter-diffusion method was employed for the facile synthesis of ZIF-8 membranes, which showed good propylene/propane separation performance [39]. A 3-aminopropyltriethoxysilane (APTES) - modified ZIF-90 membrane was developed by Huang et al. with a CO_2/CH_4 separation factor of 4.7, which is promising in the application of CO_2/CH_4 separation [40].

ZIF-8 membrane synthesis methods have been investigated and developed under different conditions for many separation applications. In particular, ZIF-8 has a relatively high chemical and thermal stability compared to other MOFs [14]. The pore size of ZIF-8 (~0.34 nm), which is larger than the kinetic diameter of H_2 (0.289 nm) and CO_2 (0.33 nm), but smaller than CO (0.376 nm), N_2 (0.364 nm) and CH_4 (0.38 nm) [41], allows it to be used potentially for gas separation processes in industry [42]. Although the pore size of ZIF-8 is slightly larger than the kinetic diameter of CO_2, ZIF-8 membranes were expected to separate H_2/CO_2 mixtures through the recognition of their size difference [43]. However, modest H_2/CO_2 separation performance has been reported [24, 26, 42, 44], requiring a substantial work on understanding the structural properties of ZIF-8 membranes and thus, improving their separation performances. There are two primary classifications of the synthesis methods: in situ growth [26, 34] and secondary growth [25, 33, 35]. Some innovative procedures have also been developed [45]. The effects of other features in ZIF-8 membrane synthesis have been discussed, including the substrate effect, the solvent effect, and the activation procedure effect. This information has been summarized by Melgar et al. [46] and Pimentel et al [22].

Herein, a ZIF-8 membrane is considered an alternative solution for separating hydrogen from biomass-derived syngas. Although many investigations have focused on ZIF-8

membrane fabrication and development, the complex mechanisms of ZIF membrane formation cause difficulties in the reproducible control of the outstanding performance of the synthesized ZIF-8 membrane. A well-integrated ZIF-8 membrane often requires many synthesis attempts because of the unstable performance of the synthesized membranes. In addition, despite the promising potential of ZIF-8 membranes for H_2 separations and the reported excellent stability of ZIF-8 material, the hydrothermal stability of ZIF-8 membranes remains uncertain under the application conditions, especially in biomass-derived syngas environments with the presence of steam. In this study, a post-treatment procedure was proposed to provide a simple, feasible way to improve the ZIF-8 membrane fabrication process and repair the imperfect ZIF-8 membrane. Moreover, the gas permeation performance of the post-treated ZIF-8 membrane was examined by single gas permeation at room temperature and mixture gas permeation at different temperatures in a simulated biomass-derived syngas environment both with and without the presence of steam. To the best our knowledge, the hydrothermal stability of the ZIF-8 membrane was for the first time studied via a long-term operation under simulated humid syngas environments at 200 ℃.

5.2 Experimental

5.2.1 Materials

Zinc chloride (99.9%) was purchased from Ajax Chemicals. Zinc nitrate hydrate (>99.99%), 2-methyimidazole (Hmim), methanol (>99.8%), and sodium formate were purchased from Sigma-Aldrich Chemical Co. All chemicals were used as received without further treatment. For permeation tests, instrument-grade hydrogen, nitrogen, argon, carbon dioxide, carbon monoxide, and a simulated biomass-derived syngas with a gas composition of 50 vol% H_2, 25 vol% CO and 25 vol% CO_2 were purchased from BOC. Deionized (DI) water was produced in a lab-based reverse osmosis water treatment plant.

5.2.2 ZIF-8 Membrane Fabrication and Post-treatment

5.2.2.1 *Seed Synthesis*

Nano-sized ZIF-8 crystals were synthesized according to the method of Cravillon et al [18]. In general, 0.386 g $Zn(NO_3)_2$ $6H_2O$ and 0.4175 g Hmim were dissolved in 25 ml methanol. The Hmim solution was then added to the Zn solution with stirring for 30 min at room temperature. The mixture was then aged under a static condition for 24 h to form the colloidal ZIF-8 seeds. The solid crystals were collected by centrifuge and were washed with methanol 3 times. Subsequently, the ZIF-8 seeds were dried in a vacuum oven at 50 ℃ overnight. Finally, a 0.1 wt% seeding solution was obtained by dispersing the ZIF-8 powder in methanol under ultrasonication.

5.2.2.2 *Membrane Fabrication*

A porous α-alumina disc support of 3 mm thickness and 22 mm diameter was prepared by hydraulic pressing followed by programmed temperature calcination. Prior to being seeded, the support was polished with fine sandpaper to obtain a smooth seeding surface and was then washed in an ultrasonic water bath. After the support was dried at 120 ℃, it was dip-coated in the prepared seed solution for 10 seconds 2 times and dried in an oven at 80 ℃ overnight.

The secondary growth solution was prepared according to the method reported by Bux et al [24]. In detail, 0.5460 g $ZnCl_2$, 0.2781 g $NaHCO_2$, and 0.4698 g Hmim were dissolved in 40 ml methanol under ultrasonication for 1 min and were then stirred for 5 min. The clear solution was carefully poured into a Teflon-lined autoclave with the seeded support loaded vertically. The autoclave was treated in an oven at 120 ℃ for 6 h. After the autoclave was cooled to room temperature, the membrane was removed and washed with methanol. Finally, the membrane was dried at room temperature for 24 h.

5.2.2.3 *Post-treatment of the Imperfect Membrane*

The dried ZIF-8 membrane was considered an imperfect membrane if it did not have a reasonable H_2/N_2 separation factor in the single gas permeation test. Then, post-

treatment was performed in the following two steps to refine the membrane. First, the imperfect membrane was gently polished to smooth the membrane surface with fine sandpaper (#1600). If it was still an imperfect membrane after the polishing treatment, then the following 2nd step was carried out. The membrane surface was further polished to deliberately break the top thin layer of the ZIF-8 membrane into small ZIF-8 particles, regenerating a uniform ZIF-8 seeded support layer. Subsequently, a 2nd membrane synthesis was conducted by repeating the procedures in section 5.2.2 followed by the polishing post-treatment. This post treatment procedure is like what has been reported by Tao et al [35].

5.2.3 Gas Permeation Test and Characterization

A single gas permeation test was conducted on the system, as shown in Figure 5.1a, at room temperature, and a mixture gas permeation test was performed on the Wiche-Kallenbach system, as shown in Figure 5.1b, at different temperatures. The membrane was loaded into a permeation cell sealed with a silicon o-ring and was then activated under argon flow before testing. In the mixture gas permeation test, the feed gas flow rate was 30 ml/min and the feed/retentate side total pressure (approximately 3 atm) was controlled using a needle valve. On the permeate side, argon was used as the sweep gas to dilute the gas concentration and the total pressure was maintained at 1 atm. The gas compositions of the feed and the permeate streams were analyzed with a gas chromatograph (Buck scientific 910 GC) configured with both a thermal conductivity detector (TCD) and a flame ionization detector (FID). An Agilent ADM 2000 flow meter was used to measure the flow rate in both tests. Scanning electron microscopy (SEM) was performed on a JEOL 700F. X-ray diffraction (XRD) patterns of the samples were collected using a Philips PW1700 instrument equipped with a Co Kα radiation source. The separation factor, $\alpha_{i/j}$ for the gas mixtures was calculated from equation 5-1:

$$\alpha_{i/j} = \frac{y_i / y_j}{x_i / x_j} \qquad (5\text{-}1)$$

where x_i and x_j represent the mole fraction of species i and j in the feed side, while y_i and y_j represent the mole fraction of species i and j in the permeate side.

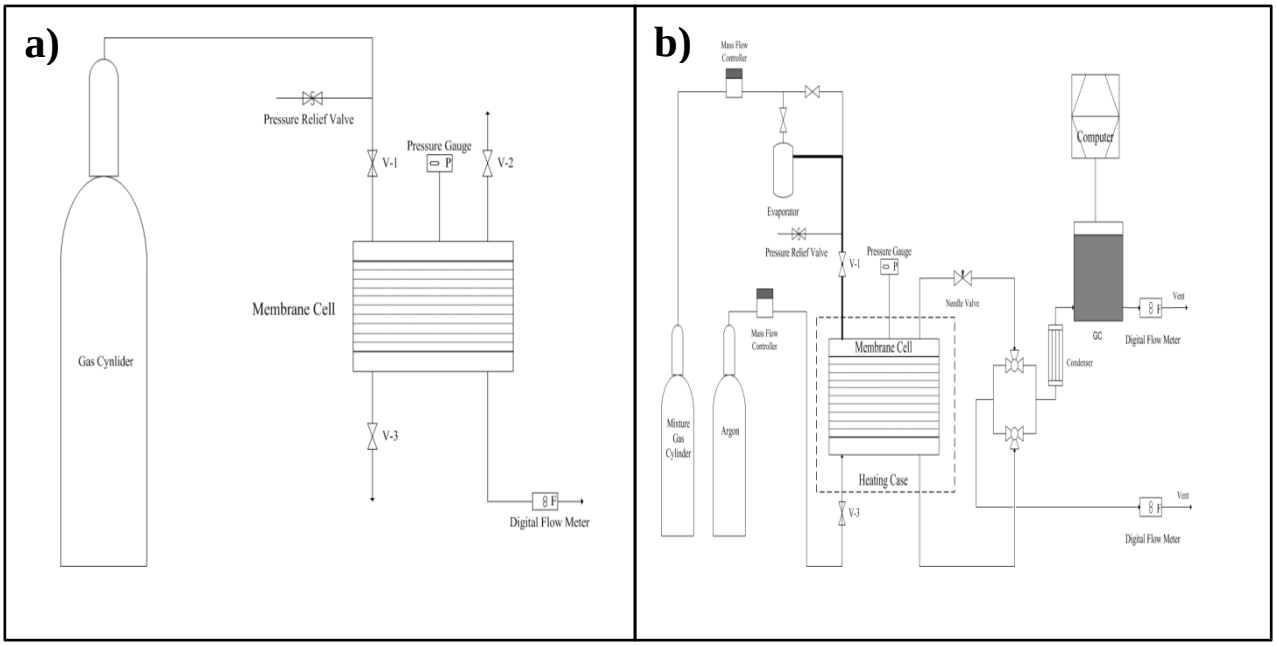

Figure 5.1 Schematic diagram of the gas permeation setup for (a) single gas and (b) mixture gas.

5.3 Results and Discussion

5.3.1 ZIF-8 Membrane Synthesis and Post-treatment

The average size of the synthesized ZIF-8 seeds was approximately 100 nm with a uniform size distribution, as shown in Figure 5.2a. Figure 5.2b and Figure 5.2c show the top surface of the support before and after the seeding procedure, indicating that the support is uniformly covered by the ZIF-8 seeds after the double dip-coating procedure. The single gas permeation results at room temperature are summarized in Table 5.1. The bare support exhibited a pure gas H_2 permeance of 11.5×10^{-6} mol m^{-2} s^{-1} Pa^{-1} and H_2/CO_2, H_2/CO, and H_2/N_2 separation factors of 3.63, 3.08, and 3.02, respectively. These separation factors suggest that gas permeation through the bare support followed the combined mechanisms of Knudsen diffusion and laminar flow [47]. Although the

gas permeances of the imperfect ZIF-8 membrane decreased more than 10 times after the membrane synthesis procedure, the separation factors of H_2/CO_2 and H_2/N_2 were not improved compared with the bare support but rather decreased to 3.03 and 2.59, respectively. The top surface and cross-section SEM images of the imperfect ZIF-8 membrane are shown in Figure 5.2d and Figure 5.2e, respectively. Although a well-integrated membrane layer was likely to be formed on the top of the support, the membrane surface was very bumpy and uneven apparently due to the formation of large ZIF-8 crystals with an average particle size over 20 μm. Figure 5.2d and e reveals that these disordered large ZIF-8 crystals are randomly cross-linked and spread throughout the support, and the membrane thickness is over 40 μm. After polishing the surface of the imperfect ZIF-8 membrane, all of the gas permeances were significantly decreased and in particular, the H_2 permeance was reduced to 20.5×10^{-8} mol m^{-2} s^{-1} Pa^{-1}, which was 3 times lower than that of the imperfect ZIF-8 membrane. Compared to the above-mentioned imperfect ZIF-8 membranes, the H_2/CO_2, H_2/CO, and H_2/N_2 separation factors were improved to 4.79, 8.87, and 13.06, respectively, which were comparable to other reports [46]. It was found that the separation factor of H_2/N_2 was higher than that of H_2/CO, though the kinetic diameter of CO (0.376 nm) was larger than that of N_2 (0.364 nm). The lower H_2/CO separation factor can be ascribed to the stronger CO adsorption compared with weak N_2 adsorption on the ZIF-8 surface [37]. Figure 5.2f shows that the top surface of the 1st polished ZIF-8 membrane was flatter and that the edges of the large ZIF-8 crystals were polished away. At the same time, some debris particles were observed on the polished membrane surface, which were assumed to be the broken ZIF-8 fragments. The cross-section image of the 1st polished ZIF-8 membrane, as shown in Figure 5.2g, demonstrates that the ZIF-8 membrane layer exhibited a reduced thickness of *ca* 20 μm after the polishing post-treatment.

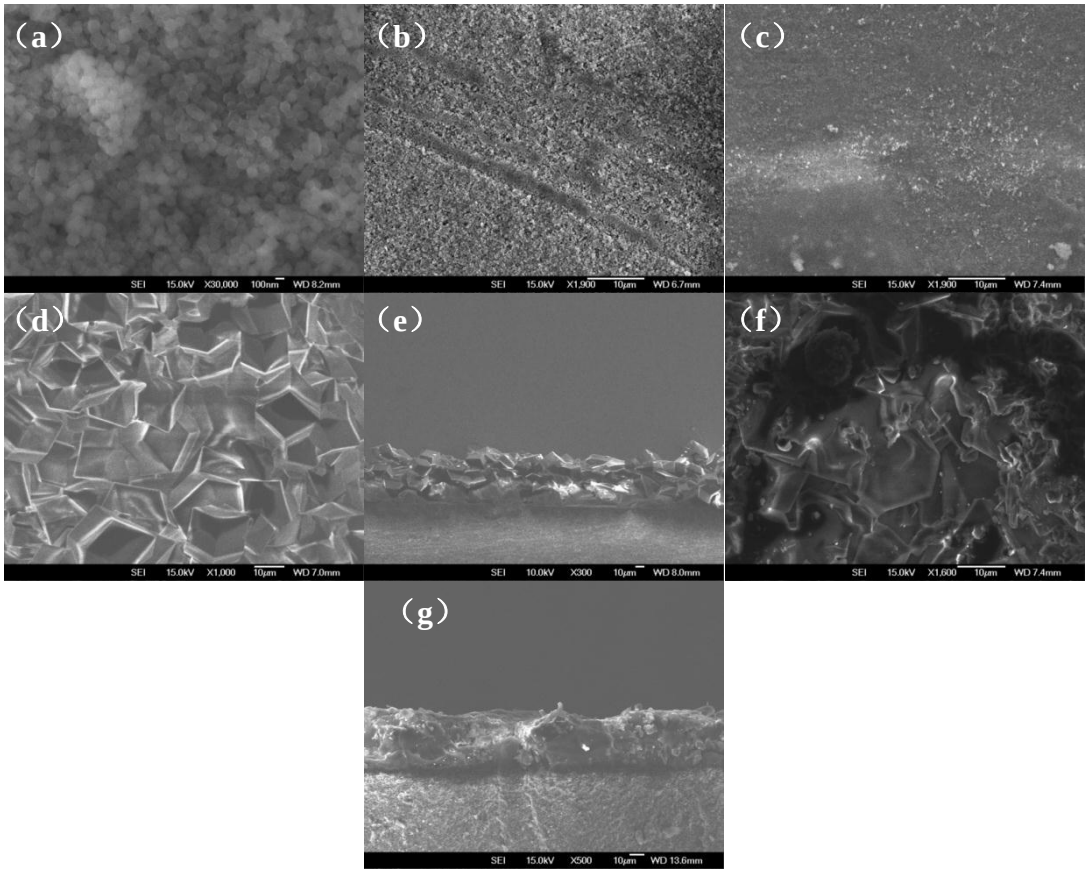

Figure 5.2 SEM images of (a) ZIF-8 seeds, (b) bare α-alumina support, (c) seeded support, (d) top surface and (e) cross-section of the imperfect ZIF-8 membrane, (f) top surface and (g) cross-section of the 1st polished ZIF-8 membrane.

The schematic diagram shown in Figure 5.3 is proposed to explain the effects of the polishing post-treatment. As shown in Figure 5.3a, before the polishing treatment, the roughness of the imperfect ZIF-8 membrane surface could result in a defective contact area between the membrane and the sealing o-ring, possibly generating an undesired shortcut for the permeating gas molecules. Rather than passing along the ZIF-8 membrane thickness to the permeate side, it is easier for the pressurized gas molecules to flow through the defects due to the incomplete sealing, where the transport resistance is smaller. Accordingly, the ZIF-8 membrane failed to achieve the gas separation performance, as expected by the molecular sieve effect. Thus, it resulted in the low separation factors of H_2/CO_2 and H_2/N_2, as reflected by the single gas permeation results of the imperfect ZIF-8 membrane (Table 5.1). In contrast, the polishing post-treatment procedure could eliminate or at least reduce significantly the sealing defects,

allowing for the formation of a flat membrane top layer, as shown in Figure 5.3b. Under this circumstance, the feed gas can be effectively sieved by the ZIF-8 membrane, improving the separation factors of hydrogen to larger molecular gases.

Table 5.1 Single gas permeances of the support and synthesized membranes at room temperature.

Samples	**Pure Gas Permeance (10^{-8} mol / m^2 s Ṗa)**				**Pure Gas Selectivity Factor**		
	H_2	CO_2	CO	N_2	H_2 / CO_2	H_2 / N_2	H_2 / CO
Support	1150	317	375	381	3.63	3.02	3.08
Imperfect Membrane	62.4	20.6	4.28	4.63	3.03	2.59	2.49
Post treatment (1st Polishing)	20.5	4.28	2.31	1.57	4.79	13.06	8.87
Post treatment (2nd time synthesis + Polishing)	20.8	4.63	2.74	1.54	4.47	13.35	7.57

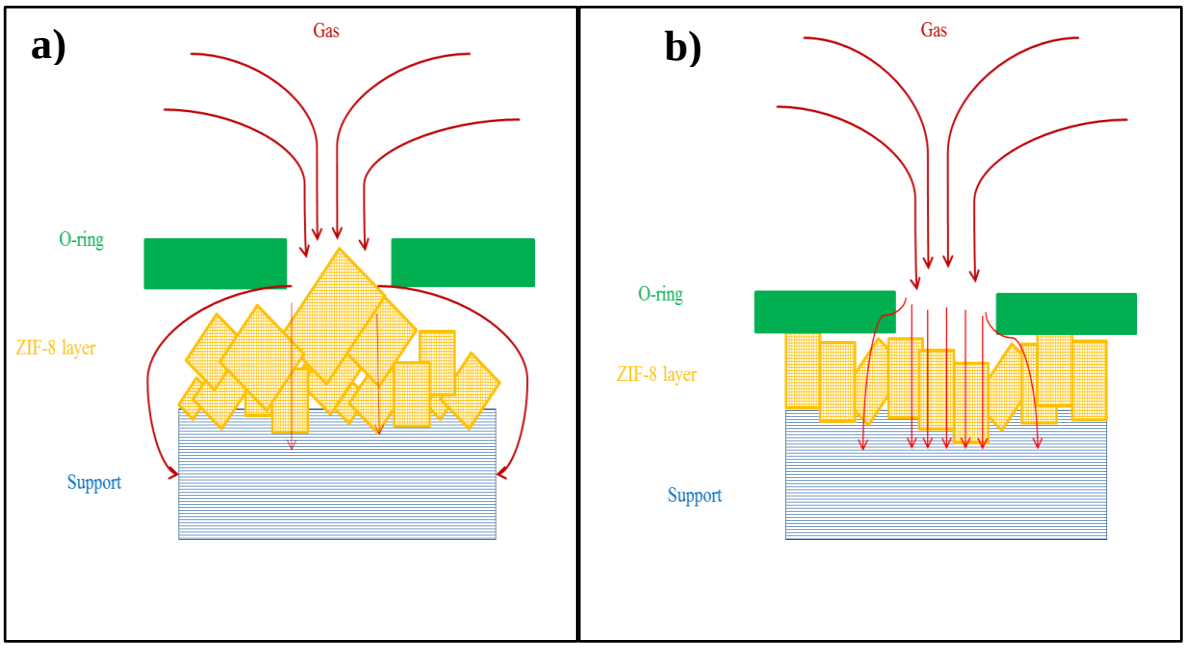

Figure 5.3 Schematic diagram of the gas permeation through the membrane, (a) before and (b) after the polishing post-treatment.

Despite the definite improvement via the polishing treatment, careful and precise control is required during this manual post-treatment process. If the membrane layer is damaged by excessive polishing, it would result in poor H_2 separation performance again. For this case, the 2nd time synthesis post-treatment was conducted in this study in an attempt to repair the membrane for reliable membrane-based H_2 separations. The single gas permeation results obtained through the ZIF-8 membrane after 2nd time synthesis and polishing are listed in Table 5.1. The single gas permeances and gas separation factors of the membrane after the 2nd synthesis and polishing are comparable to those of the 1st polished membrane. It appears that an additional rubbing of the imperfect ZIF-8 membrane produced ZIF-8 seeds effectively by fragmenting the membrane constituents before the 2nd seeded (secondary) growth [35]. In the industrial manufacture perspective, this additional seeded growth is highly desirable, since this post-treatment method can reduce the cost of the supports via repairing membranes that show poor separation performance.

In addition, Figure 5.4 shows the XRD patterns of the ZIF-8 membranes before and after the post-treatments along with those of ZIF-8 seeds and the simulated XRD

patterns of ZIF-8 and α-alumina. At this point, it is worth mentioning that the XRD patterns of the ZIF-8 membranes after the both post-treatments (i.e., both 1st polishing and 2nd time synthesis and polishing post-treatments) were well-preserved, with being comparable to those of imperfect ZIF-8 membranes and ZIF-8 seeds. This indicates that the main ZIF-8 structure in the membrane was well maintained, while removing or reducing defective structures, originally present in the imperfect ZIF-8 membranes, through the post-treatments.

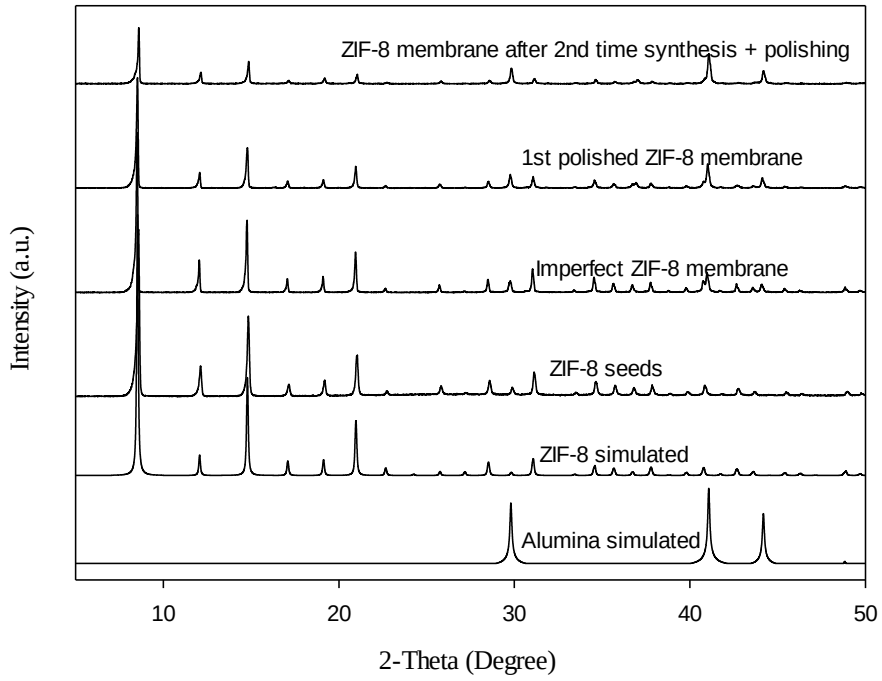

Figure 5.4 XRD patterns of the ZIF-8 seeds, the imperfect ZIF-8 membrane, the 1st polished ZIF-8 membrane and the ZIF-8 membrane after 2nd time synthesis and polishing.

5.3.2 Mixture Gas Permeation

The mixture gas permeation of a ZIF-8 membrane after the 2nd synthesis and polishing was examined at different temperatures with a mixture gas of 50 vol% H_2, 25 vol% CO_2, and 25 vol% CO, which was chosen as a simulated biomass-derived syngas composition without water vapor. As shown in Figure 5.5a, the mixture gas permeances of H_2, CO_2, and CO at 30 ℃ through the ZIF-8 membrane were 13.6×10^{-8}, 4.31×10^{-8}, and 2.89×10^{-8}

mol m^{-2} s^{-1} Pa^{-1}, respectively. These permeation values were decreased 30% for H_2 and CO_2 but slightly increased for CO as compared to the single gas permeation results (Table 5.1). Therefore, the corresponding H_2/CO_2 and H_2/CO separation factors 30 ℃ were 3.05 and 4.53, respectively, which were lower than the ideal selectivities of 4.47 and 7.57, respectively, as a similar trend was reported by Pan et al [33]. The gas permeation variation in the mixture gas can be attributed to 1) competitive adsorption and diffusion when different gases exist in the membrane system and 2) the concentration polarization impact on the feed side of the membrane. As the temperature increased, the gas permeances further decreased for all gases with the lowest degree of reduction for H_2. Therefore, the separation factors of H_2/CO_2 and H_2/CO increased monotonically with temperature. It was noted that the H_2 permeance at 200 ℃ decreased approximately 20%, whereas the CO and CO_2 permeances decreased over 50% compared to their permeances at 30 ℃. As a result, the corresponding separation factors of H_2/CO_2 and H_2/CO increased from 3.05 to 5.14 and from 4.53 to 6.38, respectively. The temperature-dependent gas permeation performance could be explained by the competition between activated diffusion and reduced adsorption with increased temperature [38]. In our case, the gas permeation was primarily in the adsorption-controlled regime, which resulted in the reduction of gas permeances as the temperature increased, especially for the strong adsorption gases CO and CO_2. Though undesirable, we cannot exclude the presence of Knudsen diffusion through the defects in the ZIF-8 membrane, which in turn contributed to decreasing the gas permeances in a partial way.

In a practical syngas environment, water vapor co-exists with the above dry syngas, and thus will affect the gas permeation performance of the ZIF-8 membrane. Here, the mixture gas permeation performance was further investigated under the simulated biomass-derived syngas environment with the presence of 10 vol% steam as temperature was increased up to 200 ℃. The resulting permeation data (Figure 5.5b) indicate that the gas permeance of H_2 was almost constant with temperature, while those of CO_2 and CO decreased monotonically with temperatures, as similar to the permeances in the absence of steam (Figure 5.5a). The lower gas permeances of all the gases than the counterparts under the dry syngas stream can be ascribed to the

condensation and occupation of water molecules in the pore aperture of the ZIF-8 structure, impeding the gas permeation through the ZIF-8 membrane. Nevertheless, the degree of reduction in the gas permeances was not significant for all gases, apparently because of the hydrophobicity of ZIF-8 materials. Specifically, the H_2/CO_2 and H_2/CO separation factors of 4.95 and 6.08 at 200 ℃ were almost close to 5.14 and 6.38, respectively, obtained under the dry syngas stream (Figure 5.5a). As 200 ℃ is the maximum temperature considered in this study and a higher temperature is desirable for energy-saving H_2 separations from the syngas stream, the weak adsorption of water at high temperatures is beneficial for preserving the performance for H_2 separations regardless of water in the feed.

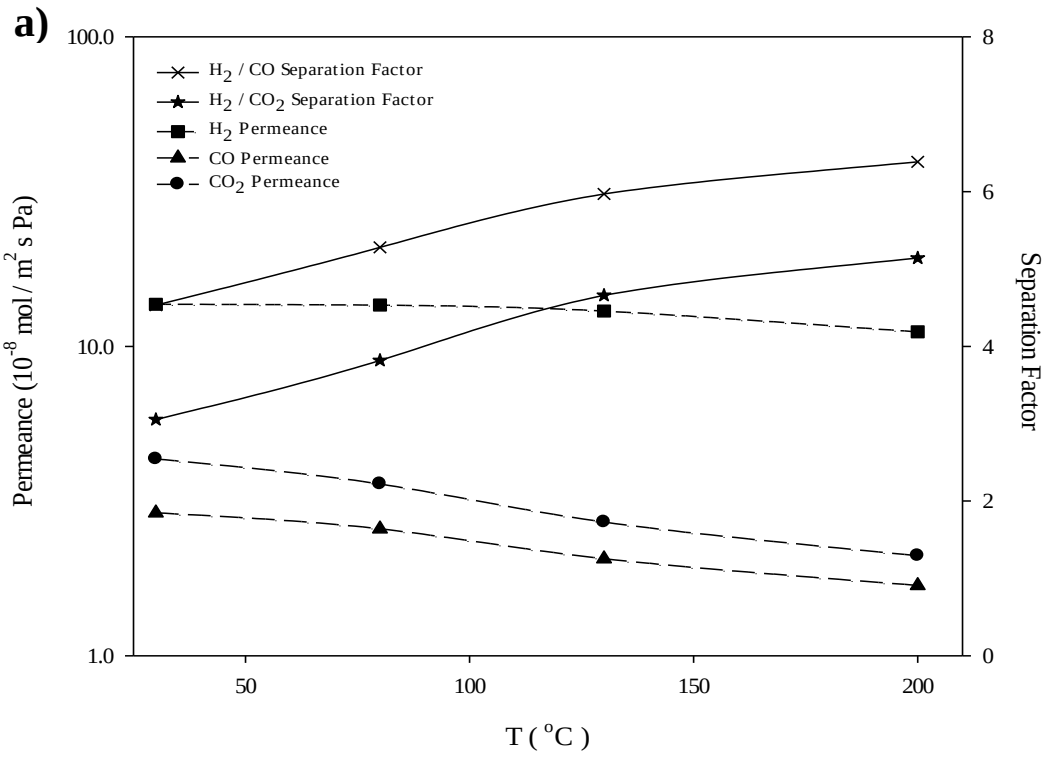

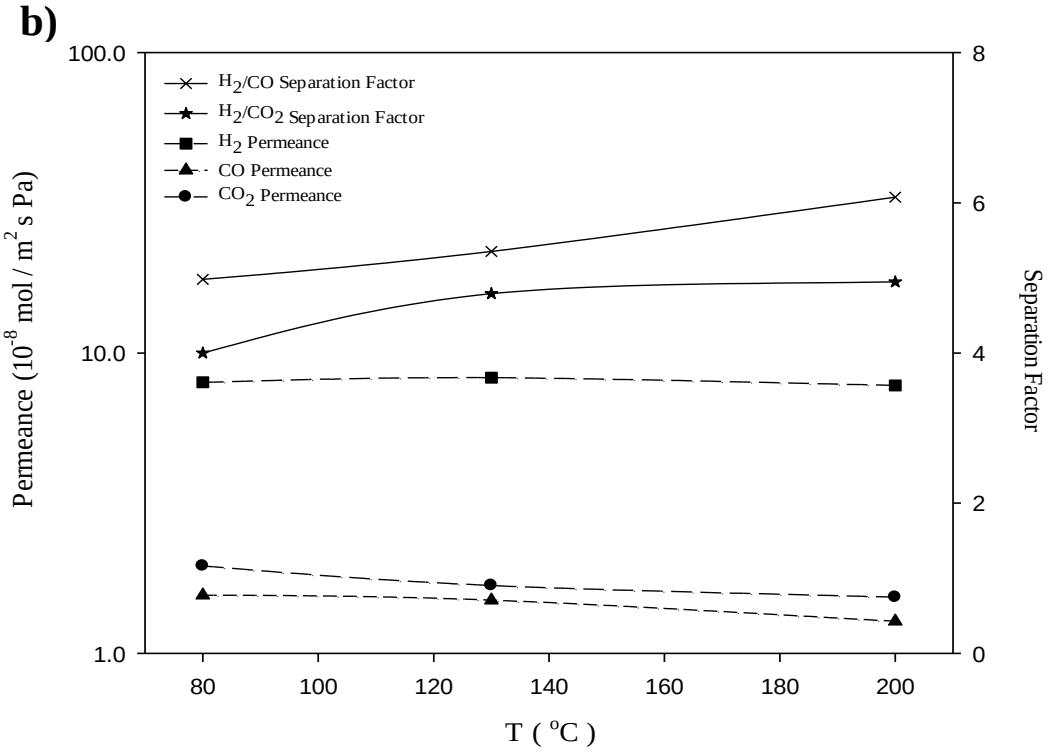

Figure 5.5 Mixture gas permeances and separation factors at different temperatures (a) without and (b) with the presence of 10 vol% steam.

5.3.3 Hydrothermal Stability of the ZIF-8 Membrane

Hydrothermal stability often prohibits many membranes, e.g., silica membranes and polymeric membranes, from being employed in syngas separation applications with the presence of steam. Although the ZIF-8 membrane shows a potential to separate H_2 from CO and CO_2 (Figure 5.5) and ZIF-8 is known as a thermally stable material, to the best of our knowledge, the hydrothermal stability of the ZIF-8 membrane has not been reported under the practical humid syngas environment. As mentioned above, the high hydrothermal stability of ZIF-8s is a key factor to ensure robust H_2 separations. Therefore, we investigated the thermal stability of ZIF-8 particles under various gaseous environments and found that the ZIF-8 structure was least stable under a steam atmosphere [48]. Although similar separation factors that indicate the preferred permeations of H_2 were observed in both dry and wet conditions at 200 ℃, it is

necessary to confirm the applicability of the ZIF-8 membrane for reliable H_2 separations from biomass-derived syngas by investigating the hydrothermal stability under a simulated syngas environment in the presence of steam. To this end, the hydrothermal stability was examined by observing the performance of the ZIF-8 membrane under the simulated syngas environment with the presence of 10 vol% steam at 200 ℃. As shown in Figure 5.6, the gas permeances and separation factors were not significantly changed up to ~10 h. However, all the gas permeances started to increase slowly after 10 h and concomitantly the separation factors were decreased. After 15 h, the H_2 permeance increased by more than 75% and the CO and CO_2 permeances were increased to almost 2 times of their initial permeances, resulting in the H_2/CO_2 and H_2/CO separation factors being lowered to 3.32 and 3.59, respectively. The performance variation indicated that the ZIF-8 membrane have a limitation for membrane-based H_2 separations as it started to lose its molecular sieve functionality after 10 h at 200 ℃ under the simulated biomass-derived syngas environment with the presence of 10 vol% steam. In addition, the single gas permeation test was conducted at room temperature by using the ZIF-8 membrane after the hydrothermal stability test. The gas permeances of H_2, CO, and CO_2 were 35.13×10^{-8}, 14.56×10^{-8} and 10.26×10^{-8} mol m^{-2} s^{-1} Pa^{-1} with the corresponding H_2/CO_2 and H_2/CO separation factors of 3.42 and 2.41, respectively. These separation factors were very close to the single gas permeation results of the imperfect ZIF-8 membrane (3.03 and 2.49 in Table 5.1). Therefore, one may conclude that the ZIF-8 membrane is not able to serve as the H_2-selective membranes for a long-term purpose, since its exposure to the steam-containing syngas environment at 200 ℃ for 15 h resulted in deteriorating the separation performance eventually toward that of the bare supports.

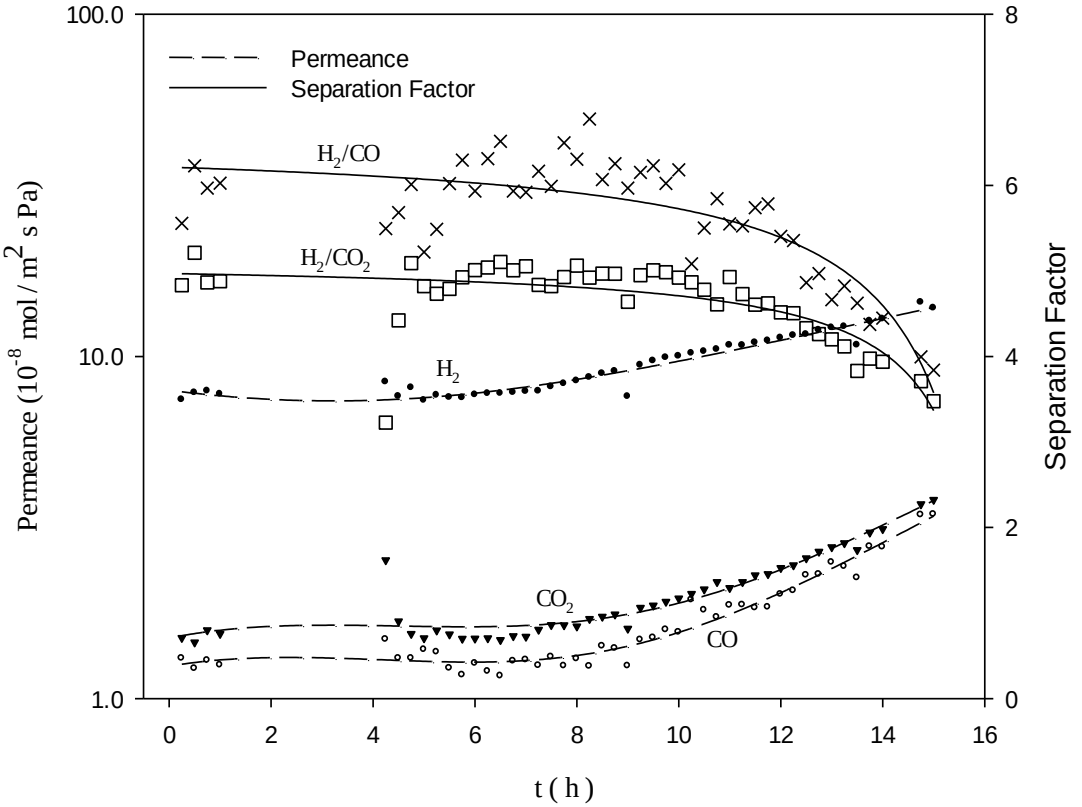

Figure 5.6 Long term mixture gas permeances and separation factors at different temperatures with 10 vol% steam.

The XRD patterns of the ZIF-8 membranes after the hydrothermal stability test were consistent with the simulated ZIF-8 pattern (Figure 5.7), indicating the ZIF-8 structure was still preserved in spite of the lowered H_2 separation performance. Along with the XRD patterns shown in Figure 5.4, this result suggests that the XRD analysis should be complemented with the permeation measurement to draw a proper conclusion relevant to the separation performance of ZIF-8 membranes. As expected, the hydrothermal exposure led to irregular-shaped ZIF-8 grains and cracks on the top surface of the ZIF-8 membranes as shown in the SEM image (Figure 5.8a). Figure 5.8b shows that the membrane thickness of the ZIF-8 membrane was slightly decreased after the hydrothermal stability test. Unfortunately, all these results were consistent with our findings on the thermal stability of ZIF-8 particles [48]. Specifically, the particles with the ZIF-8 structure could be maintained at a temperature lower than 300 °C for 5 h under steam conditions with some loss of its crystallinity, though ZIF-8 structures were

well preserved at the same temperature under inert argon conditions. Considering both the crystallinity and defect are critical for preserving the separation performance of a ZIF-8 membrane, deliberate choices for the reliable use through ZIF-8 membranes should be satisfied; inert conditions will be much beneficial for utilizing the H_2 separation performance of ZIF-8 membranes. At the same time, new approaches need be provided to preserve the H_2 separation performance of intact ZIF-8 membranes.

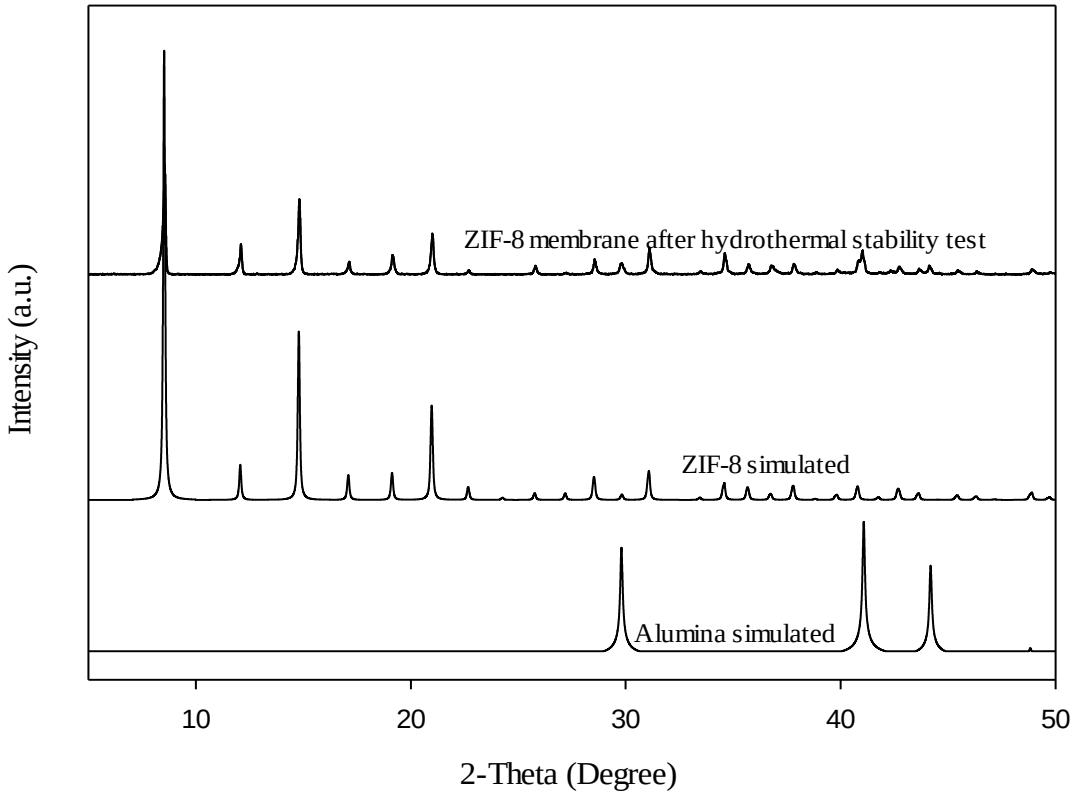

Figure 5.7 XRD patterns of the ZIF-8 membrane after the hydrothermal stability test at 200 ℃ for 15 h.

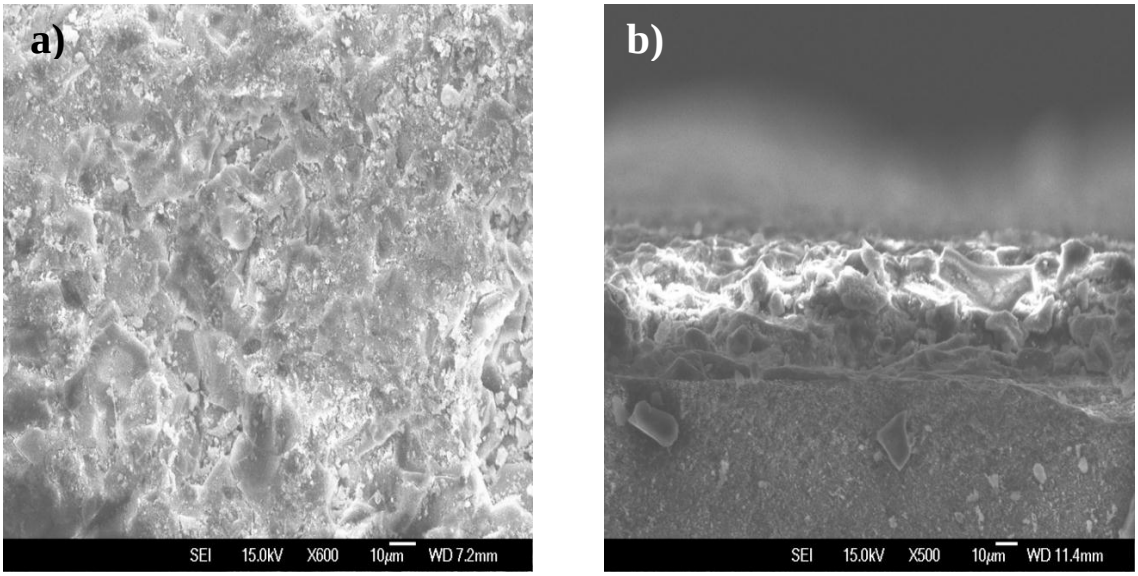

Figure 5.8 SEM images of (a) top surface and (b) cross section of the ZIF-8 membrane after the hydrothermal stability test.

Based on the hydrothermal stability test, we conclude that the ZIF-8 membrane is not suitable for long-term H_2 separations in the biomass-derived syngas environment with the presence of steam at temperatures over 200 °C. Similarly, ZIF-8 membrane applications in the water gas shift reaction and other steam-involved reactions at temperatures of over 200 °C are practically inappropriate. This directs to the need of additional post-treatments that allow for overcoming the low hydrothermal stability of ZIF-8 membranes for their realization in real applications.

5.4 Conclusions

In this study, a zeolitic imidazolate framework-8 (ZIF-8) membrane was successfully prepared with well-developed post-treatment methods. The proposed post-treatment methods, including (1) a polishing and (2) a 2^{nd} time synthesis followed by polishing, repaired imperfect ZIF-8 membranes and thus improved the reliability of ZIF-8 membrane fabrications. The gas separation performance of the post-treated ZIF-8 membrane was examined by single gas permeation at room temperature and subsequently, mixture gas permeation at different temperatures in a simulated biomass-derived syngas environment with and without the presence of steam. The results

demonstrated that the treated ZIF-8 membrane had a modest performance for H_2 separations (H_2/CO_2 and H_2/CO separation factor of 5.14 and 6.38 at 200 °C, respectively) in the simulated environments and the presence of water vapor reduced the permeation rates of all the gases with the similar H_2/CO_2 and H_2/CO separation factors (4.95 and 6.08 at 200 °C, respectively). Finally, the hydrothermal stability of the ZIF-8 membrane was investigated in simulated humid biomass-derived syngas environments. Despite the promise for H_2 separation from CO and CO_2 in the absence and presence of water in the feed, the poor hydrothermal stability limits the ZIF-8 membrane application for long-term H_2 separations in biomass-derived syngas environments over 200 °C. Currently, we are making an effort to propose new approaches that lead to preserving the H_2 perm-selectivity of ZIF-8 membranes under steam-containing feeds at temperatures higher than 200 °C.

Reference

[1] J. Hongrapipat, W.L. Saw, S. Pang, Co-gasification of blended lignite and wood pellets in a dual fluidized bed steam gasifier: The influence of lignite to fuel ratio on NH3 and H2S concentrations in the producer gas, Fuel 139, (2015) 494-501.

[2] J.A. Ruiz, M.C. Juarez, M.P. Morales, P. Munoz, M.A. Mendivil, Biomass gasification for electricity generation: Review of current technology barriers, Renew. Sust. Energ. Rev. 18, (2013) 174-183.

[3] W. Saw, H. McKinnon, I. Gilmour, S.S. Pang, Production of hydrogen-rich syngas from steam gasification of blend of biosolids and wood using a dual fluidised bed gasifier, Fuel 93, (2012) 473-478

[4] W.L. Saw, S.S. Pang, Co-gasification of blended lignite and wood pellets in a 100 kW dual fluidised bed steam gasifier: The influence of lignite ratio on producer gas composition and tar content, Fuel 112, (2013) 117-124.

[5] J. Hongrapipat, W. Saw, S. Pang, Removal of ammonia from producer gas in biomass gasification: integration of gasification optimisation and hot catalytic gas cleaning, Biomass Conv. Bioref. 2, (2012) 327-348.

[6] K. Kumabe, T. Hanaoka, S. Fujimoto, T. Minowa, K. Sakanishi, Co-gasification of woody biomass and coal with air and steam, Fuel 86, (2007) 684-689.

[7] M. Packer, Algal capture of carbon dioxide; biomass generation as a tool for greenhouse gas mitigation with reference to New Zealand energy strategy and policy, Energy Policy 37(2009) 3428-3437.

[8] S. Pang, J. Li, BIGCC system for New Zealand: an overview and perspective, New. Zeal. J. For. 51, (2006) 7-12.

[9] E.E. McLeary, J.C. Jansen, F. Kapteijn, Zeolite based films, membranes and membrane reactors: Progress and prospects, Micro. Meso. Mater. 90, (2006) 198-220.

[10] T. Yang, T.S. Chung, High performance ZIF-8/PBI nanocomposite membranesfor high temperature hydrogen separation consisting of carbon monoxide and water vapor, Int. J. Hydrogen. Energy. 38(2013) 229-239.

[11] S.L. James, Meral-organic frameworks, Chem. Soc. Rev., 32(2006) 276-288.

[12] H. Li, M. Eddaoudi, M. O'Keeffe, O.M. Yaghi, Design and synthesis of an exceptionally stable and highly porous metal-organic framework, Nature. 402 (1999) 276-279.

[13] S.T. Meek, J.A. Greathouse, M.D. Allendorf, Metal-organic frameworks: a rapidly growing class of versatile nanoporous materials, Adv. Mater. 23 (2011) 249-267.

[14] K. S. Park, Z. Ni, A. P. Côté, J. Y. Choi, R. Huang, F. J. Uribe-Romo, H. K. Chae, M. O'Keeffe, O. M. Yaghi, Exceptional chemical and thermal stability of zeolitic imidazolate frameworks, Proc. Natl. Acad. Sci. USA. 103 (2006) 10186-10191.

[15] J.L.C. Rowsell, O.M. Yaghi, Metal-organic frameworks: a new class of porous materials, Micro. Meso. Mater., 73(2004) 3-14.

[16] H.C. Zhou, J.R. Long, O.M. Yaghi, Introduction to Metal –organic frameworks, Chem. Rev., 112(2012) 673-674.

[17] J. Cravillon, S. Münzer, S-J. Lohmeier, A. Feldhoff, K. Huber, M. Wiebcke, Rapid room-temperature synthesis and characterization of nanocrystals of a prototypical zeolitic imidazolate framework, Chem. Mater. 21 (2009) 1410-1412.

[18] J. Cravillon, R. Nayuk, S. Springer, A. Feldhoff, K. Huber, M. Wiebcke, Controlling zeolitic imidazolate framework nano- and microcrystal formation: insight into crystal growth by time-resolved in-situ static light scattering, Chem. Mater. 23 (2011) 2130-2141.

[19] J. Cravillon, C.A. Schröder, H. Bux, A. Rothkirch, J. Caro, M. Wiebcke, Formate modulated solvothermal synthesis of ZIF-8 investigated using time-resolved in situ X-ray diffraction and scanning electron microscopy, CrystEngComm. 14 (2012) 492-498.

[20] X.C. Huang, Y.Y. Lin, J.P. Zhang, X.M. Chen, Ligand-directed strategy for zeolite-type metal-organic frameworks: zinc(II) imidazolates with unusual zeolitic topologies, Angew. Chem. Int. Ed. 45 (2006) 1557-1559.

[21] Y. Pan, Y. Liu, G. Zeng, L. Zhao, Z. Lai, Rapid synthesis of zeolitic imidazolate framework-8 (ZIF-8) nanocrystals in an aqueous system, Chem. Commun. 47 (2011) 2071-2073.

[22] B.R. Pimentel, A. Parulkar, E-K. Zhou, N.A. Brunelli, R.P. Lively, Zeolitic imidazolate frameworks: Next generation materials for energy-efficient gas separations, Chem. Sus. Chem. 7(2014) 3202-3240.

[23] Y.Q. Tian, C.X. Cai, Y. Ji, X.Z. You, S.M. Peng, G.H. Lee, $[Co_5(im)_{10}\cdot 2\,MB]_\infty$: A Metal-Organic Open-Framework with Zeolite-Like Topology, Angew. Chem.-Int. Edit. 41, (2002) 1384-1386.

[24] H. Bux, F. Liang, Y. Li, J. Cravillon, M. Wiebcke, J. Caro, Zeolitic imidazolate framework membrane with molecular sieving properties by microwave-assisted solvothermal synthesis, J. Am. Chem. Soc. 131 (2009) 16000-16001.

[25] X. Liu, H. Jin, Y. Li, H. Bux, Z. Hu, Y. Ban, W. Yang, Metal–organic framework ZIF-8 nanocomposite membrane for efficient recovery of furfural via pervaporation and vapor permeation, J. Mem. Sci. 428 (2013) 498-506.

[26] M.C. McCarthy, V. Varela-Guerrero, G.V. Barnett, H-K. Jeong, Synthesis of zeolitic imidazolate framework films and membranes with controlled microstructures, Langmuir 26 (2010) 14636-14641.

[27] A. Corma, H. Garcia and F.X.L.i. Xamena, Engineering Metal Organic Frameworks for Heterogeneous Catalysis, Chem. Rev., 110(2010) 4606-4655.

[28] J.Y. Lee, O.K. Farha, J. Roberts, K.A. Scheidt, S.B.T. Nguyen, J.T. Hupp, Metal organic framework materials as catalysts, Chem. Soc. Rew., 38(2009) 1450-1459

[29] J. Liu, L. Chen, H. Cui, J. Zhang, L. Zhang, C-Y. Su, Applications of metal–organic frameworks in heterogeneous supramolecular catalysis, Chem. Soc. Rev. 43, (2014) 6011-6061.

[30] H. Yin, J. Choi, A.C.K. Yip, Anti-poisoning core–shell metal/ZIF-8 catalyst for selective alkene hydrogenation. Catal. Today, (2015). http://dx.doi.org/10.1016/j.cattod.2015.08.030

[31] P. Horcajada, C. Serre, G. Maurin, N.A. Ramsahye, F. Balas, M. Vallet-Regi, M. Sebban, F. Taulelle, G. Ferey, Flexible Porous Metal-Organic Frameworks for a Controlled Drug Delivery, J. Am. Chem. Soc. 130, (2008) 6774-6780

[32] Y. Li, F. Liang, H. Bux, W. Yang, J. Caro, Zeolitic imidazolate framework ZIF-7 based molecular sieve membrane for hydrogen separation, J. Membr. Sci., 354(2010) 48-54

[33] Y. Pan, B. Wang, Z. Lai, Synthesis of ceramic hollow fiber supported zeolitic imidazolate framework-8 (ZIF-8) membranes with high hydrogen permeability, J. Membr. Sci., 421-422(2012) 292-298

[34] M. Shah, H.T. Kwon, V. Tran, S. Sachdeva, H-K. Jeong, One step in situ synthesis of supported zeolitic imidazolate framework ZIF-8 membranes: Role of sodium formate, Micropor. Mesopor. Mater. 165 (2013) 63-69

[35] K. Tao, C.L. Kong, L. Chen, High performance ZIF-8 molecular sieve membrane on hollow ceramic fiber via crystallizing-rubbing seed deposition, Chem. Eng. J. 220, (2013) 1-5.

[36] J. Yao, L. Li, W.H.B. Wong, C. Tan, D. Dong, H. Wang, Formation of ZIF-8 membranes and crystals in a diluted aqueous solution, Mater. Chem. Phy., 139(2013) 1003-1008

[37] H.L. Huang, W.J. Zhang, D.H. Liu, B. Liu, G.J. Chen, C.L. Zhong, Effect of temperature on gas adsorption and separation in ZIF-8: A combined experimental and molecular simulation study, Chem. Eng. Sci. 66, (2011) 6297-6305.

[38] Y. Pan, T. Li, G. Lestari, Z. Lai, Effective separation of propylene/Propane binary mixtures by ZIF-8 membranes, J. Membr. Sci., 390-392(2012) 93-98

[39] H.T. Kwon, H.K. Jeong, *In Situ* Synthesis of Thin Zeolitic–Imidazolate Framework ZIF-8 Membranes Exhibiting Exceptionally High Propylene/Propane Separation, J. Am. Chem. Soc. 135, (2013) 10763-10768.

[40] A.S. Huang, Q. Liu, N.Y. Wang, J. Caro, Organosilica functionalized zeolitic imidazolate framework ZIF-90 membrane for CO_2/CH_4 separation, Microporous Mesoporous Mat. 192, (2014) 18-22.

[41] D.W. Breck, *Zeolite Molecular Sieves: Structure, Chemistry, and Use*. 1974: John Wiley & Sons, Inc.

[42] G.S. Xu, J.F. Yao, K. Wang, L. He, P.A. Webley, C.S. Chen, H.T. Wang, Preparation of ZIF-8 membranes supported on ceramic hollow fibers from a concentrated synthesis gel, J. Membr. Sci. 385, (2011) 187-193.

[43] R. Krishna, J.M. van Baten, *In silico* screening of zeolite membranes for CO_2 capture, J. Membr. Sci. 360, (2010) 323-333.

[44] H. Bux, A. Feldhoff, J. Cravillon, M. Wiebcke, Y.S. Li, J. Caro, Oriented Zeolitic Imidazolate Framework-8 Membrane with Sharp H_2/C_3H_8 Molecular Sieve Separation, Chem. Mater. 23, (2011) 2262-2269.

[45] J.F. Yao, D.H. Dong, D. Li, L. He, G.S. Xu, H.T. Wang, Contra-diffusion synthesis of ZIF-8 films on a polymer substrate, Chem. Commun. 47(2011) 2559-2561.

[46] V.M.A. Melgar, J. Kim, M.R. Othman, Zeolitic imidazolate framework membranes for gas separation: A review of synthesis methods and gas separation performance, J. Ind. Eng. Chem., 28(2015) 1-15

[47] K. Keizer, R.J.R. Uhlhorn, R.J. Vanvuren, A.J. Burggraaf, Gas separation mechanisms in microporous modified γ-al_2o_3 membranes, J. Membr. Sci. 39, (1988) 285-300.

[48] H. Yin, H. Kim, J. Choi, A.C.K. Yip, Thermal stability of ZIF-8 under oxidative and inert environments; A practical perspective on using ZIF-8 as a catalyst support, Chem. Eng. J. 278, (2015) 293-300.

Chapter 6
A Proof-of-concept Study of Water Gas Shift Reaction by a ZIF-8-based Membrane Reactor

6.1 Introduction

The membrane reactor (MR) system combines the functions of catalytic reactions and the membrane separation process. By employing the MR system, many benefits could be achieved in some important reactions, like water gas shift reaction (WGSR), hydrogenation/dehydrogenation reactions and catalytic decomposition reactions etc. [1].

Water gas shift reaction (WGSR) is a traditional chemical process which has been employed to produce hydrogen from the hydrocarbons since hundred years ago. As introduced in literature review, WGSR is an exothermic reversible reaction, which means the equilibrium constant of the reaction would decrease with increasing the reaction temperature. At present, the industrial WGSR is always conducted with a series of adiabatic steps, normally combined with high temperature shift (HTS) and low temperature shift (LTS), in order to achieve the high production conversion while maintaining the reaction rate [2 - 5]. Herein, the simple MR system provides an effective strategy for WGSR and could shows the advantages including, higher reaction rate, enhanced equilibrium, improved CO conversion and purified H_2 production [1, 6]. Several studies have conducted in the MR for WGSR in the past years. For example, Battersby et al. used metal doped silica membrane reactor for the low temperature water gas shift reaction and investigated the operation effects to the performance of the membrane reactor [6]. Basile et al. employed palladium membrane reactor for the high temperature water gas shift reaction and found the reaction equilibrium could be successfully switched by removing the products during the reaction [1]. Dong et al. fabricated their MR for WGSR by using a modified ZSM-5 membrane and they also generated a simulated calculator for the WGSR MR system in their study [7]. However, till now, the membranes have been reported for the MR are either too expensive to scale up or structure instable under the WGSR reaction conditions, which limits the development of the membrane reactor in industrial applications.

Hence, based on the insight gained from the previous chapters on the ZIF-8 material and its gas separation membrane, a proof of concept study was conducted with the ZIF-8 based membrane reactor for WGSR in this chapter. The MR conducted in this study was constructed by employing the industrial LTS catalysts ZnO-CuO-Al_2O_3 and the ZIF-8

membrane fabricated as described in Chapter 5. In this study, the improvements on CO conversion and the purification of produced H_2 by employing MR were demonstrated and the stability limitations of ZIF-8 membrane reactor under the WGSR conditions were discussed.

6.2 Methodology

6.2.1 Materials

Zinc chloride (99.9%) was purchased from Ajax Chemicals. Zinc nitrate hydrate (>99.99%), 2-methyimidazole (Hmim), methanol (>99.8%), Sodium Carbonate (>99.5%), copper nitrate trihydrate (>98%), aluminium nitrate nonahydrate (>98%) and sodium formate were purchased from Sigma-Aldrich Chemical Co. All chemicals were used as received without further treatment. For water gas shift reaction, instrument-grade argon and carbon monoxide were purchased from BOC. Deionized (DI) water was produced in a lab-based reverse osmosis water treatment plant.

6.2.2 Sample Preparation

6.2.2.1 ZIF-8 Membrane

ZIF-8 membrane was fabricated, modified and characterized as described in section 5.2.2.

6.2.2.2 The Preparation of $Cu/Zn/Al_2O_3$ Catalysts

$Cu/Zn/Al_2O_3$ catalyst was prepared as described in Giessler's work [8]. In detail, 1.7376g $Zn(NO_3)_2$, 1.0124g $Cu(NO_3)_2 \cdot 3H_2O$ and 1.4797g $Al(NO_3)_3 \cdot 9H_2O$ were dissolved in 20ml DI water at 70 ℃ under stirring. Then, 2.5845g Na_2CO_3 was dissolved in 10ml DI water. Subsequently, the Na_2CO_3 solution was dropped into the nitrate mixture at 70 ℃ under stirring until the pH = 7. After stirring for 1 hour at 70 ℃, the precipitation was collected and washed with vacuum filtration. The filtrate was calcinated in the furnace from 30 ℃ at the temperature ramping rate of 2 ℃/min to

500 ℃ and hold for 3 hours. The final product was grind to fine powder and collected. Prior to the reaction, the catalyst was activated at 220 ℃ for 2 hours in an Ar/stream atmosphere.

6.2.3 The Scheme of the Reactor System

The flow arrangement of the reactor system is shown in Figure 6.1a. In water gas shift reaction (WGSR), 0.025g catalysts were packed into the catalysts chamber located at gas feed side of the membrane reactor cell. Generally, the reactant gas (10 SCCM Ar and 0.5 SCCM CO) was feed through the mass flow controllers, and the reaction pressure (feed/retentate side pressure in MR) was controlled at 30 psi by using the back pressure controller. Moisture was introduced by utilizing the vapour evaporator and the temperature of the water was set at 80 ℃. Meanwhile, 20 SCCM Ar was used as the sweep gas for MR to dilute the gas concentration in the permeate side. Two digital flow meters were used to monitor the online flow rates after the reactor. The gas compositions were analysed with gas chromatograph (Buck scientific 910 GC) configured with both thermal conductivity detector and the flame ionization detector.

The apparatus of the membrane reactor cell was shown in Figure 6.1b. In the case of MR, both V-1 and V-2 valves were open and the sweep gas was introduced through V-1 while the permeate gas flow out through V-2. When the reaction was conducted with packed bed reactor (PBR), both V-1 and V-2 valves were closed and the permeate side of the membrane became a dead end, so the whole membrane reactor cells became a pecked bed reactor configuration.

The CO conversion was calculated by using the equations below [7]

$$\text{For PBR: CO conversion } (\%) = 1 - \frac{X_{CO_{unreacted}}}{X_{CO_{feed}}} \quad [7\text{-}1]$$

$$\text{For MR: CO conversion } (\%) = 1 - \frac{F_{retentate} \cdot X_{CO_{retentate}} + F_{permeate} \cdot X_{CO_{permeate}}}{F_{feed} \cdot X_{CO_{feed}}} \quad [7\text{-}2]$$

The H_2 conversion was calculated by using the equation [7]

$$H_2\,recovery\ (\%) = \frac{F_{permeate} \cdot X_{H_2 permeate}}{F_{permeate} \cdot X_{H_2 permeate} + F_{retentate} \cdot X_{H_2 retentate}} \qquad [7\text{-}3]$$

Where F represents the standard flow rates of the gases and X represents the concentrations of the gases at different flows.

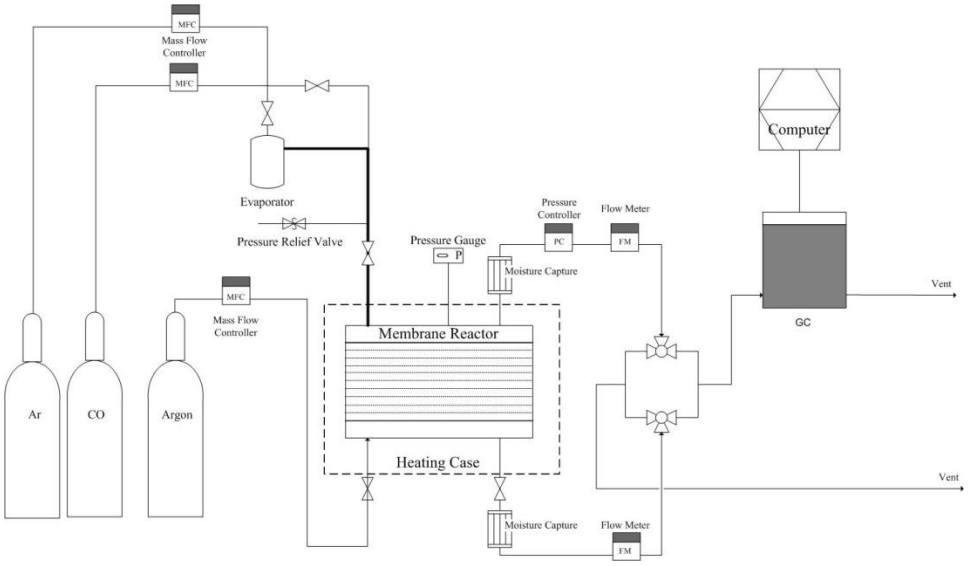

(a)

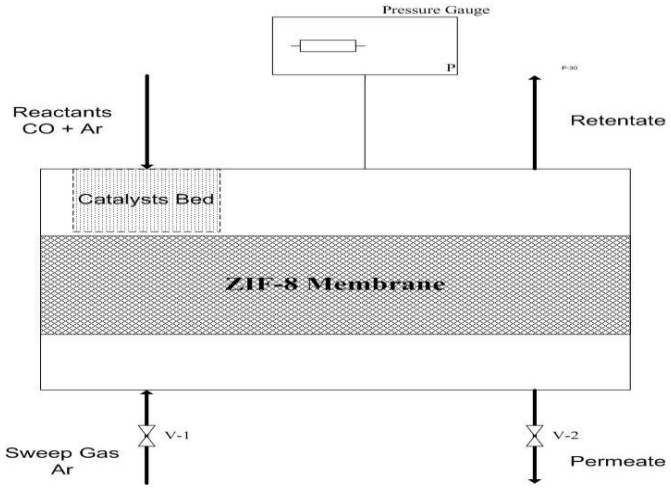

(b)

Figure 6.1 (a) The scheme of the reactor system and (b) membrane reactor cell.

6.3 Results and Discussions

6.3.1 The Improvement of CO Conversion

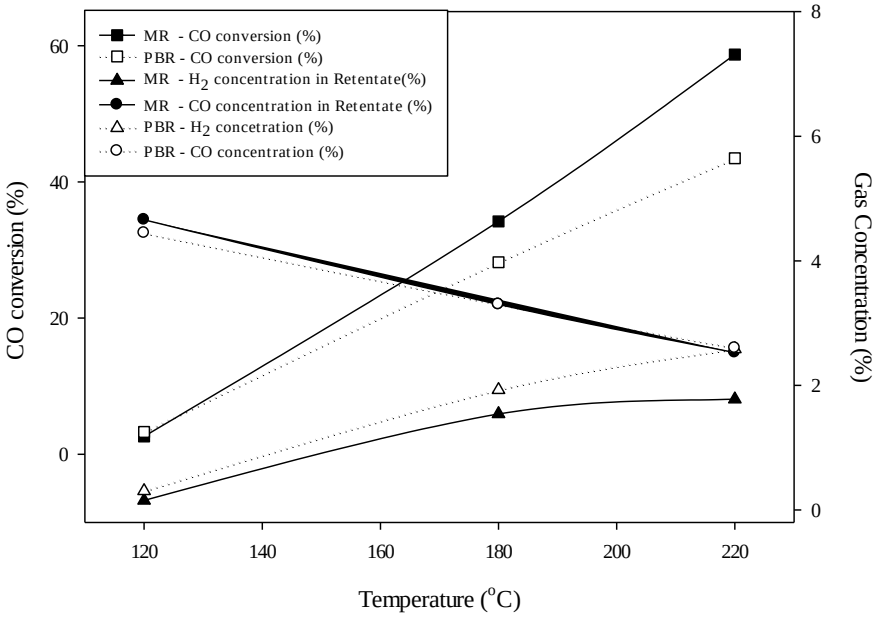

Figure 6.2 CO conversion, hydrogen and CO concentration as the function of temperature in MR and PBR.

As shown in Figure 6.2, the CO conversions in both MR and PBR were improved as the temperature increased, although the CO conversions were still lower than the equilibrium due to reaction rate limitation at high space velocity. However, the CO conversions in MR were still dramatically improved up to 35% compared to that in PBR at 220 ℃. In the meantime, the higher operation temperature resulted with better improvement of CO conversion by utilizing MR system. Besides, a larger hydrogen concentration difference between MR and PBR was observed as the temperature increased, which was caused by the improvement of hydrogen permeance at higher temperature as we reported in section 5.3.2. On the other hand, the CO concentration in MR was slightly lower than in PBR at 220 ℃, otherwise the CO concentrations in MR and PBR were quite close due to the low CO permeance on ZIF-8 membrane. Hence, we could conclude that the CO conversion improvement in MR is mainly contributed to

the lower hydrogenation concentrations in the reaction chamber (retentate side) which in turn improved the reaction rate. The results are consistent with the findings reported by Battersby etc. [6].

6.3.2 The Effect on Hydrogen Recovery and Purification

Figure 6.3 clearly indicates that the hydrogen recovery was significantly increased to over 55% by employing MR at temperature of 220 ℃. To be specific, the H_2/CO ratio in the permeate side of MR was over 3, which was much higher than the ratio of around 1 in PBR at 220 ℃, while the H_2/CO ratio in the retentate side of MR was lower than in PBR. This result implies that the produced H_2 could be captured and concentrated in the permeate side of MR during the catalytic WGSR. Besides, it was more significant of the hydrogen recovery and purification effects by employing MR at higher temperature as shown in Figure 6.3, because of the higher hydrogen permeance as the temperature increased. Hence, the higher purity hydrogen could be obtained by employing the single MR unit for WGSR, rather than the conventional PBR with additional separation and purification steps.

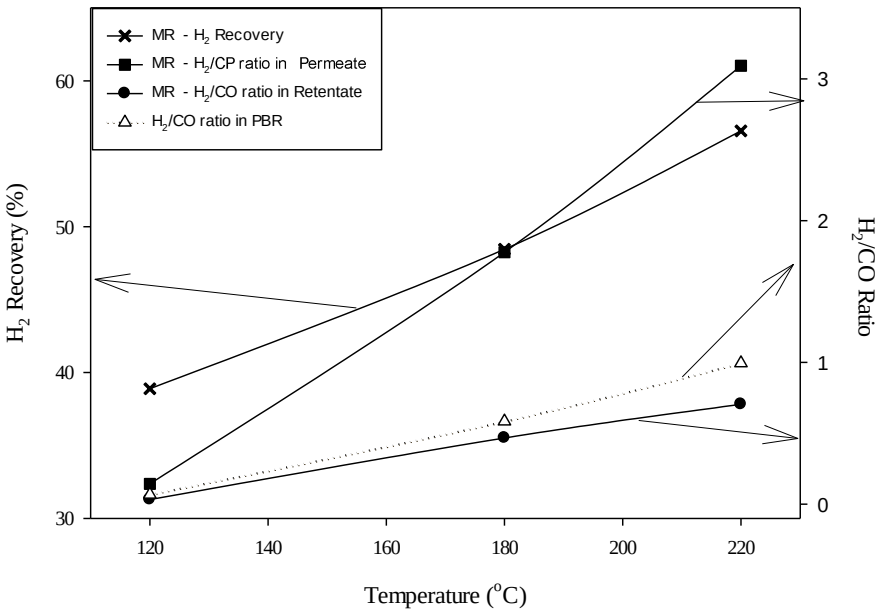

Figure 6.3 Hydrogen recovery as the function of temperature in MR, and H_2/CO ratio as the function of temperature in MR (retentate and permeate) and PBR.

6.3.3 The Stability of ZIF-8 Membrane

The WGSR was sequentially conducted in MR under the temperatures of 120 ℃, 180 ℃ and 220 ℃. As shown in Figure 6.4, the mixture gas permeances through the membrane were firstly determined to be 30.87×10^{-8} and 7.54×10^{-8} mol m^{-2} s^{-1} pa^{-1} for H_2, and CO at 120 ℃, indicating that gas permeances slightly increased compared to their single gas permeation results and mixture gas permeation results in section 5.3.2. On the other hand, H_2/CO separation factors were only 4.09 in this mixture gas system at 120 ℃, which was lower than the single gas separation performance at room temperature. The gas permeation variations in this reaction system could be contributed to 1) the higher moisture concentration in the feed gas stream would induce higher gas permeamce of H_2 and CO, 2) the lower concentrations of the feed gas (H_2 and CO) would reduce concentration polarization impacts on the their permeance and 3) the membrane performance deviations from different batches. While the lower gas separation performance was mainly caused by the higher stage cut (0.25) employed in the MR process in this study [9].

The reaction temperature in MR process was increased to 180 °C and 220 °C at 3 hours and 7.5 hours respectively, in the meantime both H_2 and CO permeances dramatically increased while the H_2/CO separation factors decreased to lower than 2 after reaction was conducted for 13 hours. These results show that the ZIF-8 membrane started to decompose at the temperature of 180 °C and the H_2/CO gas separation performance totally declined after 5 hours at temperature 220 °C. The findings are consistent with the results of the hydrothermal stability of ZIF-8 membrane reported in Chapter 5 and also verify our conclusions about the pessimist of ZIF-8 membrane applications in water gas shift reaction and other steam participated reactions at the temperature over 200 °C.

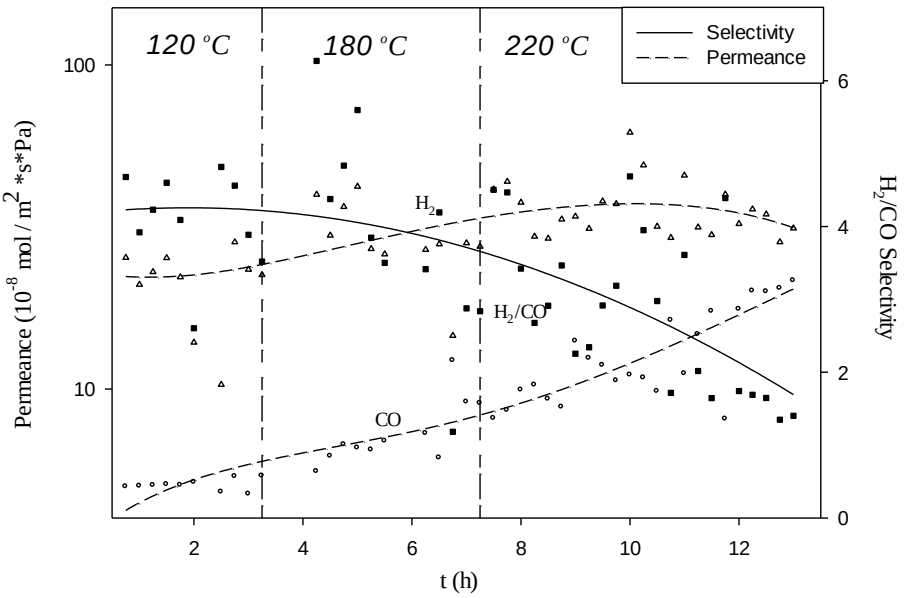

Figure 6.4 The gas permeation performance of ZIF-8 membrane in the MR process for WGSR (■: H_2/CO selectivity, Δ: H_2 permeance, ○: CO permeance).

6.4 Conclusion

The WGSR were successfully conducted through the MR and PBR in this study. The result shows that the CO conversion of the WGSR was improved up to 35% by employing the ZIF-8 based MR compared to that in PBR at 220 ℃, while this CO conversion improvement could be enhanced by increasing the operation temperature. In addition, over 55% of the produced H_2 was recovered in the MR process at 220 ℃ and the higher purify H_2 could be obtained in the permeate side of the MR without additional purification steps. However, the ZIF-8 based MR totally lost its integrity after the WGSR was conducted under the temperature of 220 ℃ for 5 hours, because the ZIF-8 material and its membrane, as we reported in previous chapters, are not hydrothermal stable over the temperature of 200 ℃ and impropriate to be employed for WGSR.

Reference

[1] A. Basile, A. Criscuoli, F. Santella and E. Drioli, Membrane reactor for water gas shift reaction, Gas. Sep. Purif. 10(1996) 243-254

[2] C. Wheeler, A. Jhalani, E.J. Klein, S. Tummala, L.D. Schmidt, The water-gas-shift reaction at short contact times, J. Catal., 223(2004) 191-199.

[3] B.R.J. Smith, M. Loganathan. M.S. Shantha, A Review of the Water Gas Shift Reaction Kinetics, Int. J. Chem. React. Eng., 8(2010) R4

[4] C. Ratnasamy, J.P. Wagner, Water Gas Shift Catalysis, Catal. Rew., 51(2009) 325-440

[5] Y. Choi, H.G. Stenger, Water gas shift reaction kinetics and reactor modelling for fuel cell grade hydrogen, J. Power. Sources., 124(2003) 432–439

[6] S. Battersby, M.C. Duke, S. Liu, V. Rudolph, J.C.D.D. Costa, Metal doped silica membrane reacto: operational effects of reaction and permeation for water gas shift reaction, J. Membr. Sci., 316(1-2)(2008) 46-52

[7] X. Dong, H. Wang, Z. Rui, Y.S. Lin,Tubular dual-layer MFI zeolite membrane reactor for hydrogen production via the WGS reaction: Experimental and modelling studies. Chem. Eng. J. 268(2015) 219-229

[8] S. Giessler, L. Jordan, J.C. Diniz da Costa, G.Q.M. Lu, Performance of hydrophobic and hydropholic silica membrane reactors for the water gas shift reaction, Separ. Purif. Technol. 32(2003) 255-264.

[9] K.L. Chong, N. Peng, H. Yin, G.G. Lipscomb, T.S. Chung, Food sustainability by designing and modeling a membrane controlled atmosphere storage system,. Journal of Food Engineering, 114(2013) 361-374.

Chapter 7

Anti-poisoning Core–shell Metal/ZIF-8 Catalyst for Selective Alkene Hydrogenation

This chapter is published as a journal article

Hang Yin, Jungkyu Choi, Alex C.K. Yip, Catal. Today. 265(2016) 203-209

7.1 Introduction

Metal-organic frameworks (MOFs) are novel emerging hybrid functional materials that consist of crystal lattice structures formed by metal ion nodes and organic ligands. These solid microporous materials have attracted considerable research interest, and various MOF materials have been developed since the archetypal MOF-5 was first reported in the late 1990s [1]. The remarkable inherent properties of these MOF materials, such as extremely high surface areas, outstanding stabilities and tunable pore sizes, provide these materials with potential for applications ranging from gas separation and storage to drug delivery [2 - 8].

The applications of MOF in the field of heterogeneous catalysis have recently received increasing attention. MOFs, which are a promising material in the catalyst industry, exhibit catalytic activity with their active metal nodes or clusters in the frameworks. Furthermore, MOFs can also serve as a catalyst support or host structure [9 - 11]. In particular, MOFs are capable of immobilizing noble metal catalysts in the matrix of their structure, thereby affecting the catalytic activity and selectivity in the reaction [12]. Moreover, many preparation methods, including the encapsulation method [13, 14], the impregnation method [15 - 17], the solid grinding method [18, 19] and the chemical vapor decomposition method [15, 20, 21], have been developed to load catalysts into MOF supports. For example, Lu et al. [13] reported an encapsulation strategy for incorporating nanoparticles within the matrix of zeolitic imidazolate framework-8 (ZIF-8) by adding surfactants to the ZIF-8 synthesis solution and optimizing the ZIF-8 crystallization conditions. Jiang et al. [18] reported a simple grinding method for depositing gold (Au) nanoparticles onto a MOF, and this Au/MOF composite exhibited an outstanding catalytic performance in the CO oxidation reaction. Although many studies on the preparation and applications of catalysts embedded in MOF materials have been conducted, there are still significant challenges for producing catalyst/MOF composites with desired morphologies and specific functionalities. In particular, an effective and feasible synthesis for preparing these composites is extremely desirable.

Herein, we report a synthesis strategy for preparing a core–shell metal/ZIF-8 composite in aqueous solution via initial deposition of the metal catalyst onto the synthesized ZIF-8 support (metal/ZIF-8) by the impregnation method, followed by secondary growth of the ZIF-8 shell layer in aqueous solution with an optimized concentration. With an effective aperture size for molecular sieving (4.0–4.2 Å), this ZIF-8 shell layer selectively allows molecules with the appropriate shape and size to access the metal/ZIF-8 core [22]. The core–shell metal/ZIF-8 (ZIF-8/metal/ZIF-8) catalyst exhibits potential benefits over typical ZIF-8-supported metal catalysts by offering high reactant/product selectivity and anti-poisoning properties when the catalyst is used in the presence of potential poisons such as thiophene. The catalytic performance of the core–shell metal/ZIF-8 catalyst in the hydrogenation of 1-hexene and cis-cyclooctene was examined.

7.2 Experimental

7.2.1 Materials

Zinc nitrate hydrate (>99.99%), 2-methyimidazole (Hmim), palladium nitrate dihydrate (approximately 40% Pd basis), gold (III) chloride trihydrate (>99.99%), sodium borohydride (>98%), methanol (>99.8%), 1-hexene (>99.8%) and cis-cyclooctene (>95%) were purchased from Sigma–Aldrich. Thiophene was purchased from Aldrich Chemical Co. Ethyl acetate (>98%) was purchased from BDH Chemicals and ZSM-5 (CBV2314) was purchased from Zeolyst International. Deionized (DI) water was used to prepare all required samples and solutions. All of the chemicals were used as received without any further treatment.

7.2.2 Sample Preparation

ZIF-8 was synthesized following the method reported by Pan et al. [23] and described in section 4.2.2 of this thesis.

The metal/ZIF-8 core containing approximately 2.5 wt% metal (Au or Pd) was prepared by dispersing ZIF-8 suspension (0.06 g/ml ZIF-8 in 4 ml of methanol for Au/ZIF-8 and 0.05 g/ml ZIF-8 in 5 ml of DI water for Pd/ZIF-8) in 2 ml of metal precursor solution ($HAuCl_4$ in methanol or aqueous $Pd(NO_3)_2$ solution) and the mixtures were stirred for 2 h. Subsequently, a 0.15 mmol/ml sodium borohydride solution (methanol solution for Au/ZIF-8 or aqueous solution for Pd/ZIF-8) was added to the precursor/ZIF-8 solution under vigorous stirring for 30 min at room temperature. The resulting solids were washed and collected by vacuum filtration and then dried overnight in an oven at 80 ℃. The Pd/ZSM-5 composites were prepared following the same method for Pd/ZIF-8.

The core–shell metal/ZIF-8 composites (ZIF-8/metal/ZIF-8) were prepared by dispersing the metal/ZIF-8 composites in the aqueous ZIF-8 solution. The synthesis conditions for the secondary ZIF-8 layer are listed in Table 7.1. After all chemicals dissolved, the solution was placed in a 50 ℃ water bath under stirring for 24 h. Finally, the core–shell metal/ZIF-8 composites were washed and collected by vacuum filtration and then dried overnight in an oven at 80 ℃.

Table 7.1 Compositions of the ZIF-8 synthesis solutions, synthesis temperatures and reaction durations for the core–shell Au and Pd/ZIF-8 composites.

Conditions	**Samples**		
	ZIF-8/Au/ZIF-8 - 1	**ZIF-8/Au/ZIF-8 - 2**	**ZIF-8/Pd/ZIF-8**
Molar ratio (Zn^{2+} : Hmim : H_2O)	1 : 140 : 7139	1 : 140 : 21000	1 : 140 : 21000
Temperature (°C)	60	50	50
Duration (h)	24	24	20

7.2.3 Characterization

Scanning electron microscopy (SEM) and transmission electron microscopy (TEM)

images were recorded using a JEOL 700F and a Philips CM-200, respectively. X-ray diffraction (XRD) patterns of the samples were collected using a Philips PW1700 instrument equipped with a Co K radiation source. The product solution was analysed using a Varian CP-3800 gas chromatograph (GC). Thermogravimetric analysis (TGA) was performed using a SDT Q600 system under a flow of air with a temperature ramp rate of 5 K/min.

7.2.4 Catalytic Alkene Hydrogenation

Catalytic alkene hydrogenation was conducted in ethyl acetate solvent inside an autoclave reactor [13, 24]. In a typical process, Pd/ZSM-5, Pd/ZIF-8 or ZIF-8/Pd/ZIF-8 samples with an equivalent amount of Pd (approximately 0.5 mg) were thoroughly dispersed in 4.5 mL of ethyl acetate solvent under sonication and stirring. Then, 0.25 mL of 1-hexene and 0.25 mL of cis-cyclooctene were added to the mixture under vigorous stirring. In certain experiments, 0.06 mL of thiophene was simultaneously added to the reactor to investigate the catalyst poisoning effect. After the reactor was flushed several times with hydrogen (H_2) to remove the residual air, the reactor was filled with H_2 to 20 psi, and the reaction was conducted at 30 ℃ for 24 h under stirring (350 rpm). Finally, the catalysts were removed from the reaction solution by centrifugation. The filtrate was analysed using a gas chromatograph (GC) equipped with a capillary column (MXT-1, 30 m × 0.53 mm × 1 μm) and a flame ionization detector (FID).

7.3 Results and Discussion

7.3.1 Characterization of the Synthesized Samples

Figure 7.1a presents a SEM image of a ZIF-8 sample prepared using the aqueous rapid synthesis method [23]. The particle size of the synthesized ZIF-8 ranged from 100 nm to approximately 300 nm, which was slightly larger than the reported size of 85 nm [23] as a result of the prolonged ZIF-8 crystallization time during the vacuumed filtration. The SEM image (Figure 7.1b) shows that ZIF-8 has no obvious variation in shape or

size after impregnation with Au particles. As shown in Figure 7.2, the synthesized ZIF-8 and the Au/ZIF-8 composites have identical XRD patterns, and these XRD patterns indicate that the ZIF-8 samples are crystalline. The weak intensity of the synthesized ZIF-8 at $2\theta = 7–8°$ compared to that of the simulated pattern could be due to the presence of residual solvent molecules or organic ligands, which interact with the ZIF-8 structures [17]. As shown in Figure 7.1c and Figure 7.1d, Au particles of approximately 1 nm were uniformly distributed in the ZIF-8 support. Although agglomeration of the Au particles was observed, as shown in Figure 7.1c, the majority of the Au particles were homogeneously distributed in the Au/ZIF-8 sample. Moreover, Figure 7.1e and Figure 7.1f shows the general morphology of the Pd/ZIF-8 sample, in which the Pd particle distribution was less uniform compared to that of Au/ZIF-8. The different metal distribution (Au and Pd) in ZIF-8 was caused by the metal precursor solutions used during the impregnation. The aqueous $Pd(NO_3)_2$ precursor has a lower diffusion and adsorption to the hydrophobic ZIF-8 compared to the $HAuCl_4$ precursor in methanol. As shown in Figure 7.1e, Pd particles agglomerated on the ZIF-8 support and were primarily located near the edge of the ZIF-8 particles. However, as shown in Figure 7.1f, some isolated Pd particles with a size of approximately 1 nm were still present in the ZIF-8 structure. In addition, the XRD patterns presented in Figure 7.2 show that the Au/ZIF-8 and Pd/ZIF-8 samples generally retained the ZIF-8 crystalline structure following impregnation with the metal precursor and reduction in sodium borohydride solutions. The XRD pattern of ZIF-8/Pd/ZIF-8 shows slightly reduced peak intensity at $2\theta = 15°$ and additional small peaks between 2θ of 15° and 18° compared to the simulated ZIF-8 pattern. This may indicate that the presence of Pd particles in the core–shell structure reduced the crystallinity of ZIF-8, specifically near the interface between the shell layer and the core. The unknown new peaks generated at $2\theta = 15–18°$ could be attributed to impurities or trace amount of new crystalline ZIF-8 structures (e.g. mixed-linker ZIF-8) resulted from variation of the imidazolate linker with Pd precursor.

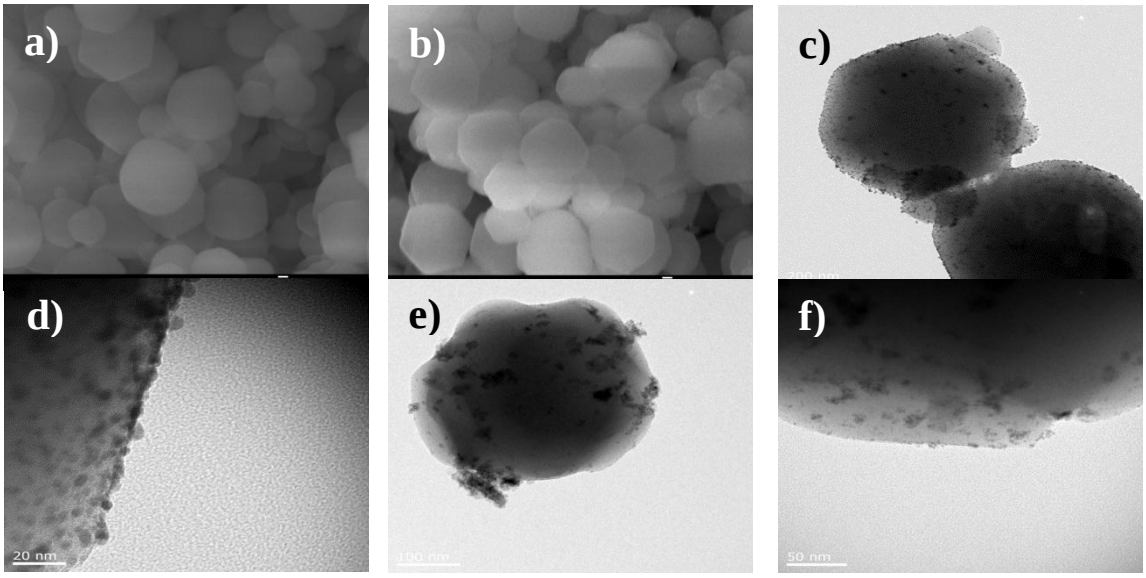

Figure 7.1 SEM images of (a) the synthesized ZIF-8 and (b) Au/ZIF-8, and TEM images of Au/ZIF-8 (c and d) and Pd/ZIF-8 (e and f).

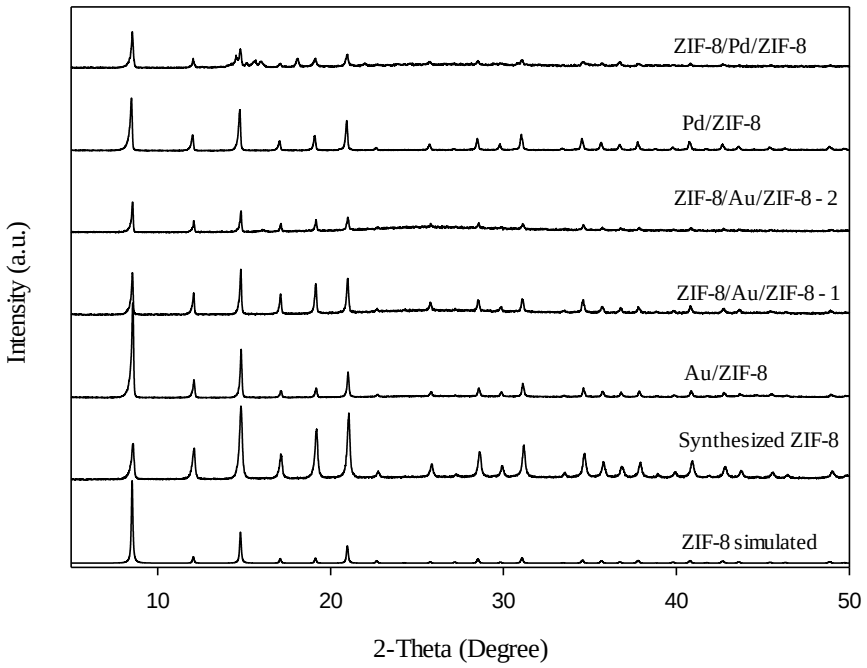

Figure 7.2 XRD patterns of the synthesized ZIF-8, metal/ZIF-8 and ZIF-8/metal/ZIF-8 samples.

The core–shell metal/ZIF-8 composite was synthesized via a secondary growth approach: pre-synthesized metal/ZIF-8 particles were used as the cores of the composite, and a ZIF-8 protective layer crystallized around the metal/ZIF-8 core in the presence of the ZIF-8 crystallization solution. Table 7.1 presents the synthesis conditions for the two core–shell Au/ZIF-8 composites. TEM images of ZIF-8/Au/ZIF-8-1 are presented in Figure 7.3a and Figure 7.3b. Figure 7.3a shows that a thin ZIF-8 shell layer (less than 20 nm) was successfully grown around the Au/ZIF-8 core. A small amount of small pure ZIF-8 particles without a core were observed after the secondary growth step as shown in Figure 7.3b. These pure ZIF-8 particles are expected to diminish and dissolve while the core–shell Au/ZIF-8 particles increase in size due to Ostwald ripening. The TEM image (Figure 7.3c) indicates that all Au/ZIF-8 cores were fully covered by a ZIF-8 shell layer in the ZIF-8/Au/ZIF-8-2 sample. The concentration of the synthesis solution for ZIF-8/Au/ZIF-8-2 was approximately 3 times more dilute than that of ZIF-8/Au/ZIF-8-1 (Table 7.1). The latter conditions with a higher nutrient concentration (ZIF-8/Au/ZIF-8-1) favour direct ZIF-8 crystallization via a nucleation/coalescence route, which results in the formation of individual pure ZIF-8 particles without the Au/ZIF-8 core. The simultaneous crystallization of pure ZIF-8 particles results in less nutrients being available for the secondary growth of the ZIF-8 layer over the pre-formed Au/ZIF-8 cores; thus, a thinner shell layer was obtained for ZIF-8/Au/ZIF-8-1. ZIF-8/Au/ZIF-8-2, however, was synthesized in a dilute crystallization medium in which direct crystallization is prevented and secondary growth via a seeding mechanism becomes dominant. Compared with the crystallization conditions for ZIF-8/Au/ZIF-8-1, heterogeneous nucleation induced by the Au/ZIF-8 cores occurred at a considerably faster rate because the cores provide surfaces for the ZIF-8 crystals to grow on, thereby eliminating the requirement of creating a new surface and minimizing the total surface free energy. The ZIF-8 shell layer of the ZIF-8/Au/ZIF-8-2 sample was thicker (approximately 100 nm) than that of the ZIF-8/Au/ZIF-8-1 sample, as shown in Figure 7.3d, because the building units (nutrients) of ZIF-8 were predominantly used to grow the shell layer [13,25]. When using a crystallization solution with the same concentration as that for ZIF-8/Au/ZIF-8-2 but with a shorter synthesis time of 20 h, the resulting ZIF-8/Pd/ZIF-8 was observed to have

a thinner ZIF-8 shell (less than 100 nm) without any core-free Pd/ZIF-8particles (Figure 7.3e and Figure 7.3f).

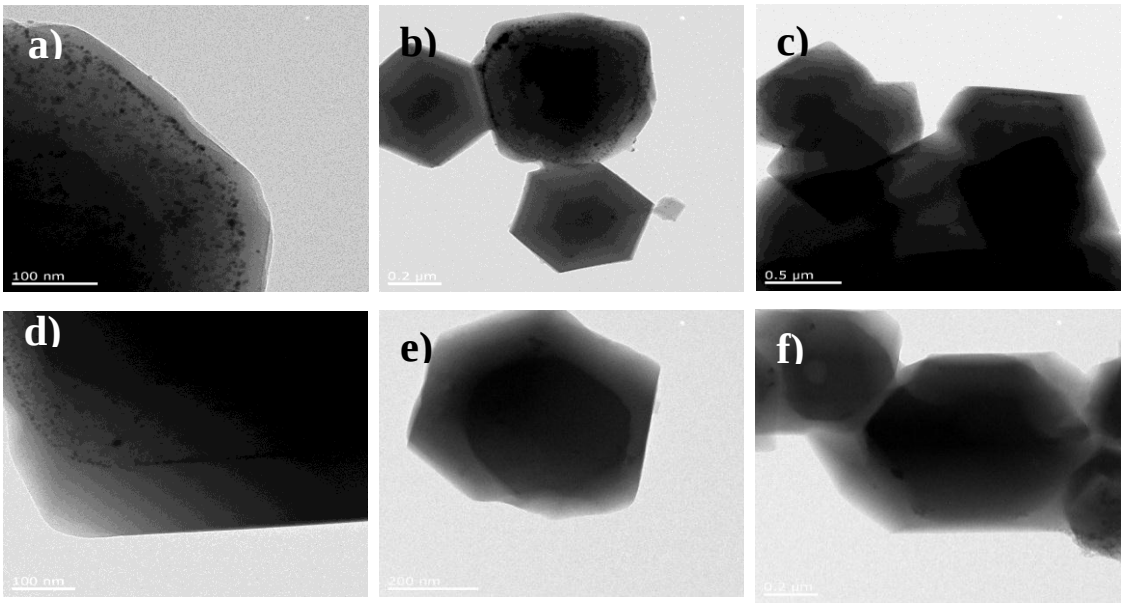

Figure 7.3 TEM images of ZIF-8/Au/ZIF-8-1 (a and b), ZIF-8/Au/ZIF-8-2 (c and d) and ZIF-8/Pd/ZIF-8 (e and f).

The TGA results (Figure 7.4) indicate that the synthesized ZIF-8 exhibited a weight loss of approximately 18% under flowing air at a temperature of 200 ℃. This weight loss corresponds to the removal of moisture and other residues from the ZIF-8 structure. The ZIF-8 structure was also found to be stable up to 400 ℃ under flowing air, which is consistent with the results reported in a previous study [17]. In contrast, the Pd/ZIF-8 structure began to quickly collapse from approximately 280 ℃, and finally, the Pd/ZIF-8 sample fully decomposed after heating to 400 ℃ under flowing air. Furthermore, the ZIF-8/Pd/ZIF-8 structure was found to decompose from approximately 320 ℃ under flowing air, which indicates that this sample possesses higher thermal–structural stability compared to Pd/ZIF-8 without the ZIF-8 protective shell layer, although it is less stable than pure ZIF-8. The lower thermal stability of Pd/ZIF-8 compared with pure ZIF-8 could be attributed to the embedded Pd particles, which damaged the metal-organic linker bonds of the ZIF-8 structure; thus, the ZIF-8 framework is more vulnerable under high-temperature conditions.

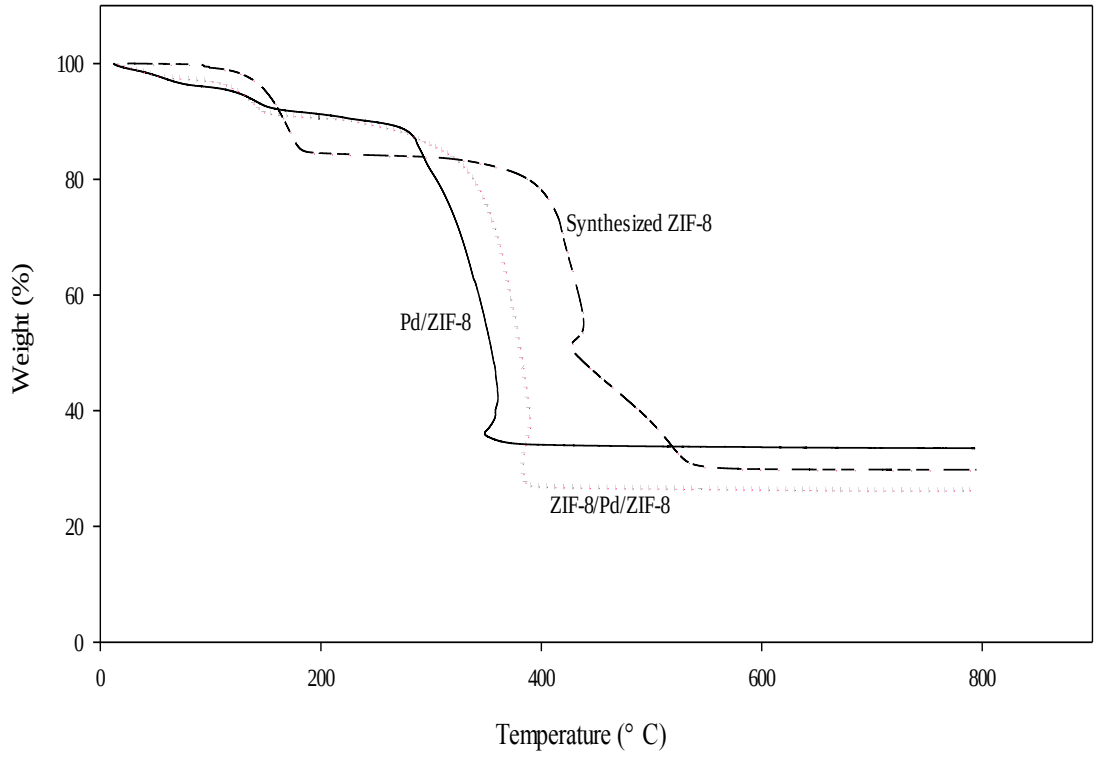

Figure 7.4 TGA results for the synthesized ZIF-8, Pd/ZIF-8 and ZIF-8/Pd/ZIF-8 samples.

7.3.2 Catalytic Alkene Hydrogenation

The catalytic hydrogenation of 1-hexene and cis-cyclooctene was conducted in the liquid phase to evaluate the catalytic performance of the prepared catalysts. Figure 7.5 shows the shape/size selectivity of the designed catalyst as a function of the specific pore size. Although the aperture size of ZIF-8 is close to 3.4 Å based on calculation from XRD [22], the hinged Zn-imidazolate-Zn units which define the edges of the XRD-derived 0.34 Å aperture size gives flexibility to allow 1-hexene with a molecular diameter of 1.7 Å to access the internal channels. However, cis-cyclooctene with a molecular width of 5.5 Å, which is larger than 1-hexeneand the effective aperture size

of ZIF-8, will be excluded from the framework and consequently prevented from contacting the active component inside the catalyst core [26, 27]. Due to the aperture flexibility, the hydrogenation of 1-hexene is possible overall of the Pd particles dispersed in the micropores of the Pd/ZIF-8 composite and ZIF-8/Pd/ZIF-8 composite. The hydrogenation of cis-cyclooctene, however, could only occur over the Pd particles located near the outer surface of Pd/ZIF-8. For reference, a Pd/ZSM-5 catalyst was also synthesized and evaluated in alkene hydrogenation.

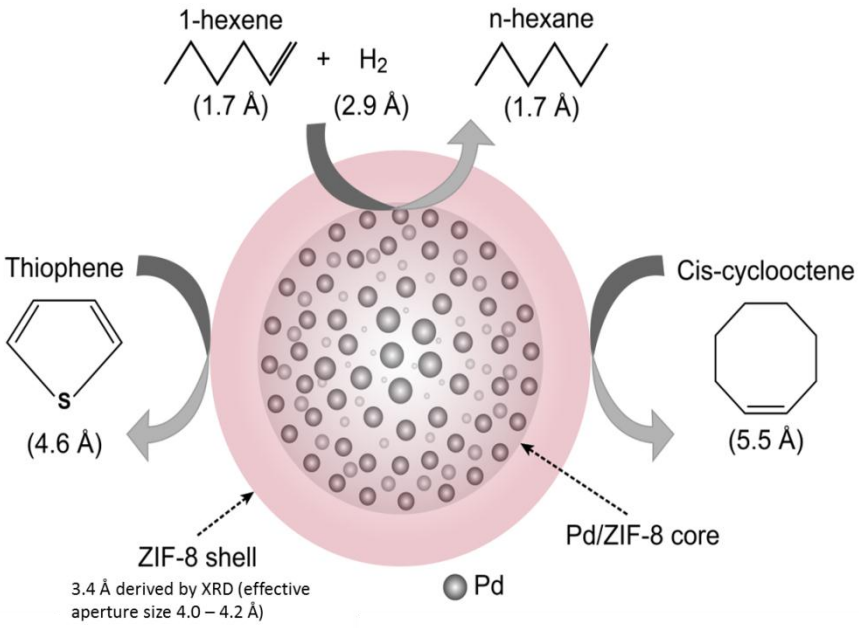

Figure 7.5 Schematic diagram of catalytic alkene hydrogenation on ZIF-8/Pd/ZIF-8.

Figure 7.6 shows the conversions of 1-hexene and cis-cyclooctene hydrogenation when catalysed by ZIF-8, Pd/ZSM-5, Pd/ZIF-8 and ZIF-8/Pd/ZIF-8. Pure ZIF-8 shows zero catalytic activity in the hydrogenation of 1-hexene and cis-cyclooctene. In contrast, the conversions of 1-hexene and cis-cyclooctene reached nearly 100% and approximately 30%, respectively, over both Pd/ZSM-5 and Pd/ZIF-8. The higher conversion of 1-hexene could be attributed to: (i) the faster turnover rate of 1-hexene over the Pd nanoparticles compared with that of cis-cyclooctene [24], and (ii) 1-hexene, which has a

smaller kinetic diameter compared with cis-cyclooctene, has a higher diffusion rate inside the microporous channel of ZIF-8. The latter also causes less mass transfer limitations to the reaction. The conversion of cis-cyclooctene over Pd/ZSM-5 was slightly higher than that over Pd/ZIF-8 due to the greater accessibility of Pd active sites in Pd/ZSM-5. ZIF-8 possesses a relatively small pore size compared with ZSM-5 (effective pore size of 4.0–4.2 Å vs 5.6 Å), which causes the hydrogenation of cis-cyclooctene to primarily occur over Pd particles located on the outer surface of Pd/ZIF-8, preventing the reaction from being catalysed by the remainder of Pd particles in the inner structure of ZIF-8.

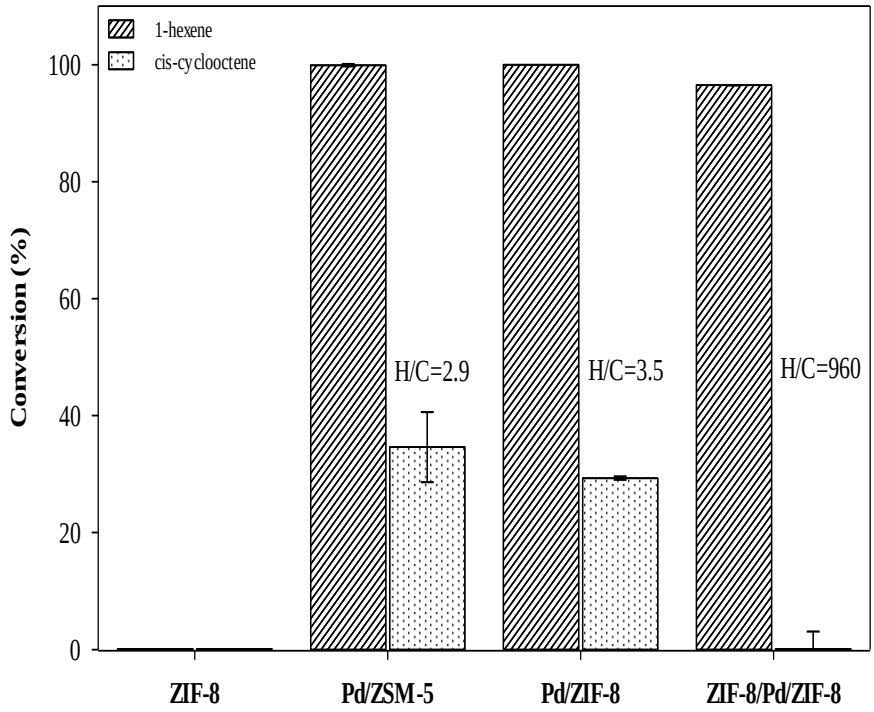

Figure 7.6 Hydrogenation of 1-hexene and cis-cyclooctene catalyzed by ZIF-8, Pd/ZSM-5, Pd/ZIF-8 and ZIF-8/Pd/ZIF-8. "H/C" is the conversion ratio of 1-hexene to cis-cyclooctene.

Interestingly, the hydrogenation results revealed that the ZIF-8/Pd/ZIF-8 core–shell composite showed remarkably higher selectivity to 1-hexene than to cis-cyclooctene (96.5% conversion of 1-hexene versus zero conversion of cis-cyclooctene over ZIF-

8/Pd/ZIF-8) with conversion ratio of 1-hexene to cis-cyclooctene (H/C) = 960. This result confirmed the hypothesis that the cis-cyclooctene molecules were excluded by the ZIF-8 shell and thus unable to contact the Pd particles for hydrogenation. In contrast, 1-hexene was able to access the Pd particles protected by the ZIF-8 shell through its flexible pores. Nevertheless, the ZIF-8 shell also increased the mass transfer limitations in ZIF-8/Pd/ZIF-8 and inevitably decreased the conversion of 1-hexene slightly compared with Pd/ZIF-8. Because the reaction exhibits a transport limitation, it could be inferred that the overall rate of 1-hexene hydrogenation is fast compared to the rate of transport to the Pd active sites, i.e., mass-transfer controlled. It is therefore advantageous to deposit the Pd sites in the subsurface layer (as shown in Figure 7.3e and Figure 7.3f) such that the transport limitations can be reduced while catalytically active Pd particles, which are liable to lose activity by attrition, can be protected. The catalytic alkene hydrogenation indicates that the ZIF-8 shell layer was successful grown over the Pd/ZIF-8 core using the synthesis method reported herein.

7.3.3 Anti-poisoning Property

It has been reported that noble metals can easily be poisoned by sulfur species [28]. This sulfur poisoning effect is often irreversible due to the formation of sulfur-metal bonds, which are not catalytically active. For example, Pd particles can be deactivated by trace amounts of sulfur containing impurities, which are commonly found in raw materials of process feedstock, e.g., in woody biomass [29]. In this study, the core–shell metal/ZIF-8 composite was evaluated to investigate its performance in protecting the active sites from sulfur poisoning by screening the poisoning component outside the ZIF-8 shell. The anti-poisoning ability of the developed core–shell catalyst was investigated by adding thiophene (with a molecular size of 4.6 Å) with alkene and H_2 to poison the catalyst in the reactor for hydrogenation. After the reaction, the spent catalyst was recovered and regenerated under vacuum at 100 ℃ for 24 h. The catalyst was then reused for alkene hydrogenation in the absence of thiophene. The catalyst performance in alkene hydrogenation after contacted with poisoning component and regeneration was investigated. Figure 7.7 shows that the conversion of 1-hexene and cis-cyclooctene over Pd/ZSM-5 after sulfur treatment and regeneration decreased to approximately 74%

and 6.2%, respectively, (nearly 100% conversion of 1-hexene and 30% conversion of cis-cyclooctene prior to sulfur treatment, as shown in Figure 7.6) due to the prior deactivation of Pd particles by thiophene. These results suggest that the catalyst treatment step using vacuum heating cannot completely regenerate the spent catalyst due to irreversible poisoning of Pd particles. The conversions of 1-hexene and cis-cyclooctene over Pd/ZIF-8 were 95% and 0%, respectively, after regeneration. The conversion of 1-hexene was almost recovered back to pre-poisoned performance. This result confirmed that the Pd sites located in the inner structure of Pd/ZIF-8 remained catalytically active for the hydrogenation of 1-hexene after the removal of thiophene. In contrast, the conversion of cis-cyclooctene was reduced to almost 0% (after poisoning by thiophene and regeneration), indicating that the ZIF-8 structure was possibly maintained and that it still retains its molecular sieving ability after regeneration of the catalyst. However, the surface Pd particles in Pd/ZIF-8 are still poisoned irreversibly by sulfur species which resulted in almost 0% conversion of cis-cyclooctene. Figure 7.7 shows the alkene hydrogenation over the core–shell Pd/ZIF-8 (ZIF-8/Pd/ZIF-8) after the catalyst underwent sulfur treatment by thiophene and after it is regenerated. The hydrogenation of 1-hexene and cis-cyclooctene are 95% and 3%, respectively, over the regenerated ZIF-8/Pd/ZIF-8, which is comparable to the conversion obtained using ZIF-8/Pd/ZIF-8 prior to sulfur poisoning (Figure 7.6). A 3% conversion of cis-cyclooctene was obtained using regenerated ZIF-8/Pd/ZIF-8, potentially due to the minor defect formed on the ZIF-8 shell during the regeneration process that exposed some Pd particles for hydrogenation. Although Pd/ZIF-8 and ZIF-8/Pd/ZIF-8 gave similar conversions of 1-hexeneand cis-cyclooctene after they are regenerated, the ZIF-8 protective layer in the core–shell composite keeps the Pd particles in the sub-surface layer thereby eliminates irreversible sulfur poisoning to the Pd sites near the surface. One may consider the regenerated Pd/ZIF-8 with catalytically inactive surface Pd particles indeed has a similar structure as ZIF-8/Pd/ZIF-8 but with a smaller (overall composite) size. The results also suggest that the designed core–shell metal/ZIF-8 composite has a narrow molecular cut size between 4.2 and 4.6 Å as reflected by the exclusion against thiophene molecules (4.6 Å) over 1-hexene (1.7 Å). This sharp molecular sieve separation cannot be readily achieved by traditional microporous zeolites.

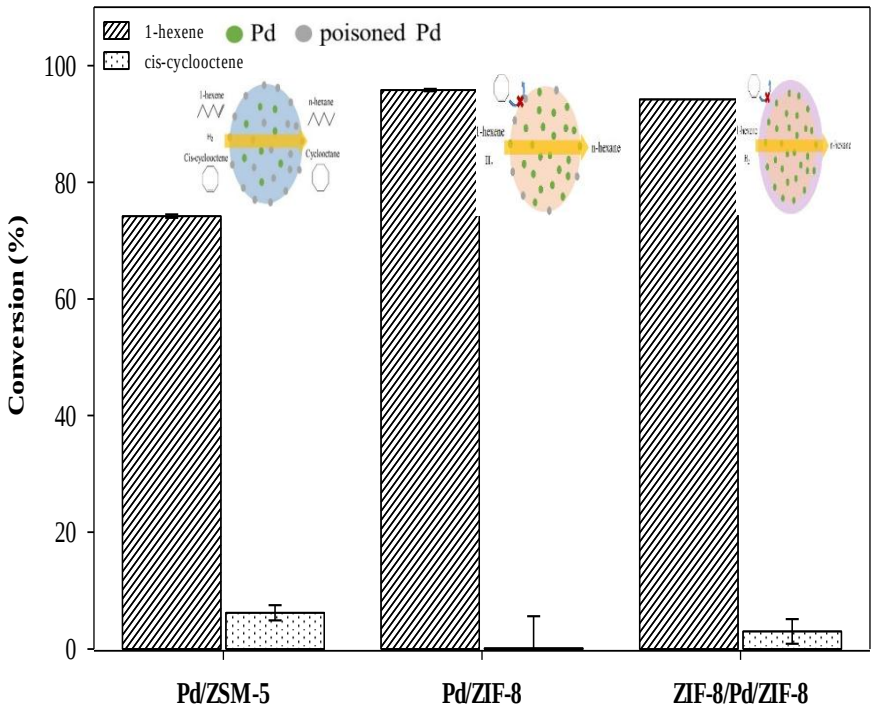

Figure 7.7 Catalytic hydrogenation of 1-hexene and cis-cyclooctene over regenerated(a) Pd/ZSM-5, (b) Pd/ZIF-8 and (c) ZIF-8/Pd/ZIF-8 after thiophene treatment.

7.4 Conclusions

A successful method for synthesizing a core–shell metal/ZIF-8composite was reported. The catalytic selectivity and anti-poisoning properties of the synthesized ZIF-8/Pd/ZIF-8 composites were investigated and compared with those of Pd/ZSM-5 and Pd/ZIF-8 in alkene hydrogenation. The core–shell ZIF-8/Pd/ZIF-8 exhibited higher selectivity to 1-hexene over cis-cyclooctene during hydrogenation. Furthermore, the ZIF-8 shell layer of the core–shell structure was able to effectively protect the subsurface Pd particles from sintering at high temperature and from poisoning by thiophene. The sulfur poisoning components were captured within the layer at the external edge of the catalyst core. The catalytic activity of the core–shell ZIF-8/Pd/ZIF-8 could be recovered after removal of the adsorbed thiophene via heat treatment under vacuum. It is concluded that

the core–shell structure reported in this work is a feasible design for ZIF-supported catalysts, allowing it to be used practically in industrial processes.

Reference

[1] H. Li, M. Eddaoudi, M. O'Keeffe, O.M. Yaghi, Design and synthesis of an exceptional stable and highly porous metal organic framework, Nature., 402(1999) 276-279.

[2] J.L.C. Rowsell, O.M. Yaghi, Metal-organic frameworks: a new class of porous materials, Micro. Meso. Mater., 73(2004) 3-14.

[3] S.L. James, Meral-organic frameworks, Chem. Soc. Rev., 32(2006) 276-288.

[4] S.T. Meek, J.A. Greathouse, M.D. Allendorf, Metal-organic frameworks: a rapidly growing class of versatile nanoporous materials, Adv. Mater. 23 (2011) 249-267.

[5] H-C. Zhou, J.R. Long, O.M. Yaghi, Introduction to metal-organic frameworks, Chem. Rev. 112 (2012) 673-674.

[6] S.G. Telfer, What are these things called MOFs, Chem. N. Z. Adv. Mater. Nanotech., 74(2010) 9-14.

[7] J.J. Low, A.I. Benin, P. Jakubczak, J.F. Abrahamian, S.A. Faheem, R.R. Willis, Virtual high throughput screening confirmed experimentally: porous coordination polymer hydration, J. Am. Chem. Soc. 131 (2009) 15834-15842.

[8] K. S. Park, Z. Ni, A. P. Côté, J. Y. Choi, R. Huang, F. J. Uribe-Romo, H. K. Chae, M. O'Keeffe, O. M. Yaghi, Exceptional chemical and thermal stability of zeolitic imidazolate frameworks, Proc. Natl. Acad. Sci. USA. 103 (2006) 10186-10191.

[9] J.Y. Lee, O.K. Farha, J. Roberts, K.A. Scheidt, S.B.T. Nguyen, J.T. Hupp, Metal organic framework materials as catalysts, Chem. Soc. Rew., 38(2009) 1450-1459.

[10] A. Corma, H. Garcia and F.X.L.i. Xamena, Engineering Metal Organic Frameworks for Heterogeneous Catalysis, Chem. Rev., 110(2010) 4606-4655.

[11] J. Liu, L. Chen, H. Cui, J. Zhang, L. Zhang, C-Y. Su, Applications of metal–organic frameworks in heterogeneous supramolecular catalysis, Chem. Soc. Rev. 43, (2014) 6011-6061.

[12] M. Meilikhov, K. Yusenko, D. Esken, S. Turner, G.V. Tendoloo and R.A. Fischer, Metals@MOFs– loading MOFs with Metal Nanoparticles for Hybrid Functions, Eur. J. Inorg. Chem., 24(2010) 3701-3714

[13] G. Lu, S. Li, Z. Guo, O.K. Farha, B.G. Hauser, X. Qi, Y. Wang, X. Wang, S. Han, X. Liu, J.S. Duchene, H. Zhang, Q. Zhang, X. Chen, J. Ma, S.C.J. Loo, W.D. Wei, Y. Yang, J.T. Hupp, F. Huo, Imparting functionality to a metal–organic framework material by controlled nanoparticle encapsulation, Nat. Chem. 4 (2012) 310-316.

[14] L.Y. Chen, H.R. Chen, R. Luque and Y.W. Li, Metal-organic framework encapsulated Pd nanoparticles: towards advanced heterogeneous catalysts, Chem. Sci., 5(2014) 3708-3714.

[15] P.Z. Li, K. Aranishi and Q. Xu, ZIF-8 immobilized nickel nanoparticles: highly effective catalysts for hydrogen generation from hydrolysis of ammonia borane, Chem. Commun., 48(2012). 3173-3175

[16] M.S. El-Shall, V. Abdelsayed, A.E.R.S. Khder, H.M.A. Hassan, H.M. El-Kaderi, T.E.Reich, Metallic and bimetallic nanocatalysts incorporated into highly porous coordination polymer MIL-101. J. Mater. Chem., 19(2009) 7625–7631.

[17] H. Yin, H. Kim, J. Choi, A.C.K. Yip, Thermal stability of ZIF-8 under oxidative and inert environments; A practical perspective on using ZIF-8 as a catalyst support, Chem. Eng. J. 278, (2015) 293-300.

[18] H-L. Jiang, B. Liu, T. Akita, M. Haruta, H. Sakurai, Q. Xu, Au@ZIF-8: CO oxidation over gold nanoparticles deposited to metal-organic framework, J. Am. Chem. Soc., 131(2009) 11302-11303.

[19] T. Ishida, M. Nagaoka, T. Akita, M. Haruta, Deposition of Gold Clusters on Porous Coordination Polymers by Solid Grinding and Their Catalytic Activity in Aerobic Oxidation of Alcohols, Chem. Eur. J. 14 (2008) 8456–8460.

[20] D. Esken, S. Turner, O.I. Lebedev, G.V. Tendeloo, R.A. Fischer, Au@ZIFs: stabilization and encapsulation of cavity-size matching gold clusters inside functionalized zeolite imidazolate frameworks, ZIFs, Chem. Mater. 22 (2010) 6393-6401.

[21] S. Hermes, M.-K. Schroter, R. Schmid, L. Khodeir, M. Muhler, A. Tissler, R.W. Fischer, Metal@MOF: Loading of Highly Porous Coordination Polymers Host

Lattices by Metal Organic Chemical Vapor Deposition, Angew. Chem. Int. Ed. 44 (2005) 6237–6241.

[22] C. Zhang, R.P. Lively, K. Zhang, J.R. Johnson, O. Karvan, W.J. Koros, Unexpectedmolecular sieving properties of zeolitic imidazolate framework-8, J. Phys. Chem. Lett. 3 (2012) 2130–2134.

[23] Y. Pan, Y. Liu, G. Zeng, L. Zhao, Z. Lai, Rapid synthesis of zeolitic imidazolate framework-8 (ZIF-8) nanocrystals in an aqueous system, Chem. Commun. 47 (2011) 2071-2073.

[24] T. Zhang, X.F. Zhang, X.J. Yan, L. Lin, H. Liu, J.S. Qiu, K.L. Yeung, Core-shell Pd/ZSM-5@ZIF-8 membrane micro-reactors with size selectivity properties for alkene hydrogenation, Catal. Today., 236 (2014) 41–48.

[25] J. Yao, L. Li, W.H.B. Wong, C. Tan, D. Dong, H. Wang, Formation of ZIF-8 membranes and crystals in a diluted aqueous solution, Mater. Chem. Phy., 139(2013) 1003-1008.

[26] P. Wang, J. Zhao, X. Li, Y. Yang, Q. Yang, C. Li, Assembly of ZIF nanostructures around free Pt nanoparticles: efficient size-selective catalysts for hydrogenation of alkenes under mild conditions, Chem. Comm., 49(2013) 3330-3332.

[27] L. Lin, T. Zhang, X.F. Zhang, H. Liu, K.L. Yeung, J.S. Qiu, New Pd/SiO2@ZIF-8 Core–Shell Catalyst with Selective, Antipoisoning, and Antileaching Properties for the Hydrogenation of Alkenes, Ind. Eng. Chem. Res., 53(2014) 10906–10913.

[28] C.H. Bartholomew, Mechanisms of catalyst deactivation, Appl. Catal. A 212 (2001) 17–60.

[29] Z. Wu, S. Goel, M. Choi, E. Iglesia, Hydrothermal synthesis of LTA-encapsulated metal clusters and consequences for catalyst stability, reactivity, and selectivity, J. Catal. 311 (2014) 458–468.

Chapter 8

Conclusion, Recommendations and Future Study

8.1 Conclusions

In this thesis, a systematic study was carried out aiming to develop a porous hybrid solid membrane reactor system for H_2 production and purification from WGSR. At the beginning, ZIF-8 was screened out from various porous material candidates and selected as the raw material of the objective membrane system. Then, the hydrothermal stability of ZIF-8 was evaluated under various environments and the application feasibilities of ZIF-8 materials were discussed. Moreover, the ZIF-8 based catalyst and gas separation membrane were successfully prepared with the fabrication methods developed in this study, and their applications were characterized under the stimulated conditions of the H_2 involved reactions. Finally, a demonstration experiment of WGSR was conducted in both the ZIF-8 membrane reactor system and the conventional packed bed reactor system. The advantages of employing the ZIF-8 based membrane reactor system were illustrated, while the stability limitations of the ZIF-8 material under the harsh conditions were verified.

The main findings of this study are generally detailed as:

Firstly, the micro porous materials of ZIF-8, GIS - NaP and MIL-47 were successfully prepared through the hydrothermal synthesis method and the crystallization mechanisms of these materials were examined. In the meantime, the composite catalysts with these porous material supports were fabricated and characterized with various methods. Finally, ZIF-8 was selected as the raw material of the membrane system after considering its fabrication feasibility and the application potentials in catalysis and gas separation membrane processes.

Secondly, a comprehensive study was performed to investigate the thermal stability of ZIF-8 under various gaseous environments and to investigate the feasibility of employing ZIF-8 in gas-phase applications. Herein, we determined that ZIF-8 exhibits its greatest stability in an inert environment and the worst stability were observed under a steam atmosphere. We also pointed out that the TGA results could accurately represent the thermal stability of ZIF-8 from the engineering prospective only if they are recorded isothermally. In summary, ZIF-8 is concluded suitable for use in catalytic

reactions and gas-separation processes at temperatures below 300 ℃ in the presence of air or water and under inert gas environments at temperature over 400 ℃.

Thirdly, a well-integrated ZIF-8 membrane was prepared through the post-treatment methods developed in this study and the ZIF-8 membrane showed a modest gas separation performance in the simulated biomass-derived syngas environment. Subsequently, the long term test results showed that the hydrothermal instability limits the ZIF-8 membrane applications in biomass-derived syngas environments over 200 °C. Lastly, we suggested that the additional efforts should be focused on preserving the integration of the ZIF-8 membranes under steam-containing feeds at temperatures higher than 200 °C.

Later on, a demonstration experiment of WGSR was carried out in both the membrane reactor system and the conventional packed bed reactor system. The result shows that the CO conversion and the H_2 recovery of the WGSR could be improved by employing the MR system, while this improvement could be enhanced by increasing the operation temperature. However, the ZIF-8 membrane based MR is not hydrothermal stable over the temperature of 200 ℃, and impropriate to be employed for WGSR before the further progressive modification on its structure.

Lastly, a core–shell metal/ZIF-8 composite catalyst was fabricated and its catalytic selectivity and anti-poisoning properties were demonstrated in alkene hydrogenation. It is concluded that this core–shell structure is a feasible design for ZIF-supported catalysts, allowing it to be used practically in industrial processes.

8.2 Recommendations and Future Study

Based on the findings and knowledge obtained from the present study, we would make the below recommendations to the future study of the ZIF-8 membrane reactor system for H_2 production and purification:

Firstly, efforts are expected to be made on the progressive modifications of ZIF-8 structure before it could be widely employed under harsh condition applications, like

WGSR. In the present study, the result clearly shows that the ZIF-8 material indeed has extraordinary potentials in the applications of catalysis, gas separation membrane as well as the membrane reactor system. However, the ZIF-8 applications in these areas are all seriously limited by its hydrothermal stability at this moment. Hence, it is critical to improve the structure stability of ZIF-8 in the future work to realize the ZIF-8's potentials in applications.

Secondly, the operation conditions optimization is highly demanded to maximize the advantages of employing MR for WGSR. From this study, we can find that the operation conditions, like reaction temperatures and membrane performance, seriously affect the performance of the membrane reactor system. Hence, the comprehensive investigation on the MR operation conditions is recommended, by combining the mathematics simulations together with experimental studies, to optimize and maximize the MR functions for different reactions.

PUBLICATIONS

Journal Articals

1. On the ZeoliticImidazolate Framework-8 (ZIF-8) Membrane for Hydrogen Separation from Simulated Biomass-derived Syngas, **H. Yin**, E. Jang, J. Choi, and A.C.K. Yip, Mesoporous and Microporous Maetrials., doi:10.1016/j.micromeso.2015.10.033.
2. Anti-poisoning core–shell metal/ZIF-8 catalyst for selective alkene hydrogenation, **H. Yin**, J. Choi, and A.C.K. Yip, Catalysis Today, 265(2016) 203-209.
3. Thermal stability of ZIF-8 under oxidative and inert environments: A practical perspective on using ZIF-8 as a catalyst support, **H. Yin**, H. Kim, J. Choi, and A.C.K. Yip, Chemical Engineering Journal, 278 (2015) 293-300.

Conference contributions

4. Synthesis and Application of core-shell Zeolitic Imidazole Framework-8 (ZIF-8) Catalyst inAlkene Hydrogenation, H. Yin, J. Choi and A.C.K. Yip, APCChE 2015, Melbourne, Australia, Sep 27 - Oct 1, 2015
5. Thermal structural stability of ZIF-8 under various gaseous environments, H. Yin, J. Choi and A.C.K. Yip, 4thMSA ECR symposium 2014, Victoria, Australia, Nov 19-21, 2014
6. Structural stability of ZIF-8 under oxidative and inert gas environment, H. Yin, J. Choi andA.C.K. Yip, ISCRE23, Bangkok, Thailand, Sep 7-10, 2014